MOLECULAR MODEL OF αB-CRYSTALLIN FUNCTION IN THE TRANSPARENCY OF THE EYE LENS AND THE STRESS RESISTANCE OF THE HEART

By

Sanjay Mishra

Dissertation
Submitted to the Faculty of the
Graduate School of Vanderbilt University
In partial fulfillment of the requirements
for the degree of

DOCTOR OF PHILOSOPHY
in
Chemical and Physical Biology

August 10, 2018
Nashville, Tennessee

Approved:
Wenbiao Chen, Ph.D.
Kevin L. Schey, Ph.D.
D. Borden Lacy, Ph.D.
Patrick. S. Page-McCaw, Ph.D.

To Swasti and Smriti:

Thank you for believing in me.

For laughing, even when the jokes were stale.

For enduring the trials and tribulations of my voyages.

For shining bright through the seasons, even on the cloudiest nights.

ACKNOWLEDGEMENTS

"It takes a village to teach a child," but it took much more to finish my Ph.D. My work would not be possible without the patience of my mentors, collaborators, and friends. Dr. Hanane Koteiche, who passed away early in my journey was most instrumental in my endevaour. I inherited many of her resources and I learned from her many techniques and most importantly - the value of documentation. Dr. Lisette Maddison was always available to walk me through my long learning paths. Dr. Ela Knapik was very generous to let me work in her lab. Drs. Shu-Yu "Simon" Wu, Rich Stein, Derek Claxton, Daniel Levic, Ping Zou and Mingyu Li not only collaborated extensively but also provided valuable support throughout my work.

I cannot praise Poonam Rathore, Guangyong Yang, Edward Monson, Marko Bajik, Abigail Poff, and Linlin Yin highly enough. Vanderbilt University hosts fantastic core facilities of which I am especially indebted to the Proteomics, Microscopy and Zebrafish Cores where Drs. Hayes McDonald, Kristie Rose, Bryan Millis; and Amanda Goodrich and Cory Guthrie always met my timelines, even though I was frequently past their deadlines. Dr. Bruce Damon, Lindsay Meyers and Patricia Mueller took care of minutiae that kept my student and immigrant status intact. Kevin Jagessar, Reza Dastvan, Alexandra Fuller and Francisco Rodriguez happily endured my volatility yet never refused to help.

All members of my committee provided extensive guidance and painstakingly taught me to be a good scientist, a better writer, and an effective presenter. Dr. Wenbiao Chen not only chaired my committee, but he also affectionately initiated me on the bewildering path of the zebrafish biology. I owe enormous gratitude to my mentor Prof. Hassane Mchaourab. While I scarcely met his expectations, he was ever more gracious responding to my failings and travails. Hassane's scientific rigor and audacities are infectious, and he taught me a great deal about life in and out of the laboratory.

My family is the foundation of my misshapen edifice. My sister, parents, and parents-in-law have not seen me in over a decade, but their invisible presence and encouragement have propelled me through my transcontinental odyssey. Finally, I can acknowledge two very important women: my loving wife and collaborator Dr. Smriti, and my vivacious daughter Swasti, who have been the bedrock of my existence. I can never thank them enough.

TABLE OF CONTENTS

Page

LIST OF TABLES

Table Page

LIST OF FIGURES

Figure Page

LIST OF ABBREVIATIONS

AF	atrial fibrillation
AUC	Analytical Ultracentrifugation
CTD	C-terminal domain
dpf	days post-fertilization
2D-PAGE	Two-dimensional polyacrylamide gel electrophoresis
DRM	desmin-related cardiomyopathy
DIGE	Difference Gel Electrophoresis
DALYs	disability adjusted life years
DBD	DNA binding domain
EPR	Electron Paramagnetic Resonance
FRET	Fluorescence Resonance Energy Transfer
GR	glucocorticoid receptors
GREs	glucocorticoid response elements
GC	Glucocorticoids
hpf	hours post-fertilization
HF	heart failure
HSP	heat-shock protein
HPA	hypothalamus-pituitary-adrenal
HPI	hypothalamus-pituitary-interrenal
iTRAQ	Isobaric tags for relative and absolute quantification
IEF	isoelectric focusing
MMTS	methyl methanethiosulfonate
MO	morpholino antisense oligo
NEI	National Eye Institute
NMD	nonsense-mediated mRNA decay
NTD	N-terminal domain
PAGE	Polyacrylamide Gel Electrophoresis
PBS	Phosphate Buffer Saline
PSC	Posterior subcapsular cataracts
PN	proteostasis network
PTU	1-phenyl 2-thiourea
SDS	Sodium Dodecyl Sulphate
SDSL	Site Directed Spin Labeling
SEC	Size Exclusion Chromatography
SE	standard error
sHSPs	small HSPs
TCEP	Tris-(2-carboxyethyl)phosphine
UPS	ubiquitin–proteasome system
VI&B	visual impairment and blindness
WIF	water-insoluble fraction
WSF	water-soluble fraction
WMISH	Whole-mount in situ hybridization

CHAPTER I

INTRODUCTION

“There is no other anatomic structure that is more mathematical in form than the lens or so complex in composition. For this very reason there is no subject in human physiology about which more divergence of opinion has been entertained than the role the crystalline lens plays in the faculty of vision." – (Gordon, 1935)

Protein folding and aggregation

Proteins are the primary molecular actors and scaffolds that maintain cell homeostasis (Brändén and Tooze, 1999). Chemically, proteins begin as linear, highly flexible, unbranched polymers of amino acid residues. However to perform their biochemically relevant roles, they must attain and maintain their evolutionarily optimized unique three-dimensional shapes (Hartl, 2017, Pal et al., 2006). The transition of a polypeptide chain from a disordered, non-native state to the ordered, native state is called protein folding (Rose et al., 2006). During protein folding, proteins undergo a reversible disorder ⇌ order transition. Folding is an exothermic process, which is driven mostly by the “hydrophobic effect”. Physiology requires correctly folded proteins to maintain cellular integrity and to carry on normal cellular and tissues functions, and the failure in properly folding proteins leads to proteopathies (also known as proteinopathies, protein conformational disorders, or protein misfolding diseases) (Reynaud, 2010, Soto, 2001, Chaudhuri and Paul, 2006, Muchowski and Wacker, 2005, Hartl, 2017).

The largest number of protein misfolding pathologies arise from aggregation of misfolded proteins (Chiti and Dobson, 2006). This is astonishing given that Anfinsen's dogma (or the thermodynamic hypothesis) attests that for proteins all of the information needed to achieve the "folded" form is encoded in the linear polypeptide sequences. (Anfinsen, 1973). However, only small, single-domain proteins that can relatively rapidly bury exposed hydrophobic amino acid residues can spontaneously fold into native conformations (Gutte and Merrifield, 1969, Anfinsen et al., 1961, Finkelstein et al., 2013). Even for proteins that can be folded *in vitro*, the time scale

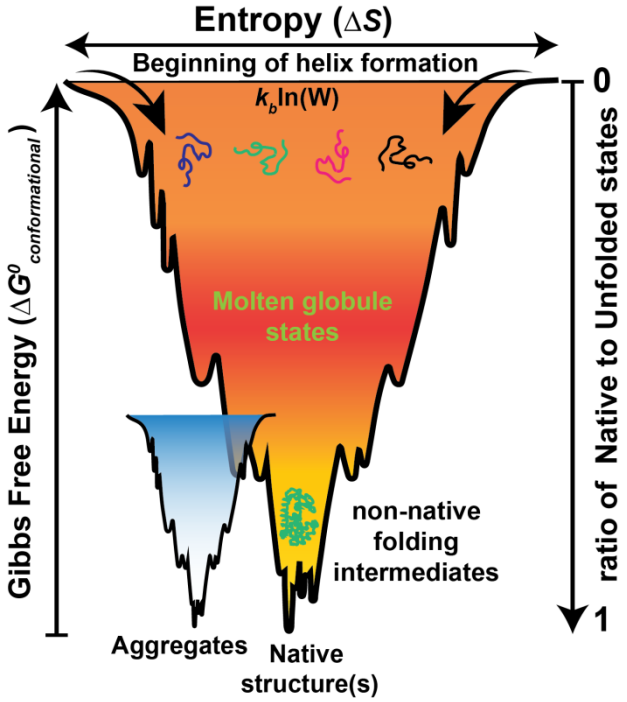

Figure 1: Cartoon of the folding funnel

Unfolded polypeptides have high entropy (ΔS, denoted by the width of the funnel), due to a large number of conformational states (W); and high free energy (ΔG, denoted by the depth of the funnel) due to low energy barriers between the conformations. Protein proceeds downhill the folding funnel towards the free energy minimum and low entropy due to a limited number of "native state(s)". As the protein traverses downhill, it encounters local minima of metastable states, or it can get trapped into aggregation states. Native states are non-unique iso-energetic conformations. (Modified from (Hartl et al., 2011)

varies from microseconds to hours (a difference of 11 orders of magnitude!), equivalent to the time difference between the life span of a mosquito and the age of the universe (Finkelstein et al., 2013). Moreover, there is an upper limit on size of protein domains "foldable" solely under thermodynamic control (Finkelstein et al., 2013). Larger proteins, composed of multiple domains, often refold inefficiently owing to the formation of partially folded intermediates, including misfolded states that tend to aggregate *in vitro* (Gutte and Merrifield, 1969, Anfinsen et al., 1961, Hartl and Hayer-Hartl, 2002).

This inefficiency of thermodynamic folding and obvious discrepancy from *in vivo* observation highlights the Leventhal's paradox (Levinthal, 1968). He postulated that even for a short 101 amino acid long peptide backbone, there would be a minimum of 3^{100} = 5 x 10^{47} conformations, if we assume just three possible configurations around each of 100 peptide bonds. If such a polypeptide chain could sample a new conformation every picosecond, (10^{12} s^{-1}), it will still take an unlikely 10^{27} years to sample all possible conformations stochastically

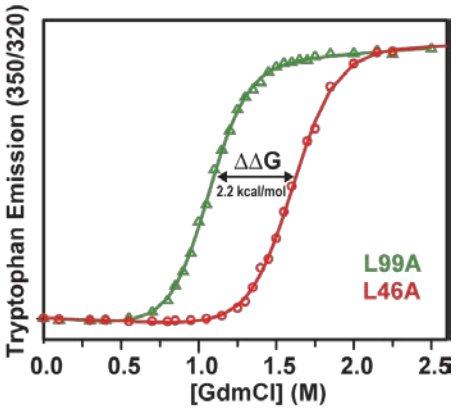

Figure 2: Denaturation curve of T4-Lysozyme mutants

Increasing concentrations of the denaturant, Guanidium Chloride (GdmCl), populates unfolded T4-Lysozyme, which red-shifts native Tryptophan fluorescence (from 320 to 350 nm) due to increase in solvent exposure. The leftward curve of L99A mutant highlights its lower stability compared to L46A. (Modified from (Claxton et al., 2008)

(Levinthal, 1969), a time scale longer than the age of the observable universe (Fowler, 1987, Fowler, 1989).

The macroscopic energetics of protein folding can be gleaned from the equilibrium transition from the folded to unfolded states. The plot of the unfolded fraction against the increasing quantity of protein denaturant (like temperature or a chaotropic agent such as guanidium hydrochloride or urea) is a highly cooperative sigmoidal curve (Figure 2) (Mishra et al., 2012, Claxton et al., 2008). At the curve's midpoint, half the protein population is folded, half is unfolded, and the population of partially folded intermediates can be assumed to be negligible.

Thus, the sigmoidal folding process can be simplistically described as an all-or-none, two-state chemical equilibrium (Zwanzig, 1997):

$$U(nfolded) \rightleftharpoons N(ative)$$

And the Equilibrium constant $K_{eq.} = \frac{[N]}{[U]}$

With the Gibbs free energy difference between the folded and unfolded populations:

$$\Delta G^0{}_{Native-Unfolded} = \Delta G^0{}_{conformational} = -RT\ ln\ K_{eq.}$$

Where:

R the gas constant (8.314 J $mol^{-1}K^{-1}$)

T the absolute temperature (Kelvin)

$\Delta G^0{}_{conformational}$ is a measure of difference in free energy between the folded and unfolded states; hence it is reflects the stability of the folded state. The folding equilibrium constant reflects the relative populations of the folded and unfolded sates. Thus, if the folding equilibrium favors the folded native state, *i.e.* $K_{eq.} > 1$, then $\Delta G^0{}_{conformational}$ will be negative.

The protein folding barriers in this “classical” two-state equilibrium can range from zero to the tens of RT and are primarily determined by protein size and the details of its structure (Halskau et al., 2008). However, typical values of $\Delta G^0{}_{conformational}$ for globular proteins, across species, are between −5 to −15 kcal/mol, which is the energy equivalent of a few hydrogen bonds (−5 kcal/mol) (Pace et al., 1981, Privalov, 1979). Such small difference in the $\Delta G^0{}_{conformational}$ means most proteins are only marginally favored to their folded state. However, the native structure(s) need to be sufficiently thermodynamically stable to ensure that enough active forms are available to perform the physiological function (Pal et al., 2006).

Proteins evolve under evolutionary drift within a narrow range of thermodynamic stability to avoid biochemical irrelevance, but with little incentive to increase stability above a certain threshold (Schreiber et al., 1994, Pal et al., 2006, Munoz et al., 2016). In fact, the narrow window of stability of proteins could possibly be an evolutionary trade-off between the activity and stability of proteins which are inversely related (Shoichet et al., 1995, Tsai et al., 2001). A corollary of this trade-off is that for an enzyme to be an efficient catalyst, it must also be flexible, which leads to a decrease in stability (Serrano et al., 1993). As shown by the Barnase/Binase pair, if a protein acquires a mutation that increases its stability without any biochemical advantage, another mutation negates the stability gain in the absence of an evolutionary pressure to favor the stability. However, if the protein accumulates a destabilizing mutation which compromises its ability to function, natural selection will rapidly remove it (Serrano et al., 1993, Ulyanova et al., 2011).

A purely thermodynamic model would suggest that proteins can fold under a thermodynamic bias cooperatively in “pre-arranged pathways”, and assistance from auxiliary “chaperones” is not obligatory to guide disordered polypeptide chains to transform into unique, biologically relevant three-dimensional structures. However, protein folding *in vivo* requires

assistance of molecular chaperones (heat shock proteins, HSPs) to attain and maintain their native folds (Broadley and Hartl, 2009, Hartl, 1996, Hartl and Hayer-Hartl, 2009, Hartl et al., 2011, Kim et al., 2013, Ellis, 1987). Indeed during their journey towards the native state, proteins encounter many valleys and hills that can slow the folding process and promote aggregation (Onuchic et al., 1997, Vallee-Belisle and Michnick, 2012). Finally, even subsequent to folding, proteins sample several conformational states away from their native energy minimum which can trap proteins into biologically unproductive, non-native alternate lowest energy minima (Capaldi et al., 2002, Vallee-Belisle and Michnick, 2007). Non-native or unfolded protein conformations populate in all physiological conditions to some extent (Bemporad et al., 2008). Misfolded proteins are not only inactive by loss-of-function but can potentially nucleate into toxic gain-of-function aggregates or form pathological amyloid fibers (Broadley and Hartl, 2009, Hartl, 2017, Klaips et al., 2018, Winklhofer et al., 2008). Therefore, intricate cellular systems called the proteostasis networks (PN) exist to assure protein homeostasis (or proteostasis) during folding and subsequent to it (Clark et al., 2012, Klaips et al., 2018, Morimoto and Cuervo, 2014, Strauch and Haslbeck, 2016, Voisine et al., 2010).

The Proteostasis Network

The all-encompassing term “proteostasis network” refers to an integrated network of a large array of proteins that oversee the “cradle-to-grave” fate of proteins (Hartl et al., 2011). Within the proteostasis network (PN), some PN factors assist in protein folding, some prevent or correct misfolding, some prevent aggregation of the misfolded proteins while others direct proteins to degradation pathways (Broadley and Hartl, 2009, Powers et al., 2009, Hartl et al., 2011, Taipale et al., 2010, Kaganovich et al., 2008, Fang and Mayor, 2012, Tyedmers et al., 2010). Specifically, the PN includes molecular chaperones and co-chaperones, the ubiquitin–proteasome system (UPS), and the autophagy machinery (Labbadia and Morimoto, 2015).

While the molecular chaperones and their regulators assist in *de novo* folding, refolding, or recognition of unfolding of proteins, the UPS ensures the quality control and mediates the degradation of irreversibly misfolded proteins to prevent aggregation and deleterious effects of dysfunctional proteins. In human cells, the PN comprises ~2000 proteins including 332 chaperones, ~280 involved in synthesis; and ~1400 proteins of UPS and autophagy components (Hartl et al., 2011, Klaips et al., 2018).

The PN dynamically responds to physiological conditions (Hartl, 1996, Hartl and Hayer-Hartl, 2002, Hartl and Hayer-Hartl, 2009, Hartl et al., 2011, Kim et al., 2013, Klaips et al., 2018). During cellular stress, such as exposure to sub-optimal temperature, caloric restriction, intense metabolic activity, oxidative and osmotic stress, and xenobiotics exposure, the stress response pathways of the PN are mobilized to reduce protein synthesis and increase the cellular capacity for protein folding and degradation (Gidalevitz et al., 2006, Labbadia and Morimoto, 2015, Morimoto and Cuervo, 2009, Voisine et al., 2010). Many diseases, such as cataract, neurodegeneration, cardiovascular disease and even some cancers involve deficiencies in proteostasis (Balch et al., 2008, Clark et al., 2012, Da Silva-Ferrada et al., 2016, Ge et al., 2010, Hartl et al., 2011, Hartl, 2017, Henning and Brundel, 2017, Klaips et al., 2018, Labbadia and Morimoto, 2015, Morimoto and Cuervo, 2014, Taylor and Dillin, 2011, Treweek et al., 2015, Voisine et al., 2010). While a common risk factor for many of these diseases is old age, the ageing itself accompanies gradual decline in cellular proteostasis capacity due to lifelong demand on the proteostatic network to keep the aging proteome healthy (Labbadia and Morimoto, 2015, Kikis et al., 2010, Voisine et al., 2010).

Since all biological systems need a healthy proteome to function, the stress responsive PN is among the most conserved, yet highly evolved systems (Kultz, 2003, Powers and Balch, 2013, Schroder et al., 1993). All known organisms have some kind of proteostasis system and

the core chaperone machineries (heat-shock protein [HSP] Hsp70s, Hsp90s, chaperonins, and small HSPs [sHSPs]) evolved early in prokaryotes (Klaips et al., 2018). A heat stress, as defined by a sudden exposure to temperatures just a few degrees above the physiological optimum, even in extremophiles significantly induces roughly 50–200 genes in organisms from archaea to human cell lines. (Richter et al., 2010). The stress response genes of humans account for almost a fifth (18%) of the 368 phylogenetically most highly conserved proteins (Kultz, 2003). Since proteins are most stable in the environment in which they were evolved to function, a robust yet flexible proteostasis is crucial to ensure survival and fitness of any organism when it encounters a less hospitable condition (Anfinsen, 1973, Strauch and Haslbeck, 2016, Balch et al., 2008). An efficient PN provides an evolutionary advantage to the host species because of better survivability. Not unexpectedly, complexity and the membership of the PN increases with the increasing complexity of the proteome of the taxa (Figure 3) (Klaips et al., 2018). About one fifth of proteins of PN in humans are chaperones (Brehme et al., 2014), which connect the three branches of PN, i.e. protein synthesis, folding and conformational maintenance; and protein degradation (Klaips et al., 2018).

Molecular Chaperones

Molecular chaperones are defined as proteins that interact with, stabilize or help another protein to acquire its functionally active conformation, without being present in the final structure (Hartl et al., 2011, Hartl and Hayer-Hartl, 2009, Hartl, 1996, Ellis, 1993, Ellis, 1987). Accordingly, chaperones include several different classes of structurally unrelated proteins which form cooperative pathways and networks. A common characteristic among all members of chaperone protein families is that they function as stress proteins or heat-shock proteins (HSPs). Under the conditions of stress, such as aging, pH extremes, nutrient limitation, osmotic variation, hypoxia, chemotherapeutic agents and noxious chemicals in which the concentrations of aggregation-prone folding intermediates increase, the heat shock elements, located in the promoter regions of the HSP genes are activated by heat shock transcription factors (Sorger, 1991).

Chaperones are central to the function of the PN where they function as oligomers

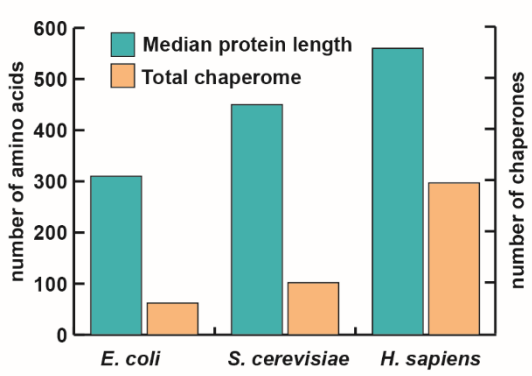

Figure 3: The chaperone complexity increases with the proteome

The average protein length (in number of amino acids, left y-axis) and total number of chaperones (right y-axis) in the proteomes of a prokaryote (*Escherichia coli*), a unicellular eukaryote (*Saccharomyces cerevisiae*), and humans (*Homo sapiens*); based on data from (Klaips et al., 2018, Brocchieri and Karlin, 2005)

either with members of the same family: “homo-oligomers”, or with members of other families, “hetero-oligomers”. Functionally, a chaperone can either function as a “holdase”, that is it binds partially folded intermediate states of target proteins in an ATP-independent manner; or it can act as a “foldase”, that is it can actively refold the client proteins powered by the free energy of ATP hydrolysis (Mattoo and Goloubinoff, 2014). Most “holdases” are stress-induced but the “foldases” come in both stress-induced and constitutively expressed versions (Richter et al., 2010). Structurally, chaperones are broadly classified according to their monomeric molecular weight into the DNAJ/Hsp40, chaperonin/Hsp60, Hsp70, Hsp90, Hsp100, and small Hsp (sHSP) families (Macario et al., 2013). While Hsp70s, Hsp90s Hsp100, and the chaperonins (Hsp60s) are foldases and actively participate in *de novo* protein folding and refolding through ATP- and cofactor-regulated binding and release cycles, the sHSPs are holdases and function in an ATP-independent manner to buffer aggregation of destabilized proteins (Jakob et al., 1993, Haslbeck, 2002, Kappe et al., 2003, Haslbeck et al., 2005, Sun and MacRae, 2005b).

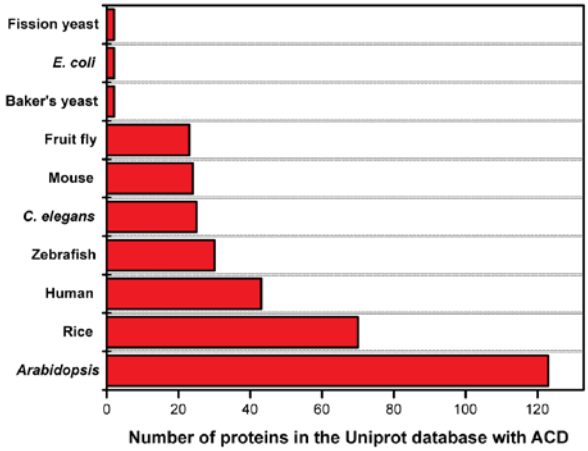

Figure 4: sHSPs are found across all taxa

44242 proteins, including 99 in viruses, 2239 in Archaea, 27814 in eubacteria, and 13756 in eukaryotes share the Alpha crystallin/Hsp20 domain (ACD) .

Small heat shock proteins (sHSP)

Among chaperones, the sHSP superfamily consists of widespread, not yet fully characterized, proteins of diverse sequences and sizes (Haslbeck et al., 2005) which are at the crossroads of protein folding and degradation pathways. Upon heat exposure, 12% of cytosolic proteins in cultured human cells (Mymrikov et al., 2017) and up to one-third of cytosolic proteins in yeast (*Saccharomyces cerevisiae*) (Haslbeck et al., 2004) become potential clients of sHSPs. This indicates the important role of sHSPs in the maintenance of proteome stability (Klaips et al., 2018, Richter et al., 2010). The sHSPs are ancient proteins, and the members of the sHSP family have been found throughout the biological kingdoms, including archaea and viruses (Jaenicke and Slingsby, 2001, Maaroufi and Tanguay, 2013). Although sequentially diverse, a common defining feature of the sHSP family is the presence of the “α-crystallin domain” (ACD), a highly conserved 80-100 residues long consensus sequence (de Jong et al., 1998), flanked by highly divergent N-terminal domain and C-terminal extension.

Based on the presence of the ACD, 44242 proteins were categorized into the Protein sequence analysis & classification database InterPro (ID IPR002068) as of Dec 2017. InterPro classifies known proteins into families and predicts the presence of domains using predictive models, called signatures. From this search, the increasing diversity in sHSPs with biological evolution becomes evident (Figure 4) (Kriehuber et al., 2010). There are 12 representative sHSPs found in *Drosophila melanogaster*, 18-20 in *Caenorhabditis*, up to 15 in vertebrates (10 in mammals and 13 in zebrafish (*Danio rerio*, synonym *Brachydanio rerio*), Table 1) and 19 in *Arabidopsis* (Aevermann and Waters, 2008, Morrow et al., 2004, Elicker and Hutson, 2007, Franck et al., 2004, Siddique et al., 2008, Maaroufi and Tanguay, 2013). In complex organisms, such as in vertebrates sHSPs can be expressed either ubiquitously or in organ-specific manner, depending on their physiological role. For example, in humans αA-crystallin (hspb4) is expressed almost exclusively in the eye lens, whereas αB-crystallin (hspb5) and Hsp27 (or

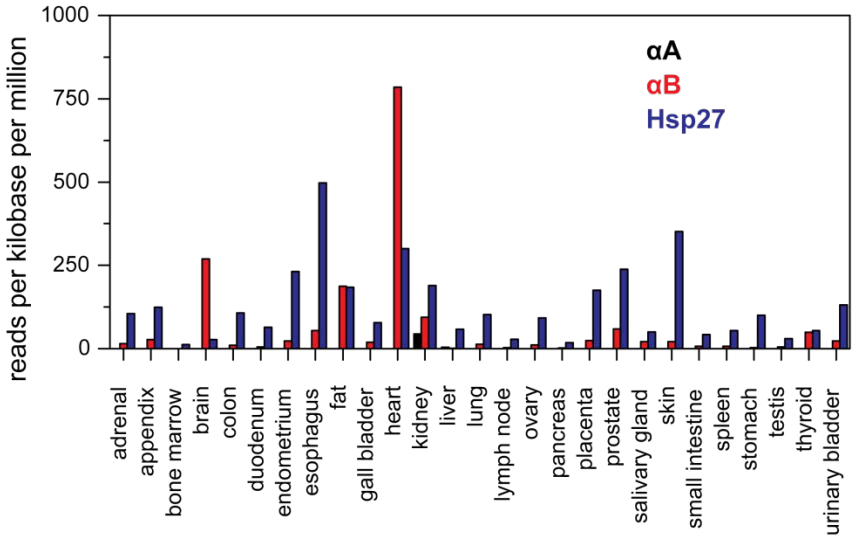

Figure 5: Prevalence of the major sHSPs in the human tissues

Based on query from the NCBI BioProject PRJEB4337 database of RNA-seq transcriptome or gene expression in 27 different tissues from 95 human individuals. (Fagerberg et al., 2014)

hspb1) are expressed nearly ubiquitously in low dosage but highly expressed in long-lived cells of muscle and brain (Figure 5). (Iwaki et al., 1989, Iwaki et al., 1990). This diversity in expression and in taxonomic representation might reflect specific roles for sHSPs to respond to increasingly complex demands of stress tolerance in diverse physiological conditions (Braun et al., 2011). However, unlike their large counterparts, the sHSPs seemed to have evolved independently in the main eukaryotic lineages, including animals, plants and fungi (Huang et al., 2008).

Table 1: Small heat shock proteins in vertebrates

Gene	Other names	Found in vertebrate taxa
hspb1	HSP27	Teleosts, amphibians, avians, mammals
hspb2	MKBP	Teleosts, amphibians, avians, mammals
hspb3		Teleosts, amphibians, avians, mammals
hspb4	αA-crystallin	Teleosts, amphibians, avians, mammals
hspb5	αB-crystallin	Teleosts (two in zebrafish), amphibians, avians, mammals
hspb6	HSP20, HSPB13	Teleosts, amphibians, avians, mammals
hspb7	cvHSP	Teleosts, amphibians, avians, mammals
hspb8	HSP22, E2IG1, H11	Teleosts, amphibians, avians, mammals
hspb9	HSPB14	Teleosts, mammals
hspb10	ODF1	Mammals
hspb11	HSP30	Teleosts, amphibians, avians
hspb12		Teleosts, chicken
hspb15		Teleosts

Based on references: (Franck et al., 2004, Kappe et al., 2003, Marvin et al., 2008, Elicker and Hutson, 2007)

The ACD**,** the evolutionarily conserved hallmark of the sHSP family, is a hydrophobic-residue rich, compact ß-sheet sandwich structure composed of two antiparallel layers of three and four ß-strands connected by a short inter-domain loop (Figure 6) (Kriehuber et al., 2010, Poulain et al., 2010, Berengian et al., 1997, Berengian et al., 1999). The minimal sHSP protomer consists of a dimer of ACDs, which can adopt two alternate dimer interfaces: a

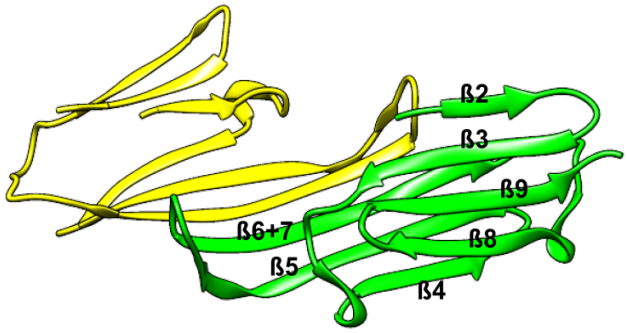

Figure 6: Structure of the ACD of αB Crystallin

Cartoon of crystal structure of excised alpha-crystallin domain (residues 67–157) dimer from human αB-crystallin, visualized from the PDB file 2WJ7 from (Bagneris et al., 2009)

metazoan 'ß7-interface' where the dimer interface is formed by the interaction of the anti-parallel ß6+7 strands of the two protomers, or a 'ß6-swapped' interface where dimerization occurs via reciprocal strand swapping of the ß6 strands into the ß-sandwich of the neighboring monomer (Strauch and Haslbeck, 2016, Bagneris et al., 2009, Basha et al., 2012, Stengel et al., 2010). The ACD is essential for the formation of dimers and higher-order assemblies *in vitro* (Sun and MacRae, 2005b, Sun and MacRae, 2005a, Bhattacharyya et al., 2006).

The N-terminal region of sHSPs flanking the ACD is highly variable in both the sequence and the length. It varies from 24 residues in *C. elegans* Hsp12.2 to 247 residues in *S. cerevisiae* Hsp42 (Haslbeck et al., 2005). The disordered and poorly conserved N-terminal region is hydrophobic and is suggested to be involved in substrate binding and in higher order oligomeric assembly (Clark, 2016, Jaya et al., 2009, McDonald et al., 2012). The C-terminal region, flexible and unstructured, shows sequence variability with a polar tendency. This region participates in stabilizing and solubilizing the oligomeric assemblies (Jaya et al., 2009, Van Montfort et al., 2002, Poulain et al., 2010). The N and C-terminal regions are thought to provide the

conformational flexibility at non-interfacial regions in the monomer, which can prevent co-assembly between highly homologous sHSPs (Hochberg et al., 2018).

While termed “small” due to their relatively smaller monomeric size, sHSPs form large and dynamic oligomeric assemblies of variable number of subunits (ranging from 9 to 50) (Haslbeck, 2002) (Figure 7). This oligomerization is essential to the role of sHSPs in substrate binding and consequent chaperone function. Among highly polydisperse mammalian sHSPs, such as α-Crystallins and Hsp27, upon heat-treatment or phosphorylation, the assemblies undergo a shift in the oligomeric equilibrium towards sHSP disassembly, which activates their

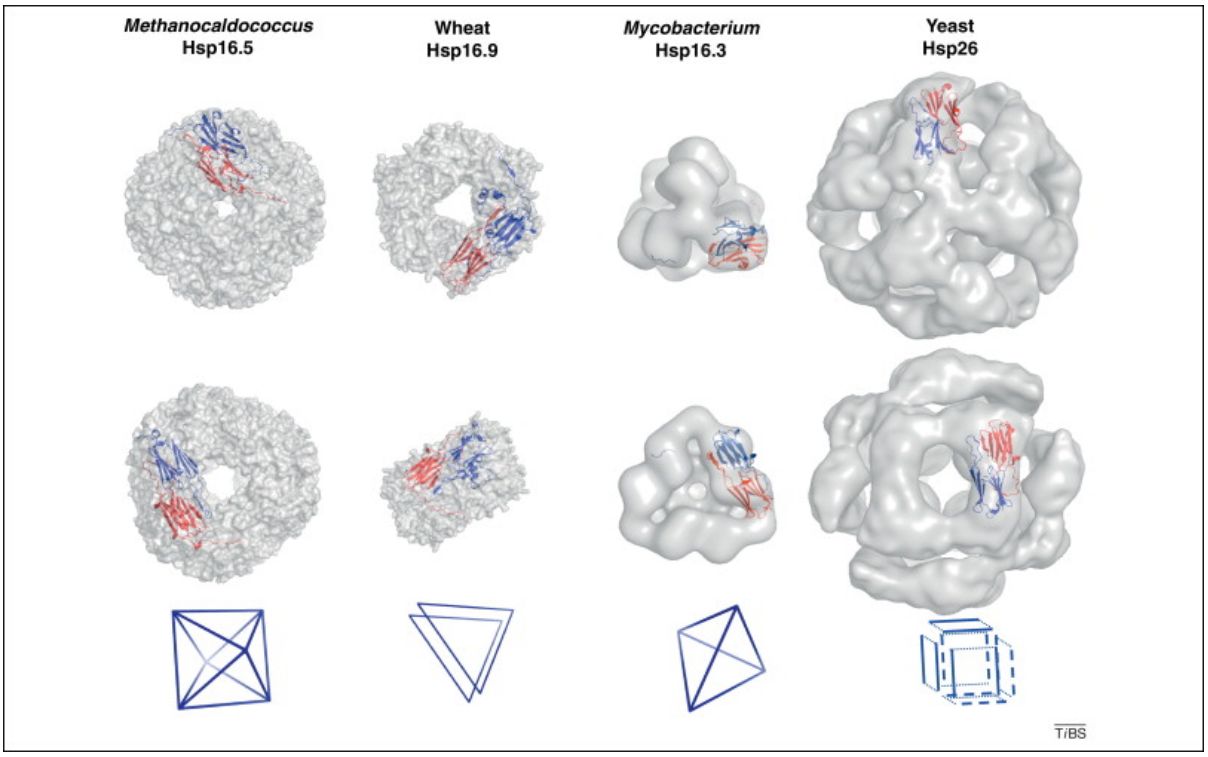

Figure 7: Molecular structures of some sHSPs at the atomic scale

Oligomeric structures derived from X-ray and EM data. Ribbon diagrams of a single dimer structure are superimposed on the surface representations, shown in two orientations rotated by 90°. The bottom row shows molecular symmetry of the molecules, with solid lines representing the location of one dimer; copied from (Basha et al., 2012)

chaperone-like activity *in vitro* (Shashidharamurthy et al., 2005, Mchaourab et al., 2005, Koteiche and McHaourab, 2006, Haslbeck and Vierling, 2015, Fleckenstein et al., 2015). Both, the rearrangement of sHSP oligomers through sub-oligomeric species or the increased rates of subunit exchange between the oligomeric ensembles can activate the sHSPs towards client proteins. The disassembly is thought to exposes the hydrophobic interior of the oligomeric shell, whereby functional binding sites are presented to the thermodynamically unstable client substrates. For homogenous oligomers of Archean and plant sHSPs, the activation of chaperone can be achieved through structural rearrangements without significant oligomeric dissociation (Giese and Vierling, 2002, Suzuki et al., 1998b).

Binding of substrate proteins by sHSP

As a prominent member of the PN, sHSPs are the first responders to a large array of physiological stresses (Haslbeck and Vierling, 2015). sHSPs respond to the stresses by both transcriptional activation and by biochemical mobilization. Among human sHSPs, Hsp27, αB-crystallin and Hsp22 are stress-inducible (Vos et al., 2010). Under heat shock conditions, a large number of cytosolic proteins associate with or are kept soluble by sHSPs. For example, all human sHSPs, except HspB7 suppressed the aggregation of cytosolic proteins of human embryonic kidney cells (HEK293) after heat stress. However, while HspB1/Hsp27, HspB3, HspB4/αA-crystallin, and HspB5/αB-crystallin bound the heat labile client proteins promiscuously, other sHSPs respond in more or less substrate-dependent manner (Mymrikov et al., 2017).

The ability of sHSPs to suppress temperature-dependent insolubilization of proteins or protection of enzyme activities reflects the chaperone activity of sHSPs. A general consensus is that instead of any defined sites on the client proteins, the sHSPs bind with thermodynamically

unstable early unfolding intermediates of aggregation-prone proteins (McHaourab et al., 2002) through hydrophobic interactions (Basha et al., 2012, Kim et al., 2013). The client proteins are bound tightly by sHSPs with binding capacity (*n*) reaching up to one substrate protein per sHSP monomer (McHaourab et al., 2009). Although, some sHSP-substrate complexes can be essentially irreversible, other sHSP-bound substrates can be released and subsequently refolded by the ATP-dependent Hsp70/Hsp40 chaperone system (Lee et al., 1997, Lee and Vierling, 2000). Thus sHSP as holdase create a reservoir of refoldable substrate (Ehrnsperger et al., 1997). In the event of extreme proteostatic challenge such as heat stress, sHSP provide an efficient, ATP-independent first line of defense against accumulation of aggregation prone unfolded proteins (Suss and Reichmann, 2015, Haslbeck and Vierling, 2015).

Since the first demonstration of α-crystallin as a molecular chaperone by suppressing thermally induced aggregation of various enzymes (Horwitz, 1992), variants of this convenient and experimentally simple method are frequently used to assay chaperone activity of sHSP (Basha et al., 2012). These methods typically involve denaturation of substrate proteins (by heat or by reduction of disulfide bonds) to form aggregates in the presence and absence of the test sHSP. The extent of aggregation is measured by light scattering, by pelleting the insoluble precipitate; or by assaying the residual enzyme activity. From the suppression of aggregation, the stoichiometry of sHSP that keeps the test protein soluble is empirically inferred as the chaperone efficiency (Jakob et al., 1993, Lee et al., 1997, Van Montfort et al., 2001a, Berengian et al., 1997, McHaourab et al., 1997).

However, the nonequilibrium conditions of these aggregation-based assays confound the experimental observable, light scattering, which reflects competition between the aggregated substrate and the substrate-chaperone complex. Furthermore, these assays subject proteins to conditions that promote aggregation by extreme destabilization of the native state

leading to a large positive ΔG_{unf}, as defined by the positive difference $G_U - G_F$, between the free energies of the unfolded (G_U) and the folded states (G_F). A positive ΔG_{unf} indicates that the unfolded state is highly favorable due to the conditions of the aggregation assays. However, mutations or post-translational modifications that can shift the folding equilibrium of proteins toward non-native states and potentiate them as clients of sHSP are often structurally similar with small difference in ΔG_{unf}. Moreover, sHSPs can detect the increased excursions of destabilized proteins toward aggregation-prone non-native states even under conditions that favor the native state in the absence of substrate aggregation (McHaourab et al., 2002). The denaturing conditions in the assays utilizing the aggregating proteins can promote the existence of heterogenous ensembles of bound substrates that differ in conformations. The conditions in these assays can also affect the structural and functional integrity of the sHSP and therefore can confound the chaperone activity by the aggregation regime of the substrate-chaperone complex.

Given these limitations of the traditional assay, an assay for equilibrium measurements of sHSP-substrate interactions has been developed utilizing lysozyme from phage T4 (T4L) (McHaourab et al., 2002). In this assay, the T4L mutants are labeled at a surface exposed mutant cysteine-151 with the fluorescent probe, monobromobimane, which reports complex formation (Sathish et al., 2003, Mishra et al., 2012). T4L is a well-established paradigm for studying the determinants of the structure and stability of proteins (Baase et al., 2010). T4L is particularly suited to elucidate the interactions with sHSP because of its relatively small size, absence of disulfides, and a two-state folding equilibrium over a wide range of temperatures, pH, and ionic strengths. With the availability of a large number of mutations with altered thermodynamic stability, which have been solved to atomic resolution, T4L makes an attractive model substrate to understand how sHSPs interact with substrates (Rennell et al., 1991,

Claxton et al., 2008, Sathish et al., 2003). In the modified chaperone efficiency assay, the complex formation of defined stoichiometry between sHSPs and T4L is followed fluorescently under conditions where T4L does not aggregate and the equilibrium population of its native state is exponentially higher than that of the ensemble of unfolded states. This assay of chaperone activity is thus more favorable than monitoring complex formation under conditions that induce substrate aggregation (Mulder et al., 2001). Also, using T4L-mutants which destabilize the native state with subtle gain in the free energy of unfolding (ΔG_{unf}) while still maintaining the native folds, is also physiologically more relevant (Claxton et al., 2008).

Using this fluorescence based assay, it has been shown that sHSPs act as "stability sensors" to detect unstable proteins even in the absence of stress, and the sHSPs bind unfolded states of proteins which are present only fleetingly (Shashidharamurthy et al., 2005, McHaourab et al., 2002, Koteiche and McHaourab, 2003). The affinity of binding of sHSPs including αA- and αB-crystallin, Hsp27, and Hsp16.5 to T4L destabilized mutants have been show to correlate with the T4L mutant's ΔG_{unf} , although the mutants were structurally indistinguishable (McHaourab et al., 2009). The sHSP/substrate complex forms when the free energy of binding to sHSP is similar to the free energy of transition of the substrate from theromodynamically metastable excited states to the stable native state (McHaourab et al., 2002). It has also been shown that the recognition and binding of substrate, in its non-native state, involves changes in the oligomeric state of sHSP and the substrate undergoes significant unfolding during the binding (Claxton et al., 2008). The assay has revealed that sHSPs bind the substrate in two distinct modes, each associated with the recognition of a different conformational state of the substrate. While the highly destabilized T4L is bound by sHSP in a low-affinity mode, where each sHSP subunit bound one T4L molecule; the marginally destabilized T4L was bound in a high-affinity mode – four sHSP subunits binding a monomer of

T4L (McHaourab et al., 2009, Koteiche and McHaourab, 2003, Sathish et al., 2003, Shashidharamurthy et al., 2005, Claxton et al., 2008).

The chaperone interactions between sHSPs and substrate can be described by a minimalistic model of three coupled equilibria: the folding equilibrium for the substrate (I), the equilibrium between the inactive and active states of the sHSP chaperone (II), and the formation of the substrate-chaperone complex equilibrium (III).

$$N \leftrightharpoons I_1 \leftrightharpoons \cdots \leftrightharpoons I_i \leftrightharpoons U \qquad \text{(I)}$$

$$sHSP \leftrightharpoons (sHSP)_{active} \qquad \text{(II)}$$

$$(sHSP) + \binom{I_i}{U} \leftrightharpoons \binom{C_i}{C_u} \qquad \text{(III)}$$

Equation (I) describes the equilibrium of the substrate in its native (N), partially folded intermediates ($I1$ ….Ii), and fully unfolded states (U). Equation (II) describes the transition of the sHSP to an active high affinity binding mode. Equation (III) couples the Equations (I) and (II) and describes the binding of the active sHSP to partially (I) or globally unfolded (U) states of the substrate to form the complex (C). The mutations and the chemical modifications that cause the recruitment of the sHSPs towards the substrate do so by shifting the equilibrium of Equation (I) towards high-energy non-native states of the substrate. In their non-native state, the energy gap of the states towards folding is much bigger than towards binding with sHSP, which provides the thermodynamic driver of the chaperone-substrate complex formation.

The activation of sHSP, either by disassembly or by expansion due to restructuring of the oligomeric ensemble can increase its affinity of binding the substrate, by shifting the equilibrium as described by the Equation (II). Sites on both the N-terminal and ACD have been shown to be involved in the substrate binding (Jaya et al., 2009). The substrate can access

these binding sites buried in the interior of the sHSP shell either dynamically through equilibrium dissociation, as in Hsp27 (McDonald et al., 2012); or by opening the outer shell through expansion, as in an engineered variant of Hsp16.5 (Shi et al., 2006a). Thus, increasing the access of the substrate to the binding sites by both the dynamic dissociation or by expansion can be possible mechanisms to activate the sHSPs.

Destabilizing changes, such as by mutations, by chemical modifications, or by structural changes due to systemic stress potentiates a large number of proteins to become substrate of sHSP (Nakamoto and Vigh, 2007, Kakkar et al., 2014). Similar modifications can cause sHSPs to also become pathologically activated where they can either indiscriminately bind proteins early on their $N \leftrightharpoons U$ equilibrium; or loose the chaperone activity and not respond optimally to the proteostatic demands (Macario et al., 2005, Macario and Conway de Macario, 2007, Gidalevitz et al., 2006, Koteiche and McHaourab, 2006). The outcome of both these scenarios can be pathological. Most importantly, accumulating destabilizing changes in both the chaperones and the substrates are common manifestations in the aging process (Kikis et al., 2010, Charmpilas et al., 2017).

Ageing is the non-homogeneous accumulation of biochemical and functional impairments (Michael and Bron, 2011, Higuchi-Sanabria et al., 2018). Cellular aging is characterized by the unmitigated accumulation of damaged and misfolded proteins through a functional decline in proteostatic machinery (Kikis et al., 2010). The inefficiency of PN with age leads to reduced cellular viability leading to development of protein misfolding diseases such as cataract, neurodegeneration, cardiovascular disease and even cancers (Lopez-Otin et al., 2013). Although genetic and auxiliary causes can expedite early onset of most of these diseases, the common risk factor remains aging which highlights that ageing most likely manifests either

through a decline in the cellular proteostasis capacity or through an increased demand on the PN to maintain the aging proteome (Erickson et al., 2006, Tower, 2011).

Unique Challenge of Proteostasis in Long Living Cells

Of the estimated total of 3.72×10^{13} cells in the human body, many undergo frequent mitotic cell division so they are continuously replaced and are thus much younger than the organism (Bianconi et al., 2013, Spalding et al., 2005a, Seim et al., 2016). While cells such as monocytes live for just about 2 days (Seim et al., 2016), cells of skin or intestine, exposed to harsh environments are also very short lived. For example, the intestinal epithelial cells have an average life of about 5 days, the average age of the non-epithelial cells or skeletal muscle could be only 15.1-15.9 years for individuals 37 and 38 years old and approximately 10% of fat cells are renewed annually (Spalding et al., 2005a, Marshman et al., 2002, Spalding et al., 2008). However, post mitotic cells such as cortical neurons, heart myocytes and eye lens fiber cells live for the life of the individual (Spalding et al., 2005b, Spalding et al., 2005a, Lynnerup et al., 2008, Senyo et al., 2013, Bergmann et al., 2009, Seim et al., 2016).

The demand on the PN for such long-living post mitotic cells is extremely critical because such cells cannot dilute their accumulated “cellular garbage” or “clinker” by mitosis (Bernhard and Laufer, 2008, Stroikin et al., 2005, Hirsch, 1978). In actively dividing cells, accumulated metabolic by-products and aggregated dysfunctional proteins get offloaded by polarized asymmetric inheritance between the daughter cells, where one of the daughter cells becomes free of the maternal “garbage” while the other sister cell carrying the proteostatic baggage is marked for apoptosis (Rujano et al., 2006, Aguilaniu et al., 2003, Stewart et al., 2005). Retention of long-lived asymmetrically retained proteins (LARPs) during cell division contributes to the aging in budding yeast (*S. cerevisiae*) by accumulating posttranslational modifications

(Thayer et al., 2014). Thus, it is remarkable that the long living cells such as lens fiber cells and cardiac myocytes can protect themselves against aging for as long as possible by evolving a very efficient proteostatic system.

The lens as a model system to study proteostatic collapse

The eye lens is so unlike any other biological object, that Democritus considered it to be a postmortem artefact (Owens, 2000, Wade, 1998). But a transparent lens is an evolutionary ancient organ, and is common to most vertebrate and invertebrate eyes (Lamb et al., 2007, Ogura et al., 2013). The eye is an organ that produces image by comparing the multidirectional light intensities, through photoreceptors in multiple spatial orientations. Thus, while an eye can be a simple camera eye as in box jellyfish, a compound eye as in insects and mollusks; or the complex camera eyes of cephalopods and humans (Nilsson, 2009); they all rely on a crystalline lens for forming the vision (Schwab et al., 2012, Jonasova and Kozmik, 2008).

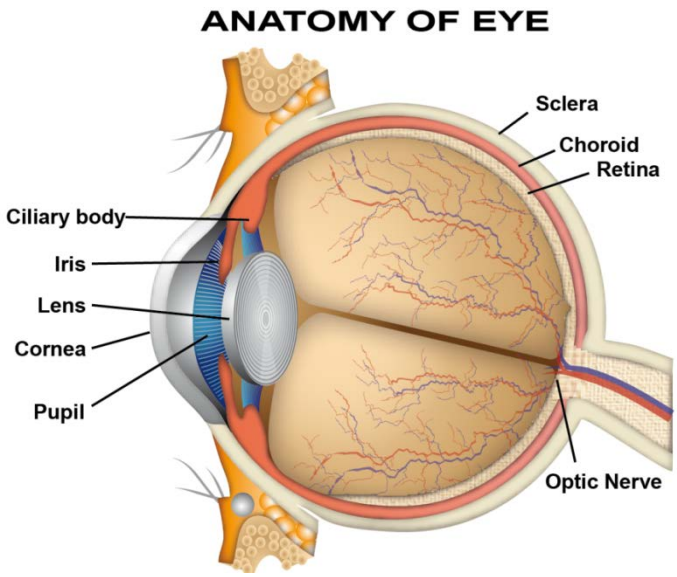

Figure 8: Schematic illustration of the anatomy of the human eye

The human eye (Figure 8) uses a cellular lens to focus images onto the light sensitive retina membrane lining the inside of the eyeball (Land, 2005, Treisman, 2004). Two concentric spheres -- a transparent **cornea**, and the opaque **sclera** fuse together to make the outermost coat of the eyeball (Davson and Perkins, 2017). A pigmented muscular diaphragm, called the **iris** controls the amount of light that passes through the **pupil** which functions as an aperture. Behind the pupil, the crystalline **lens**, suspended through ligaments, delineates the external **aqueous humor** from the internal **vitreous body**. Cornea, aqueous humor, lens, and vitreous body are the optically clear part of the eye. The iris, ciliary body, and choroid make the intermediate tunic and provide the main blood supply to the eye. The innermost layer of the eye is the photoreceptor layer called the **retina**, which is innervated by the **optic nerve** to carry the visual stimuli to the brain.

The purpose of the eye lens is to project a focused, undistorted image of the visual surroundings onto the neural retina (Bassnett et al., 2011). Several structural and biochemical adaptations serve to minimize light scatter and enable the lens as living, cellular structure to function as the biological glass (Slingsby et al., 2013, Wistow, 1993). Foremost, the lens attains transparency by the programmed elimination of nuclei and other light-scattering organelles from fiber cells. Further, the scattering at the cell borders is minimized by the close apposition of lens fiber cells by lens-exclusive adhesive proteins.

To focus light, a lens must also have a refractive index higher than the surrounding medium. In vertebrates, the tear film-cornea interface and the crystalline lens are the major refractive components in the eye and act together as a compound lens to project an inverted image onto the light sensitive retina. (Fuensanta and Doble, 2012) The high refractive index of the lens cells is achieved by accumulating very high concentrations (>300mg/mL) of soluble

structural proteins called crystallins: α, β, and γ, which can account up to 90% of the total lens proteins (Carlson, 2014, Graw, 2004).

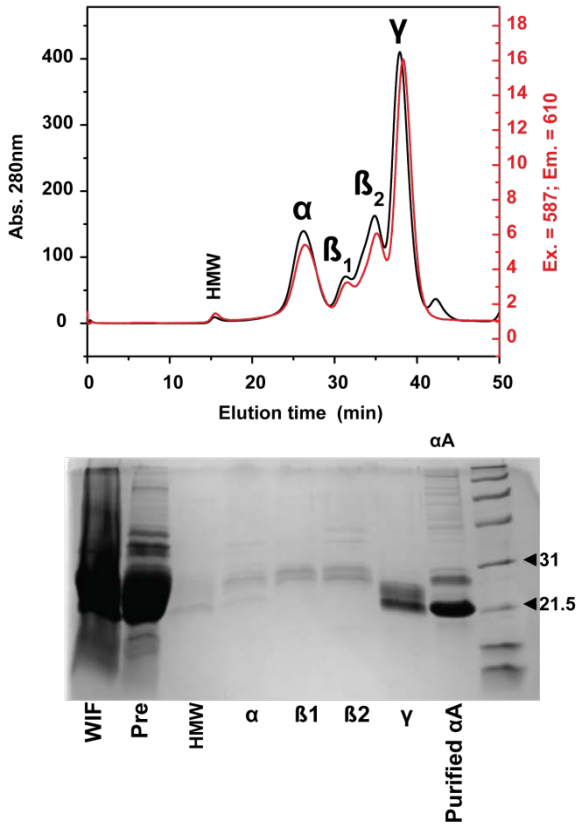

Figure 9: Protein profile of the zebrafish lens

Top panel: Size Exclusion Chromatography of the lens homogenate from 3 month old adult lens (black trace) and 10 day old embryo (red trace). Bottom panel: SDS-PAGE of the proteins separated by the SEC. (WIF: Water insoluble fraction, Pre: proteins before centrifugation to clear the homogenate). Equal volumes of the proteins were run on the SDS-PAGE, and were not normalized for concentrations.

Of the crystallins, α-Crystallins are generally the major component of the vertebrate lens and can account for about half of the total protein in most species (Augusteyn, 2004, Thomson and Augusteyn, 1985). In humans, the proportion of α-crystallins in the lens increases from

37.4% (at 26 weeks prior to birth) to 42.6% (after 52 weeks from birth) of the total lens protein (Thomson and Augusteyn, 1985). In contrast, the α-crystallins comprised less than 1% of total lens protein in zebrafish lens extract (Figure 9) at 4.5-day and only increased to ~7% in the adult lenses (Posner et al., 2011, Wages et al., 2013).

Among α-crystallins, αA is expressed almost exclusive in the lens cells in mammals and zebrafish, with low levels detected in some non-lenticular tissues such as in the spleen and pancreas (Srinivasan et al., 1992, Deng et al., 2010, Posner et al., 2002, Runkle et al., 2002). On the other hand, αB-crystallin is expressed ubiquitously throughout the eye (retinal pigment epithelium, optic nerve, extraocular muscle, iris, ciliary body, cornea), and several non-ocular sites, such as heart and nasal epithelium (Figure 23) (Robinson and Overbeek, 1996). In mouse, αB crystallin transcription precedes αA transcription, and at birth the expression patterns of αA- and αB-crystallins are similar in lens. Subsequently, αA expression is upregulated exclusively in fiber cells while αB is downregulated in fiber cells but continued everywhere else (Robinson and Overbeek, 1996). In zebrafish, the αA-crystallin transcript can be detected at 12 hours post fertilization (hpf); while αB transcripts were detected 24hpf onward (Marvin et al., 2008, Elicker et al., 2007, Elicker and Hutson, 2007, Zou et al., 2015, Wages et al., 2013, Posner et al., 2011, Dahlman et al., 2005, Runkle et al., 2001, Posner et al., 1999). Importantly, both zebrafish and humans express αA to αB in similar ratios of ~3:1 in the adult lens despite different overall concentrations of α-crystallins (Wages et al., 2013, Posner et al., 2011, Ma et al., 1998). Interestingly, αB-crystallin is the most abundant crystallin found in the lens epithelium (Cvekl and Duncan, 2007, Wang et al., 2004).

Paradoxically, such high protein concentrations of proteins in lens, approaching a paracrystalline state (Piatigorsky, 1993, Sun et al., 1984), should cause very high light scattering. But probably light scattering is virtually eliminated through destructive interference

due to short-range-order interactions between crystallins (Delaye and Tardieu, 1983, Trokel, 1962, Benedek, 1971). Using Small-angle X-ray scattering on intact calf lens and on crystallin solutions (3-510 mg/ml), it has been shown that because of their high concentration, crystallins do not behave as independent scatterers (Delaye and Tardieu, 1983). But even a minor disruption in this ordered arrangement due to fluctuations in density on spatial scales longer than approximately half the wavelength of incident light can render the lens cloudy or opaque (Benedek, 1971). Venus' flower basket (*Euplectella aspergillum*) can achieve a similar glass-like transparency due to distinctive layered design of biosilica fibers, which vary refractive index in a non-uniform profile with a high-index core and a low-index cladding (Aizenberg et al., 2004). The lens proteome has also evolved possibly to match the refractive index between lens membranes and cytosol to minimize scatter (Slingsby et al., 2013).

An important premise of the model of lens transparency by short-range spatial order, as in dense liquids or glasses, is that the size and shape of the scattering particle are globular with an average molecular weight of 557,000 ± 40,000. The α-crystallins, by virtue of their large oligomeric sizes, are thus best suited to provide transparency of the lens (Delaye and Tardieu, 1983). They are also among the oldest proteins in the body, as established by radiocarbon dating studies which compared the ^{14}C content of the lens crystallins at the center of the lens to the so-called “bomb pulse” (*i.e.* a significant increase in the atmospheric ^{14}C content due to nuclear-bomb testing) (Lynnerup et al., 2008, Vries, 1958). For long living vertebrates such as the Greenland shark (*Somniosus microcephalus*) and the bowhead whales (*Balaena mysticetus*) where life expectancy can range in centuries, the lifelong proteostatic demand to maintain lens crystallins is astounding (George et al., 1999, Nielsen et al., 2016). The age of the Greenland shark and conversely the age of the nuclear crystallins have been measured to be 392 ± 120 years (Nielsen et al., 2016). Interestingly, in bowhead whales which live to over 200

years of age, none have been found to have obvious cataracts (George et al., 1999, Borchman et al., 2017).

Faced with low turnover of its proteins and a life-long oxidative and radiation challenge, optical clarity of the lens is thought to be maintained through protein homeostasis mostly through α-crystallins as the sHSP. But the very high concentration of crystallins in the lens poses its own unique challenge to the lenticular PN (Ellis, 2001, Zhao et al., 2011b). Macromolecular crowding is expected to promote aggregation of non-native protein chains substantially by increasing their effective concentrations, necessitating molecular chaperones as essential in maintaining proteins folded under crowded conditions of lens (van den Berg et al., 1999, Tokuriki et al., 2004, Ellis, 2001).

Despite of the presence of an efficient PN, visual impairment and blindness (VI&B) due mostly to the old age causes considerable and increasing economic burden (Baltussen et al., 2004, A et al., 2016). Globally, the burden of VI&B, as measured by disability adjusted life years (DALYs), increased by 47% from 1990-2010 (Koberlein et al., 2013). In fact, it is difficult to estimate the net economic cost of the VI&B because the indirect costs are much higher than the direct costs due to reduced mobility and ability to work. According to World Health Organization (WHO) and International Federation on Aging, in developing countries 94 million older people suffer from moderate to severe visual impairment, twice as many as those who have significant hearing impairment, which is the second leading cause of old-age disability according to United Nations Population Fund (2012).

Cataract – a global disease

According to the WHO, “A cataract is clouding of the lens of the eye, which impedes the passage of light.” In 2010, cataract was responsible for more than half of all global blindness affecting about 20 million people (Khairallah et al., 2015) . Although rarer in the industrialized world, in the poorer South and South East Asia, cataract blinds more than 40% of the population (Foster and Resnikoff, 2005) .

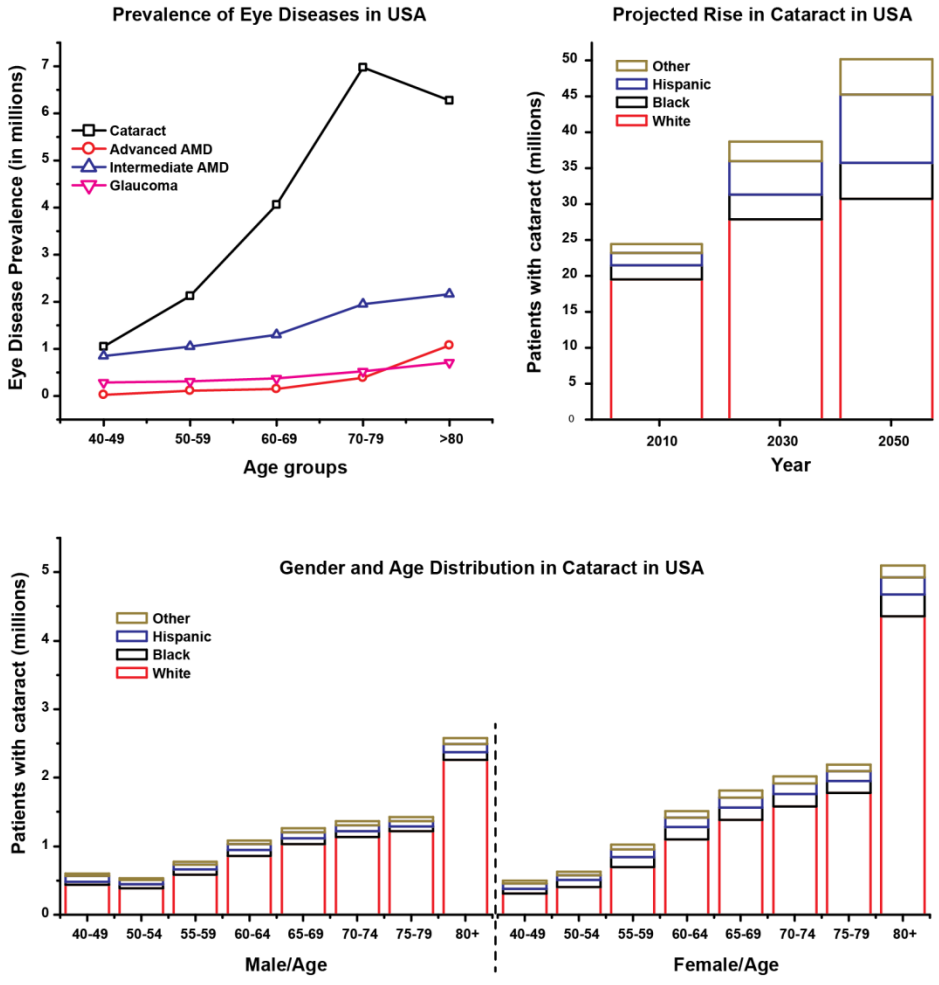

Figure 10: Burden of cataract in the USA

(Based on the data from the CDC until 2010 for which the latest figures were available)

The risk of cataract increases with each decade of life, starting around age 40 (Figure 10). In the USA, 70 percent of white Americans, 53 percent of blacks and 61 percent of Hispanic Americans develop cataract by age 80 according to the National Eye Institute (NEI). As the global life expectancy grows, the number of people suffering with cataract will also grow. In the US alone, the number of cataract cases rose by about 20 percent, from 20.5 million to 24.4 million between the years 2000 to 2010 (Figure 10). These numbers are expected to double to about 50 million by the end of 2050. It is estimated that globally, the number of people blinded by cataract is increasing by approximately 1 million per year.

By just providing cataract surgery to 95% of those who need it would avert over 3.5 million DALYs per year globally (Baltussen et al., 2004). However, while cataracts are easy to surgically remove, patients' access to surgery is often limited in poorer countries resulting in potentially blinding lifelong disability. Even in the U.S., Hispanic Americans are expected to have the most rapid increase in the prevalence of cataract from current 1.76 million cases to

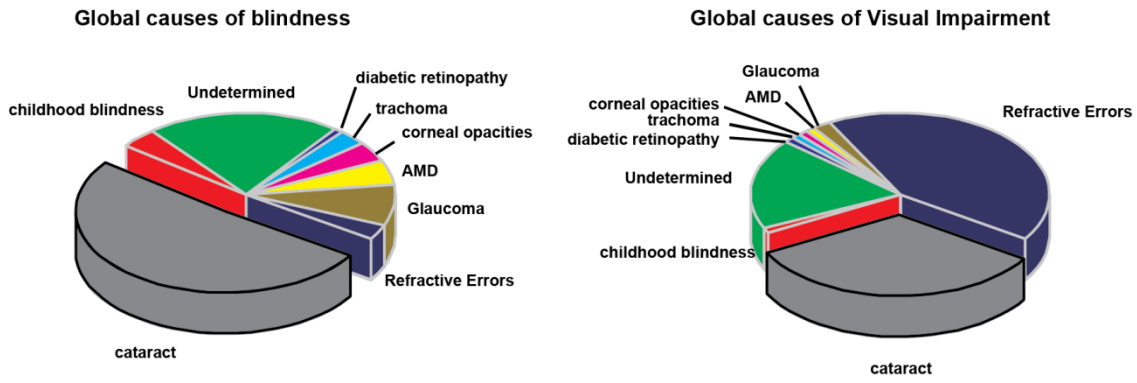

Figure 11: Cataract is the major cause of global blindness

(Plotted based on the data from the WHO, until 2010 for which the most updated figures were available)

9.51 million by 2050 (Figure 10). Undiagnosed and uncorrected cases of cataract cause about a third of all cases of visual impairments in both developed and developing countries. In fact, despite increased access to surgical procedures, cataract is the first cause of blindness followed by uncorrected refractive error and macular degeneration (Figure 11) (Khairallah et al., 2015).

There are three main types of age-related cataracts defined by clinical appearance: nuclear, cortical, and posterior subcapsular (Asbell et al., 2005).

Nuclear cataract: This is the most common type of age-related cataract. As the lens ages, new layers of fibers are added compressing the lens nucleus (the central portion of the lens). The aging nucleus becomes harder (nuclear sclerosis cataract) and gradually turns yellow, due mostly to an increase in lens thickness but also due to accumulation of a yellow pigment (Mc, 1959), deposition of more absorbing (or scattering) lens constituents (Mellerio, 1987), or due to photo-oxidation of the aromatic amino acids of the lenticular proteins (Pescosolido et al., 2016, Moffat et al., 1999).

Cortical cataract: The cortex of the lens (peripheral edge of the lens) is made of the newest lens fibers. New fibers are regularly added to the outside of the lens under the outer coating or capsule of the lens. With ageing, opaque “cortical spokes” can develop within the cortex of the lens causing loss of transparency in the lens.

Posterior subcapsular cataract: These cataracts are granular opacities occurring mainly in the central posterior cortex just under the posterior capsule. They are called "subcapsular" because the opacity forms beneath the lens capsule that encloses the lens and holds it in place. Posterior subcapsular cataracts (PSC) are generally associated with exposure to toxic agents, posterior intraocular disease, ionizing radiation, or blunt trauma. Long term exposure to steroids are a known risk factor for development of PSC (Black et al., 1960).

While mostly an age related disorder, cataract also affects many children worldwide and it causes more visual disability than any other form of treatable blindness. More than 200,000 children suffer from complications related with cataract accounting for 10-30% of childhood blindness (Gogate et al., 2011). While increased Vitamin A supplementation has helped reduce the number of children going blind due to corneal scars, an increasing number of children (35%) now go blind from congenital cataract (Gogate et al., 2009). It is estimated that the prevalence of childhood cataract is 10 times higher in low-income economies compared to high-income economies (Foster et al., 1997). Using the median incidence of 1.69 per 10,000 cases translates to around 314,000 new childhood cataract (both congenital and developmental) cases every year (Sheeladevi et al., 2016).

Development of the mammalian lens

The overall morphology of all vertebrate eyes, including the lens, is highly conserved across the kingdom despite important distinctions between taxa (Schwab et al., 2012, Parker, 2004). The development of the vertebrate eye begins very early in the embryo development and a single continuous eye field begins to take shape as early as the late gastrulation (Gilbert, 2003). All cellular lenses share the characteristic elongation of cells as a common ontogenic and phylogenetic feature. In some vertebrates a tiny parietal or median eye, equivalent to the mammalian pineal, consists of a lens which is made of just a monolayer of elongated cells (Chow and Lang, 2001). These primitive lenses might represent the evolutionary beginning of the more modern vertebrate lenses because they morphologically resemble the lens placode (Ung and Molteno, 2004).

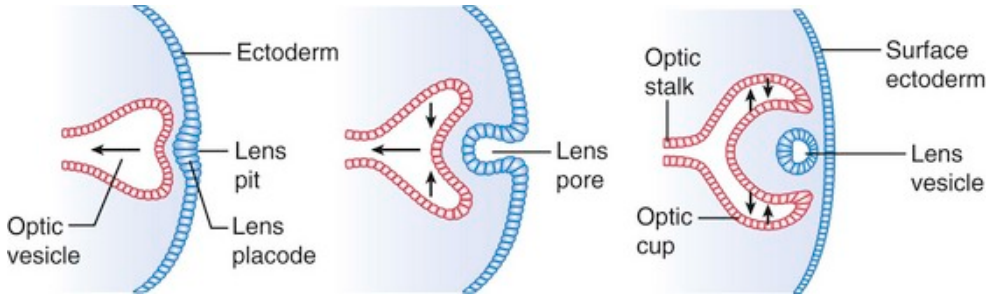

Figure 12: Early development of the embryonic human eye lens

Schematic of the anterolateral evagination of the forebrain leading to the formation of optic vesicle, while the basement membrane of the surface ectoderm forms the lens vesicle (Image taken from ClinicalGate iKnowledge webpage)

In humans, the lens forms during the 5th week of gestation (Figure 12) (Chow and Lang, 2001). In mammals the elongated lens progenitor cells develop from an epithelial monolayer over the presumptive retina, which thickens into columnar cells called the lens placode (Wistow, 1993). The optic pit in the eye primordium grows towards the surface ectoderm with which it finally coalesces. The optic vesicle underlying the pit becomes the presumptive retina and the ectodermal cells thicken and elongate to form the lens placode. In mice, αB-crystallin expression is the hallmark of lens placode formation (Robinson and Overbeek, 1996). In mouse, transcripts of αA-crystallin were first observed at the lens cup stage (Robinson and Overbeek, 1996). The localized thickening and elongation of the lens placode cells form the lens pit. The lens pit fills the space created by the invagination of the optic vesicle as it transforms into optic cup. The lens pit continues to deepen and finally detaches from the ectoderm to form a hollow lens vesicle. Upon separation of the lens vesicle, the cells at the posterior pole elongate, exit mitosis, and differentiate as primary lens fibers (Figure 13). The cells at the anterior pole remain mitotically active and form the epithelium. Elongating fiber cells encroach on the vesicle lumen and eventually contact the anterior-most epithelial cells, which establishes an anterior–

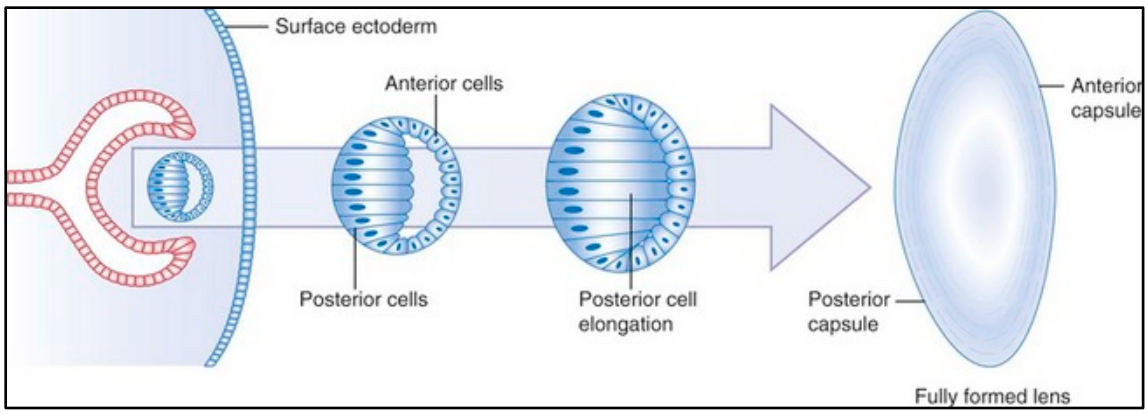

Figure 13: Differentiation of lens fiber cells

Posterior epithelial cells of lens vesicle elongate and migrate to form primary lens fibers, which fill the core to form the nucleus of the lens. The anterior cells migrate toward equator and proliferate to form secondary lens fibers to encase the nucleus.(Image taken from ClinicalGate iKnowledge webpage)

posterior (A–P) boundary. Once this polarity is established, secondary lens fiber differentiation initiates.

The lens epithelium contains stem/progenitor-like cells, which are the source of future fiber cells (Cvekl and Ashery-Padan, 2014). These stem cells allow the lens to grow throughout life and to match the size of a growing eye as new fiber cells overlay the old (Wistow, 1993). The lens epithelium provides support to the fiber cell compartments through its connection with the aqueous humor, which fills the anterior chamber of the eye. The human lens grows rapidly in the embryo and during the first postnatal year, after which it continues to grow at a much slower, nearly linear rate, throughout life (Figure 14). Because the epithelial basement membrane (lens capsule) completely encloses the lens, desquamation of aging cells is impossible, and due to the complete absence of blood vessels or transport of metabolites in this area, there is no subsequent remodeling of these fibers, nor removal of degraded lens fibers (Lynnerup et al., 2008).

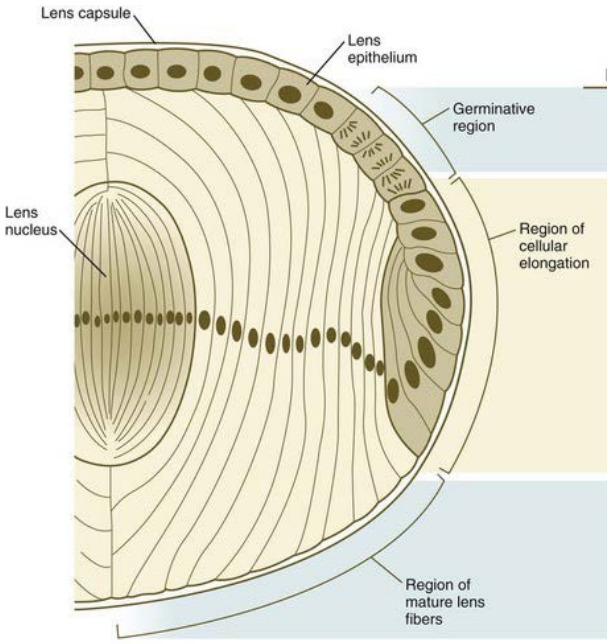

Figure 14: Organization of the adult vertebrate eye lens

As the lens grows, the epithelial cells from the germinative region stop dividing, elongate, and differentiate into lens fiber cells which produce high concentrations of lens crystallin proteins. The newly laid down fiber cells constitute the cortex region; the fiber cells laid down during the early growth period of the lens compose the nucleus region of the adult lens (Image taken from ClinicalGate iKnowledge webpage, modified from (Papaconstantinou, 1967)

Development of lens is controlled by several transcription factors, among which Paired Box 6 (PAX6) plays a most prominent role throughout early eye development and in later development of the retina and lens (Washington et al., 2009). Dominantly inherited mutations or deletions of the PAX6 cause aniridia, characterized by absence of an iris accompanying keratopathy, cataract and glaucoma (Glaser et al., 1994, Risley, 1915). Genes that are activated by *PAX6* in fruit fly -- *Eya* (eyes absent) and *Six* are expressed in humans suggesting that despite major differences in the structure and development of the vertebrate and insect eye, the

basic genetic apparatus remains conserved throughout phylogeny and PAX6 is a master regulatory gene throughout the metazoan (Halder et al., 1995).

PAX6 also plays important role in regulating the activity of the lens crystallin genes (Cvekl et al., 2017, Cvekl and Ashery-Padan, 2014, Ninkovic et al., 2010, Cvekl and Duncan, 2007). Multiple Pax6-binding sites were identified in the lens-specific promoter of the mouse αA-crystallin gene and the high expression of αA-crystallin could be under transcriptional regulation of PAX6 (Yang and Cvekl, 2005, Sax et al., 1997). Genetic ablation of PAX6 by *Cre-Lox* recombination in mice downregulated αA-crystallin expression (Ninkovic et al., 2010). The transcriptional regulator *Foxe-3* operating downstream of *Pax-6* facilitates the breaking off of the lens vesicle from the surface ectoderm and the transformation of posterior cells into lens fibers. Another transcription factor, Pituitary homeobox 3 (PITX3) directly regulates Foxe3 during early lens development (Ahmad et al., 2013, Medina-Martinez et al., 2009). Under the influence of *Sox-2*, *Pax-6*, and the oncogene *Maf*, the lens epithelial cells transform into lens fiber cells (Carlson, 2014). PITX3 maintains the mitotic activity of lens epithelial cells, fiber cell differentiation and activation of fiber cell-specific crystallins (Shi et al., 2006b, Ho et al., 2009).

Development of the zebrafish lens

Zebrafish, a fresh water fish native to the flood plains of India, has laterally placed eyes and lenses that protrude from the eye ball with no restriction from the iris. As a vertebrate, zebrafish shows nearly all the morphological hallmarks that characterize lenses of other vertebrates (Figure 15 and Figure 17), with two cell types-lens epithelial cells and lens fiber cells. Although zebrafish lens is relatively large and spherical, compared to mammalian and avian lenses which are more ellipsoid in shape (Fadool and Dowling, 2008, Gestri et al., 2012, Soules and Link, 2005).

Due to fast, extracorporeal development, relatively large sized eyes, and mostly transparent embryos, zebrafish offer several advantages as a model system to study the ocular physiology and lens proteostasis (Richardson et al., 2017). In fact, starting at 3 days post-fertilization (dpf), the panoramic visual system of the zebrafish becomes functional as assessed

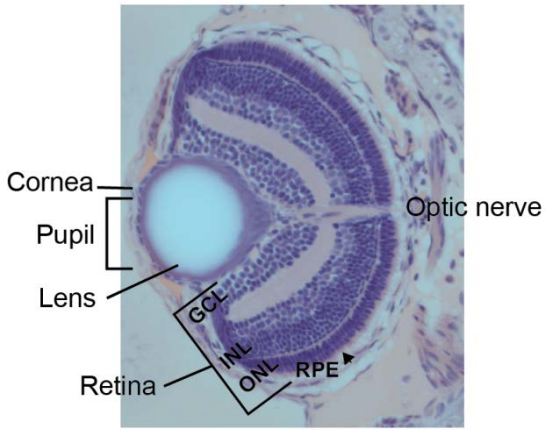

Figure 15: Histology of the embryonic zebrafish eye.

Coronal section shows the vertebrate typical layering in larval zebrafish eye: ONL, outer nuclear layer; INL, inner nuclear layer; GLC, ganglion cell layer; ON, optic nerve; RPE, retinal pigment epithelium; 5dpf embryos were fixed, dehydrated in ethanol series, embedded in JB-4 resin and 4µm sections were stained with H&E as described in (Zou et al., 2015).

by behavioral tests, such as optokinetic reflex/response (OKR) or optically evoked startle response; and by physiological tests such as Electroretinograms (ERGs) (Easter and Nicola, 1995, Easter and Nicola, 1996, Page-McCaw et al., 2004, Fleisch and Neuhauss, 2006).

Zebrafish eyes become apparent as a flattened evagination between 11-12 hpf (Dahm, 1999, Dahm et al., 2007, Greiling et al., 2010, Gestri et al., 2012, Soules and Link, 2005). As in all vertebrates, the formation of lens placode of zebrafish is induced from the ectoderm (Fadool and Dowling, 2008). The characteristic accumulation of melanin granules marking the retinal pigment epithelium becomes evident by 1dpf (Schmitt and Dowling, 1994, Dahm et al., 2007).

By the end of the first day of embryonic development, zebrafish eyes develop as a cup-shaped, bi-layered retinal anlage enclosing the prospective lens. However, the zebrafish lens delaminates from the surface ectoderm as a solid cluster of cells, like that of taxonomically closer *Xenopus*, rather than through invagination and formation of a hollow lens vesicle as in

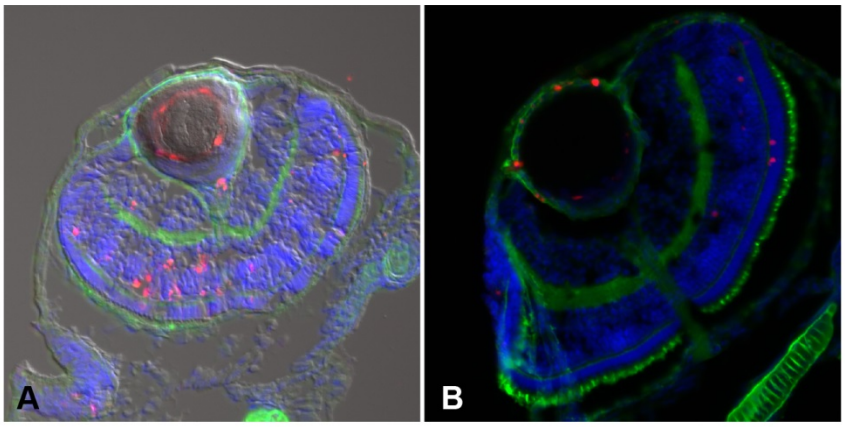

Figure 16: Denucleation at the fiber cell maturation zone

Breakdown of nuclei occurs at the lens periphery where lens fibers mature, producing double stranded DNA which stains positive for terminal deoxynucleotidyl transferase dUTP nick end labeling (TUNEL). 3dpf embryos were fixed in 4% PFA, embedded in OCT, cryosectioned and stained with TUNEL kit (Roche). (A) white field DIC overlaid with TUNEL activity in red, nuclei stained with DAPI (4',6-diamidino-2-phenylindole) in blue, and type II collagen in green. (B) Fluorescence image.

birds and mammals, and the detachment of the prospective lens is facilitated by apoptosis (Dahm et al., 2007, Schmitt and Dowling, 1994, Soules and Link, 2005).

The outermost cells in the equatorial region of this cluster become mitotically active beginning at 21 hpf and form a monolayer of epithelial cells. Like other vertebrates, the anterior lens epithelium proliferates, giving rise to elongating cells that differentiate into the crystalline fiber cells at the lens core. But in contrast to other vertebrate species, the epithelial layer does not end close to the lens' equator, but extends much farther towards the posterior pole. After the formation of a monolayer of lens epithelial cells, the differentiation and elongation of secondary lens fibers leads to a final lens that looks morphologically similar to that of other vertebrate species (Greiling et al., 2010). But in zebrafish, the primary fiber cells elongate in a circular fashion resulting in an embryonic lens nucleus with concentric shells of fibers (Dahm et al., 2007).

Between 2.5 and 3 dpf, the lens grows through the addition of secondary lens fiber cells (Dahm et al., 2007). As in other vertebrates, secondary fiber cell differentiation proceeds throughout life via pyknosis - the programmed degradation of nuclei and the intercalation of adjacent fibers via protrusions at the fiber cells' edges (Figure 16). This adds progressive layers of fiber cells around the lens nucleus. However, unlike mammalian or avian lenses the zebrafish secondary fibers differentiate in a narrow zone close to the equatorial epithelium (Dahm et al., 2007, Greiling et al., 2010).

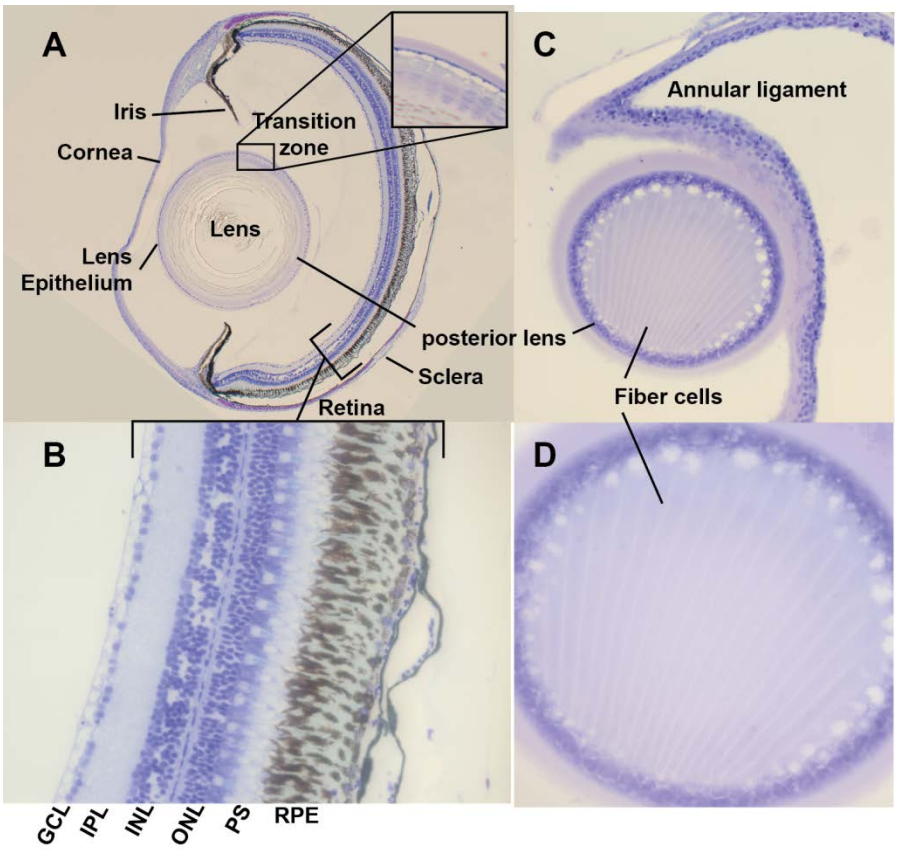

Figure 17: Histology of the adult zebrafish eye

Toluidine blue stained radial section of adult zebrafish eye shows morphological similarity with other vertebrates. (A) Zebrafish lens is more spherical but in transition zone (shown in subset) outer epithelial layer cover elongating fiber cells. (B) The retinal layers: RPE, retinal pigmented epithelium; PS, photoreceptor segment; ONL, outer nuclear layer; INL, inner nuclear layer; IPL, inner plexiform layer; GCL, ganglion cell layer; (C) the annular ligament of zebrafish is equivalent to the mammalian trabecular meshwork (C&D): cells from the posterior lens vesicle elongate to form lens fiber cells.

Eyes excised from 3 month zebrafish were fixed, dehydrated in ethanol series, embedded in JB-4 resin and 4µm sections were stained with Toluidine blue.

The adult zebrafish lens has the typical vertebrate morphology (Figure 17). It is enclosed by a lens capsule and its anterior surface is covered by a monolayer of epithelial cells. The mature zebrafish lens consists of a nuclear region and a cortical region encompassing a compact

accumulation of concentric circles of secondary lens fibers (Dahm et al., 2007). Lenses in the eyes of aquatic animals generally provide more optical power than those in terrestrial animals because the power of the cornea is significantly reduced in water (Pierscionek and Regini, 2012). Accordingly, fish cornea, in direct contact with the optically dense water medium provides little refractive power and fishes form a dense, spherical lens with a steep gradient of refractive index that provides focusing power while minimizing spherical aberration (Slingsby et al., 2013, Pierscionek and Regini, 2012).

Differences between zebrafish and mammalian lens development

While the zebrafish lens (Figure 15 and Figure 17) is similar in the development and final

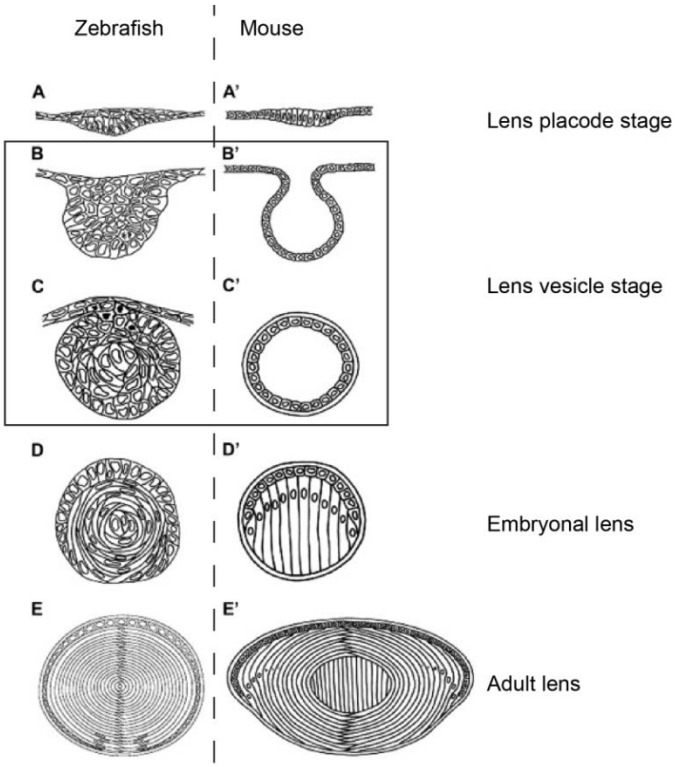

Figure 18: Schematic drawing of zebrafish and mouse eye lens

Comparative embryonic development of zebrafish (A–E) and mammalian (A'–E') lenses as well as their adult morphologies. (Modified from (Dahm et al., 2007)

morphology to vertebrate lenses (Figure 8), there are also several significant differences between zebrafish and mammalian lenses (Figure 18), at some developmental stages, as described below:

Lens placode stage: Both lenses begin as a lens placode (A, A′).

Lens vesicle stage: The zebrafish lens placode delaminates as a solid cluster of lenticular cells without obvious organization (B and C) and does not form a lens vesicle. In other vertebrates, invagination of the surface ectoderm (B′) leads to separation of the fluid-filled lens vesicle (C′).

Embryonic lens: In zebrafish, the primary fiber cells elongate in a circular fashion resulting in an embryonic lens nucleus with concentric shells of fibers (D), but in mammals the elongation of the posterior epithelial cells fills up the lens vesicle (D′) which establishes the anteroposterior elongated cells that make the embryonic nucleus of the adult mammalian lens.

Secondary fiber cells: Secondary fibers are formed by the proliferation and elongation of the differentiating lens fibers in both the zebrafish and mammals (E and E′). But in zebrafish, the secondary lens fiber cell differentiation is spatially restricted to a narrow zone close to the equatorial epithelium; while in mammals, secondary fibers grow out in both the anterior and posterior directions from the meridional zone, thereby creating concentric shells of secondary fibers surrounding the fetal lens nucleus.

Cataract is a proteostatic disease

Cataract is one example of diverse late onset “protein-conformational disorders” (Voisine et al., 2010) which makes it an attractive phenotype to understand protein homeostasis (Moreau and King, 2012). Crystallins, the primary constituent proteins of lens, form in the lens nucleus almost entirely around the time of birth with a decreasing formation throughout life (Lynnerup et al., 2008). While the mature lens fiber cells have no further turnover of their protein content, to

maintain the lens transparency, the lens proteins must remain soluble for a lifetime. The only other tissue with similar life-long demand for permanence is the dental enamel (Lynnerup et al., 2008, Spalding et al., 2005b). Furthermore, the eye lens is subjected to lifelong wear and tear of mechanical stress due to lens accommodation, and chemical stress due to photo-oxidative damage and deterioration in the proteome. However, crystallins like all long-lived proteins undergo several chemical changes as they age, including the epimerization of the naturally occurring L-aspartic acid into the racemic mixture of L- and D-forms (Truscott et al., 2016, Truscott and Friedrich, 2016).The D/L ratio of aspartate in proteins linearly increases with age (Helfman and Bada, 1975), but increases faster in lens than in tooth enamel highlighting higher biochemical stress on the lens proteome (Masters et al., 1977). D/L ratio of aspartate is particularly higher in cataractous lenses (Masters et al., 1977, Garner and Spector, 1978).

For the lens to remain transparent despite the physiological stresses, the strength of the interaction between native ß/γ- and α-crystallins must be maintained at the optimal levels and even small changes in this interaction can increase light scattering leading to cataract (Asherie, 2011). Disruption in the short-range order alone, even without aggregation of a lens crystallin can increase the light scattering and can cause cataract (Asherie, 2011, Banerjee et al., 2010, Banerjee et al., 2011). For example, while the human nuclear cataract-associated mutant γD^{E107A} is nearly identical to the wild type in structure, stability, and solubility properties, its interaction with α-crystallin increases primarily due to the change in surface electrostatic potential in the mutant protein, which increases the amount of light scattering (Banerjee et al., 2010, Banerjee et al., 2011).

Thus, lens opacity leading to cataract can occur by causes affecting chaperone activity of α-crystallins such as mutations: R116C in αA-crystallin (Brocklebank et al., 1982) and R120G in αB-crystallin (Vicart et al., 1998); or by changes in the ß and γ-crystallins, such as V76D

mutation in γ-crystallin (Wang et al., 2007) potentially overwhelming the chaperone pool of α-crystallins. A large number of mutations in crystallins are the major contributors to all congenital cataracts (Hejtmancik, 2008, Graw, 2004, Graw, 2009, Clark et al., 2012). Truncations and post-translational modifications in crystallins and other lenticular proteins are implicated in senile cataracts (Truscott and Friedrich, 2016).

Heart as a model system to study proteostatic collapse

Heart, the first formed organ in a developing fetus (Woodcock and Matkovich, 2005, Moorman et al., 2003), pumps blood throughout a metazoan organism to meet the energy and metabolic needs of organs and tissues (Da Silva-Ferrada et al., 2016). As a biomechanical device, the heart contracts and expands during the entire life resulting in an extensive mechanical stress (Boudoulas et al., 2015, Henning and Brundel, 2017). Maintenance of the resting heart rate is critically important for the survival and while factors that influence heart rate also affect life expectancy, an abnormal heart rate directly influences longevity (Boudoulas et al., 2015). The optimum functioning of the heart relies on an extremely organized network of interconnected cells that include: cardiomyocytes (the contractile muscle unit of the heart), endothelial and smooth muscle cells (forming blood vessels that ensure blood transport), fibroblasts (which produce extracellular matrix and confer support) and immune cells (Da Silva-Ferrada et al., 2016).

Cardiomyocytes, like the lens fiber cells, are long living terminally differentiated muscular cells responsible for generating the contractile force in the intact heart (Woodcock and Matkovich, 2005). There is but a limited renewal of cardiomyocytes in humans and less than 50% of cardiomyocytes are exchanged during the lifespan (Bergmann et al., 2009, Senyo et al., 2013) Not only do the number of cardiomyocytes not increase after birth, their renewal gradually decreases from 1% turning over annually at the age of 20 to 0.3% at the age of 75 leading to

slow and continuous decrease in the overall number of cardiomyocytes with age (Bergmann et al., 2009). To compensate for the loss in the total number, and the loss of the mechanical efficiency due to progressive stiffening, the remaining cardiomyocytes undergo aging-induced hypertrophy which preserves some performance at the single cell level (Bernhard and Laufer, 2008). With age, the heart undergoes a significant shift towards enhanced glycolysis possibly possibly due to proteomic remodeling of energetic and structural pathways. Further, aging heart also accumulates extracellular structural proteins and damaged proteins suggesting an age dependent decline in the protein quality control systems (Dai et al., 2014, Quarles et al., 2015).

Thus, cardiomyocytes have high proteostatic demands, consistent with their constitution and physiology, such as highly specialized proteins participating in electrical conduction and contraction; high metabolic demand chiefly met by oxidative phosphorylation; and largely terminally differentiated nature (Carra et al., 2017, Henning and Brundel, 2017). As a result, inadequate proteostasis including aberrant protein folding, protein aggregate formation, and increased protein degradation to clear the toxic misfolded and oxidized proteins is associated with many cardiac diseases (Henning and Brundel, 2017, Wiersma et al., 2016, Willis and Patterson, 2010). Not surprisingly, an extensive PN caters to the heart proteome and several sHSPs, including Hsp27/HSPB1, HSPB5, HSPB6, HSPB7, and HSPB8, are abundantly expressed in the human heart (Quarles et al., 2015, Willis and Patterson, 2010, Tannous et al., 2010, Golenhofen et al., 2004). Persistent atrial fibrillation (AF) has been suggested to be caused by exhausted sHSP levels in atrial tissue and genetic or pharmacological induction of sHSP can protect against cardiomyocyte remodeling in experimental models for AF (Hu et al., 2017).

Titin (also known as connectin), a giant sarcomeric protein, greater than 1 μm in length of molecular mass of up to ≈3800 kDa, is the molecular spring responsible for the passive

stiffness of myocardia responsible for the diastolic filling (LeWinter and Granzier, 2014, Hidalgo and Granzier, 2013, Linke and Hamdani, 2014). While the thin (actin) and thick (myosin) filaments of the sarcomere actively generate force, the titin filaments keep the thick filaments centered in the sarcomere and allow an optimum active force development (Linke and Hamdani, 2014).

The N-terminus of titin anchors in the Z-disc of the sarcomere (Granzier and Labeit, 2004, Hidalgo and Granzier, 2013, LeWinter and Granzier, 2014), where Desmin, an important Z-disk protein plays the critical role in the maintenance of structural and mechanical integrity of the contractile apparatus (Paulin and Li, 2004, Knoll et al., 2011). The rest of Titin can be divided into (1) an elastic I-band region, (2) a thick filament-binding A-band region, and (3) the M-band region where the C-terminus is embedded (LeWinter and Granzier, 2014) (

Figure 19). Elastic titin filaments traverse the I-band in a monomeric state, except in the

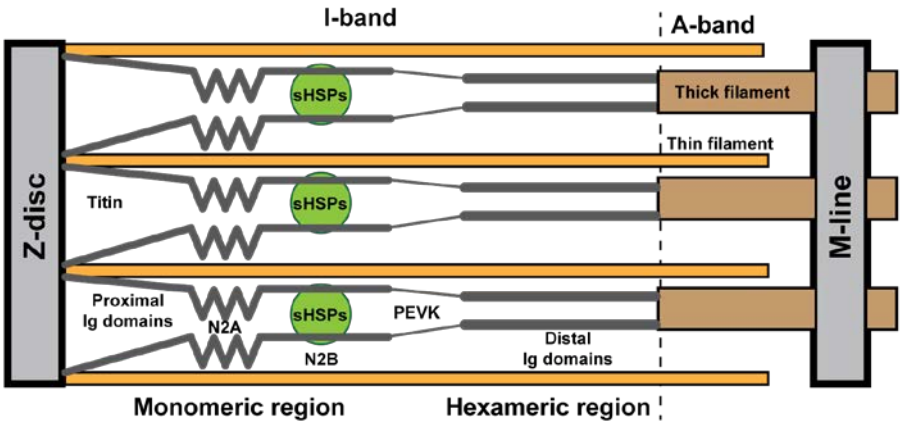

Figure 19: Schematic of titin organization in the sarcomeric I-band

Titin filaments traverse the I-band in a monomeric state but form hexamers in the Ig region. sHSPs associate with unfolded Ig domains between the Z-disk–I-band junction and PEVK and can protect against titin aggregation and prevent myocyte stiffening. Modified from (Kotter et al., 2014, Golenhofen et al., 2002)

distal immunoglobulin-like (Ig) domain region where they form hexamers. sHSPs associate with unfolded Ig domains in a region between the Z-disk–I-band junction and PEVK, and are thought to protect against titin aggregation and prevent abnormal myocyte stiffening (Kotter et al., 2014, Golenhofen et al., 2002).

Under baseline conditions, αB-crystallin is the most abundant sHSP in the heart, and its levels can increase to a dramatic 3% of total cellular protein under conditions of stress, highlighting an important role for αB-crystallin in the cardiac proteostasis (Tannous et al., 2010, Iwaki et al., 1990, Bhat et al., 1991). αB-crystallin associates with desmin and mutations in either one of them leads to heart failure in humans and mice, suggesting a potential compensatory interplay between the two in cardioprotection (Diokmetzidou et al., 2016).

The R120G mutation in αB ($CryAB^{R120G}$) is associated with desmin-related cardiomyopathy (DRM), which is characterized by the formation of desmin- and αB containing aggregates within muscle fibers (Vicart et al., 1998, Hershberger et al., 2013). Mice with cardiac specific overexpression of $CryAB^{R120G}$ develop cardiomyopathy at 3 months and die at 6–7 months from heart failure (HF) (Wang et al., 2001). Cardiac-specific αB-crystallin overexpression rescued desmin-deficient heart failure in $Des^{-/-}$ mice (Diokmetzidou et al., 2016). However the effect of R120G mutation in DCM is an example of toxicity due to aggregation-prone sHSP itself and the pathology can be ameliorated by reversing the aggregation (Sanbe et al., 2007, Sanbe et al., 2005).

Another αB mutation (R157H) that decreased binding to titin without affecting the distribution of the mutant is also associated with dilated cardiomyopathy (Inagaki et al., 2006). Under cardiac stress conditions, such as in ischemia, αB and other muscular sHSP translocated from cytosol to the Z-/I-area of myofibrils (Golenhofen et al., 2004). While αB-crystallin has binding sites in both cardiomyocytes and the skeletal muscle fibers, in skeletal muscles αB

localized diffusely throughout the entire I-band, whereas in cardiomyocytes αB was preferentially located at the N-line position of the I-band (Golenhofen et al., 2004).

Hsp27/HSPB1 is also found associated with sarcomeres, is induced in ischemia, and has been suggested to have a cardioprotective role (Chiesi and Bennardini, 1992, Hollander et al., 2004, Robinson et al., 2010, Brundel et al., 2006). Both HSP27 and αB-crystallin suppressed acidic stress induced stiffening in cardiomyocytes caused by unfolding of Ig domain of titin (Kotter et al., 2014). In diseased human muscle and heart, both sHSPs associated with the titin springs, in contrast to the cytosolic/Z-disk localization seen in healthy muscle/heart (Kotter et al., 2014). HSP27 translocates to myofibril fraction from the cytosolic in rat hearts after ischemic injury where it then colocalizes with the Z-line and may be involved in Z-line protection (Yoshida et al., 1999). Increased expression of HSP27 protected canine myocytes from simulated ischemia-reperfusion injury (Vander Heide, 2002).

While the importance of sHSPs in the cardiac proteostasis is evident, their precise role in the cardiac function is still being evaluated. Zebrafish represents a relatively simple model system to understand the role of sHSP in the maintenance of heart proteome. Although zebrafish heart is less developed relative to the mammalian heart, phenotypes of several zebrafish mutants have faithfully recapitulated human cardiomyopathies highlighting conservation of the cardiac physiology among vertebrates (Bakkers, 2011, Wilkinson et al., 2014, Chico et al., 2008). The zebrafish heart expresses two paralogous αBa and αBb-crystallins, both homologous to human αB (Posner et al., 2005, Smith et al., 2006). The lessons learned from monitoring the role of αB-crystallin paralogs in the zebrafish heart can help us understand the role of αB-crystallin in human heart. The amenability of zebrafish to forward and reverse genetics, ease of maintenance and fecundity coupled with the transparency of embryos make zebrafish a valuable model to understand the role of sHSPs in the cardiac physiology

(Bakkers, 2011, Bournele and Beis, 2016, Nguyen et al., 2008, Wilkinson et al., 2014, Chico et al., 2008).

Glucocorticoid receptor signaling in relation to crystallins and sHSP

Along with the factors of the PN, other biological pathways also play important role in overcoming the physiological stresses (Cavadas et al., 2016). These stress responding signaling and trafficking pathways interact with the PN, and function as the carriers of the stress signals across the body to prepare organs for the impending stress (Pratt et al., 2006). A physiological stress, distinct from the cellular stress, can be an actual or anticipated disruption of homeostasis (Vyas et al., 2016, McEwen, 2007). Glucocorticoids (GC) are primary stress-involved hormones that are essential in maintaining homeostatic functions (Kadmiel and Cidlowski, 2013, Rhen and Cidlowski, 2005, Oakley and Cidlowski, 2011). GCs, derivatives of cholesterol, are produced by the adrenal gland in mammals at increased levels during stress and they bind ubiquitous glucocorticoid receptors (GR) to trigger signal transduction that provides potent anti-inflammatory and immunosuppressive activity (Vandewalle et al., 2018). The GR, expressed nearly ubiquitously in human organs, is a member of the nuclear receptor superfamily, which also includes transcription factors, receptors for thyroid hormone, retinoids and other small lipophilic molecules (Matthews et al., 2015, Kayes-Wandover and White, 2000).

In the ligand-free state, the GR is located in the cytoplasm complexed with accessory protein including heat-shock proteins (Kirschke et al., 2014, Matthews et al., 2015). Upon activation by the glucocorticoid ligand, GR hyper-phosphorylates, dissociates from resting complex and translocates to the nucleus, where it can bind to glucocorticoid response elements (GREs) in the promoter regions of target genes to transactivate (Schaaf et al., 2008, Kirschke et al., 2014, Kadmiel and Cidlowski, 2013).

In humans, alternative translation and splicing of the primary transcript of the single GR (hGR) gene (NR3C1) produces multiple isoforms (Lu and Cidlowski, 2004, Lu and Cidlowski, 2006). Alternate splicing of Exon 9 generates hGRα and hGRß transcripts, which produce proteins that differ in their carboxyl termini (Oakley et al., 1996). However, several more isoforms of each of the two hGRα and hGRß proteins exist because of alternate translation of their respective primary transcripts (Kadmiel and Cidlowski, 2013, Lu and Cidlowski, 2004, Lu and Cidlowski, 2006). While hGRα is a ligand-activated transcription factor which, in the hormone-bound state, modulates the expression of glucocorticoid-responsive genes by binding to specific GRE DNA sequences; hGRβ is transcriptionally inactive, although it binds GREs in the promoter regions of target genes with a greater capacity than hGRα in the absence of GCs, and thus probably functions as a dominant negative regulator (Bamberger et al., 1995, de Castro et al., 1996, Oakley et al., 1996, Yudt et al., 2003).

Glucocorticoid response is conserved between taxa

Cortisol is the primary corticosteroid in teleosts that is released in response to stressor activation including water and electrolyte homeostasis (Bury and Sturm, 2007, Steenbergen et al., 2011, Kwong et al., 2013, Wendelaar Bonga, 1997). GC production in fish is regulated by the hypothalamus-pituitary-interrenal (HPI) axis, equivalent to the mammalian hypothalamus-pituitary-adrenal (HPA) axis (Alsop and Vijayan, 2009).

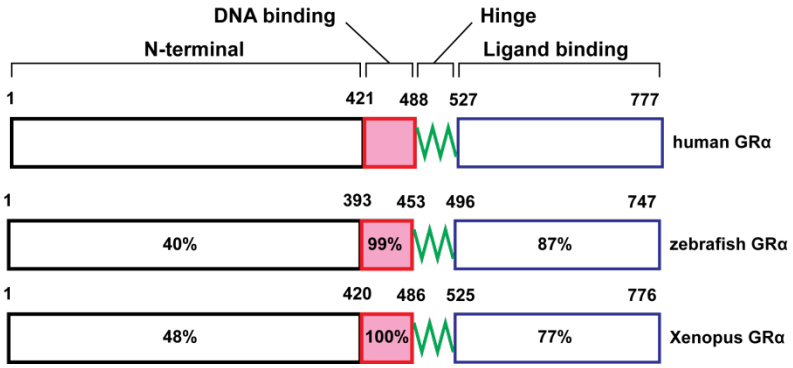

Figure 20: Schematic of the α-subtype glucocorticoid receptor

The homologous GRα have 3 major domains: the N-terminal domain (NTD), middle DNA-binding domain (DBD) with a hinge region, and the C-terminal ligand-binding domain (LBD). The numbers denote the amino acids, and the % homology is relative to human sequence.

Unlike other bony fish which have two GR genes, zebrafish has only one GR gene nr3c1, which is homologous to the human gene (Figure 20) (Schaaf et al., 2009, Schaaf et al., 2008). Both the human and zebrafish genes contain 9 exons with the first exon being noncoding. The canonical zf-GRα isoform is 59.3% similar to hGRα with near complete (98.4%) identity in the DNA binding domain (DBD). The N-terminal domain (NTD) of zfGRα is only ~40% conserved compared to hGRα, but the C-terminal ligand binding domain (LBD) is highly conserved (86.5%) among the two (Schaaf et al., 2009). Similarly, the zebrafish also expresses the C-terminal GR splice variant zf-GRß with high similarity to the human GRβ isoform, which has been shown to be a dominant-negative inhibitor of the canonical GRα and may be involved in glucocorticoid resistance (Schaaf et al., 2008, Schaaf et al., 2009). Both receptor isoforms were detected throughout the zebrafish body (Schaaf et al., 2008). While the majority of GR-deficient mice (~90%) died at birth reflecting retarded lung maturation and atelectasis, null mutants of zebrafish zf-nr3c1 were viable, phenotypically inconspicuous, fertile, and segregated according to Mendelian ratio although with compromised survivability (Facchinello et al., 2017, Cole et al., 1995).

GCR and sHSP are partners in the stress response

Since sHSPs are an integral component of the stress response system across taxa, hormone responsiveness is a common characteristic of sHSP genes (Klemenz et al., 1994, Tabibzadeh and Broome, 1999). In insects, such as in the fruit fly (*Drosophila melanogaster*) and oriental fruit fly (*Bactrocera dorsalis*), the expression of sHSPs is regulated by the molting hormone ecdysone (Shen et al., 2011, Dou et al., 2017, Ireland and Berger, 1982, Michaud et al., 1997). The human hsp27 gene is estrogen responsive, and macrophages release Hsp27 in dose-dependent manner by estrogens (Rayner et al., 2010, Devaja et al., 1997). Aberrant levels of steroid hormone receptors and αB-crystallin were found in peritoneal endometriosis, an infertility disorder due to progesterone resistance (Moberg et al., 2015).

α-crystallins accounted for more than 98% of the total soluble bovine lens proteins binding dexamethasone, a widely used anti-inflammatory and immunosuppressive synthetic glucocorticoid (Jobling et al., 2001). While the interaction of dexamethasone with purified α-crystallin could be due to nonspecific partitioning with the hydrophobic sites of α-crystallin, dexamethasone induced accumulation of αB crystallin mRNA and protein in fibroblast cultures (Scheier et al., 1996). In fact, αB-crystallin was the only HSP which was induced by dexamethasone in the fibroblast cultures, independent of general stress response (Aoyama et al., 1993). A putative GRE within the promoter region of the αB crystallin gene has been shown to bind the glucocorticoid receptor by *in vitro* footprint analysis, although this GRE was not involved in the hormone-mediated gene activation (Scheier et al., 1996).

The αB-crystallin and Myotonic dystrophy kinase binding protein (Mkbp)/HspB2 genes, both members of the small heat shock protein gene family, are arranged head-to-head in the human, mouse and rat genomes (Liu and Piatigorsky, 2011). Mkbp/HspB2 is expressed

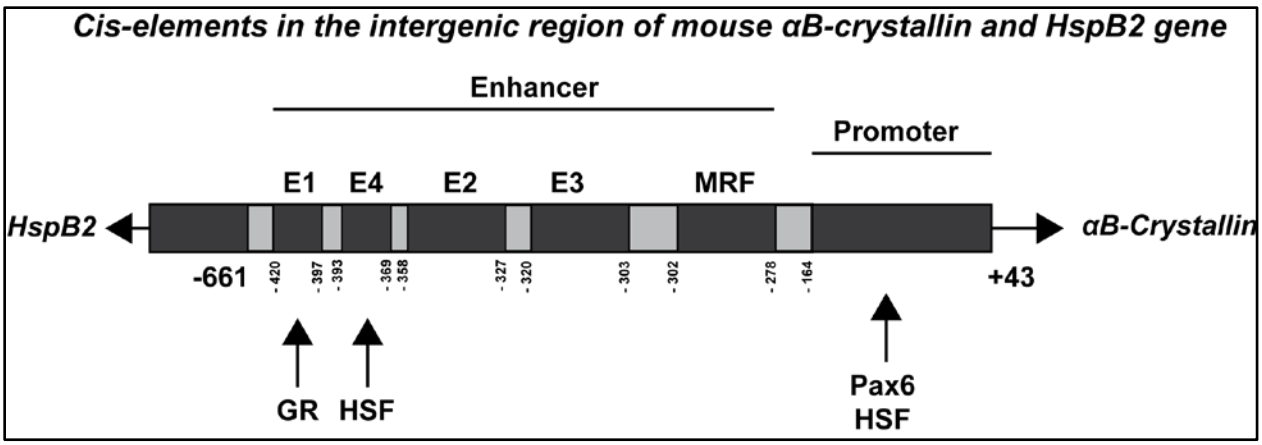

Figure 21: Cis-elements in the mouse αB-crystallin and HspB2 genes

preferentially in skeletal muscle and heart but not in the lens (Suzuki et al., 1998a). Both HspB2 and αB share some cis-elements (

Figure 21) and a GC responsive site αBE1, in the enhancing region equally affects the activity of the promoters of both αB and HspB2 (Cvekl et al., 2017, Swamynathan and Piatigorsky, 2007)

The GC medications are frequently used to treat a chronic inflammatory conditions such as arthritis, immune disorders, allergic reactions, skin and eye conditions, breathing problems, bowel diseases, and cancers (Burns, 2016, Raju, 1999, Sulaiman et al., 2018). Currently, synthetic glucocorticoids are among the most commonly prescribed drugs (Buttgereit et al., 2013). However, because of their wide ranging physiological role, GCs elicit pleiotropic side effects including posterior subcapsular cataract (PSC) (Black et al., 1960, Skalka and Prchal, 1980, Loredo et al., 1972, James, 2007). 39% of rheumatoid arthritis patients, who received long-term corticosteroid therapy developed PSC (Black et al., 1960). Not only systemic, but topical and inhaled steroids also induce cataract (Jobling and Augusteyn, 2002). In fact, up to

22% of cataract cases could be related to steroid use, a proportion which is bound to rise because of ever increasing prescriptions of steroids (Veenstra et al., 1999).

PSC is particularly debilitating for patients. While only approximately 5–15% of cataracts are classified as PSC, they account for about 40% of cases that require surgery (Leske et al., 1997, James, 2007). Importantly, among the cataract patients that undergo cataract surgery, cardiovascular disease are more prevalent than the general population, suggesting that severe cataract could be an indicator of the underlying collapse of proteostasis (Nemet et al., 2010). However, PSC opacity does not significantly correlate with the intensity or the duration of the GC dose; or the age of patients (Skalka and Prchal, 1980). Interestingly, chronic endogenous hypercortisolism (endogenous Cushing syndrome) rarely causes PSC, suggesting physiological differences in endogenous versus exogenous GCs (Bouzas et al., 1993).

In the whole body systems, only the steroids possessing glucocorticoid activity cause steroid-induced PSC, suggesting a key role for GR activation in the development of PSC. Notably, excised chick lenses in culture lost transparency when exposed not only to GCs but also to androgen, estrogen and mineralocorticoid. Thus, at least some loss of transparency in lens can be induced independently from biological activities of steroids (Kosano and Nishigori, 2002). In some adult animal models, such as in rats and in chickens, the steroids did not induce cataract, and low survival due to high concentration of administered steroids can confound results (Jobling and Augusteyn, 2002). In rabbits, cortisone induced only anterior subcapsular cataract along with diabetes (Jobling and Augusteyn, 2002). While some embryonic animals develop steroid induced cataract, GRs have not been identified in those animals such as chick, and thus GCs were thought to act on lens cells indirectly. However, while GCs could exert their effects on the lens indirectly, non-specifically, or through non-classical mechanisms, most likely specific GR are involved in the GC physiology (Sulaiman et al., 2018).

The human lens contains a functional glucocorticoid receptor. Anti-GR antibodies could detect GR in the lens epithelium, and PCR amplification and sequencing has confirmed that GRα is present in human and mouse epithelial cells; and in human, rat, rabbit and bovine lens cells (James et al., 2003, Gupta and Wagner, 2009). The lens GRα receptor could induce or repress the transcription of genes known to be associated with glucocorticoid receptor activation in other cell types (James et al., 2003, Jobling and Augusteyn, 2001, Gupta and Wagner, 2009). Thus, it is pertinent to explore the interaction of GCR with the lenticular crystallins in the context of the development of cataract, and in other proteostatic disorders.

Research overview

αB-crystallin as a typical sHSP shares most of the properties of vertebrate sHSPs including the presence of the highly conserved ACD, the hydrophobic N-terminal region and a flexible C-terminal extension (Sharma et al., 1997, Ghosh et al., 2006, Bhattacharyya et al., 2006, McHaourab et al., 2009). Although the structures of isolated ACD dimers have been resolved, there is insufficient structural insight available for the native oligomer assembly of mammalian sHSP, owing to their polydispersity and dynamics (Ghosh and Clark, 2005, Jehle et al., 2011). The αB-crystallin oligomers dynamically undergo subunit exchange through dissociation into smaller multimers, probably into dimers (Thornell and Aquilina, 2015, Benesch et al., 2008, Ecroyd et al., 2007, Aquilina et al., 2003). Similarly, *in vitro* Hsp27 undergoes concentration-dependent equilibrium dissociation to the dimer, which is favored by phosphorylation *in vivo* or by mutations mimicking the phosphorylation (Bova et al., 2000). This polydispersity and dynamics of the sHSP oligomers, a hallmark of all mammalian sHSPs, is critical for their role as chaperone enabling high affinity binding to destabilized proteins (Basha et al., 2012, Jehle et al., 2011, McHaourab et al., 2009, Koteiche and McHaourab, 2006, Shi et al., 2013, Shi et al., 2006a, McHaourab et al., 2012).

Phosphorylation of mammalian αB-crystallin in response to stress and aging has been shown *in vitro* to activate its chaperone function presumably through changes in the oligomer size and/or the rate of subunit exchange (Koteiche and McHaourab, 2003, Peschek et al., 2013, Thornell and Aquilina, 2015, Bakthisaran et al., 2016). However, zebrafish αBa-crystallin, a homolog of human αB-crystallin, displayed much higher chaperone-like activity towards the model substrate T4L approaching that of activated mutants of mammalian sHSPs (Koteiche et al., 2015). αBa-crystallin also formed bigger average oligomer than its mammalian homolog, which suggests that the elevated chaperone-like activity of αBa-crystallin could stem from the expanded oligomeric state. Oligomer expansion has already been shown to enhance chaperone-like activity of sHSPs in cataract-linked mutants of α-crystallins (Koteiche and McHaourab, 2006, Kumar et al., 1999, Shroff et al., 2000), and in engineered variants of Hsp16.5 (Shi et al., 2006a, Shi et al., 2013, Mishra et al., 2018).

Particular sequence elements in the NTD of Hsp27 have been shown to play important role in the dynamics of the oligomeric transition towards larger oligomers (Shashidharamurthy et al., 2005). A 14-amino acid peptide (hereafter referred to as the P1 peptide), unique in primate Hsp27 found at the junction of the NTD and ACD, affects the aforementioned concentration-dependent equilibrium dissociation of Hsp27. Deletion of the P1-peptide in Hsp27 shifted the equilibrium towards the larger oligomers and reduced the chaperone activity (Shashidharamurthy et al., 2005). Contrastingly, insertion of this sequence at the homologous position in the highly homogenous Hsp16.5 expanded the oligomeric structure from 24-subunits to 48-subunits concomitantly enhancing the chaperone activity (McHaourab et al., 2012, Shi et al., 2013, Shi et al., 2006a, Mishra et al., 2018).

Zebrafish uniquely expresses two paralogous αB-crystallins: αBa and αBb (Smith et al., 2006, Posner et al., 2005, Posner et al., 1999). Despite high sequence conservation between

the human and zebrafish αB homologs, the terminal regions flanking ACD are fairly variable (Figure 22).

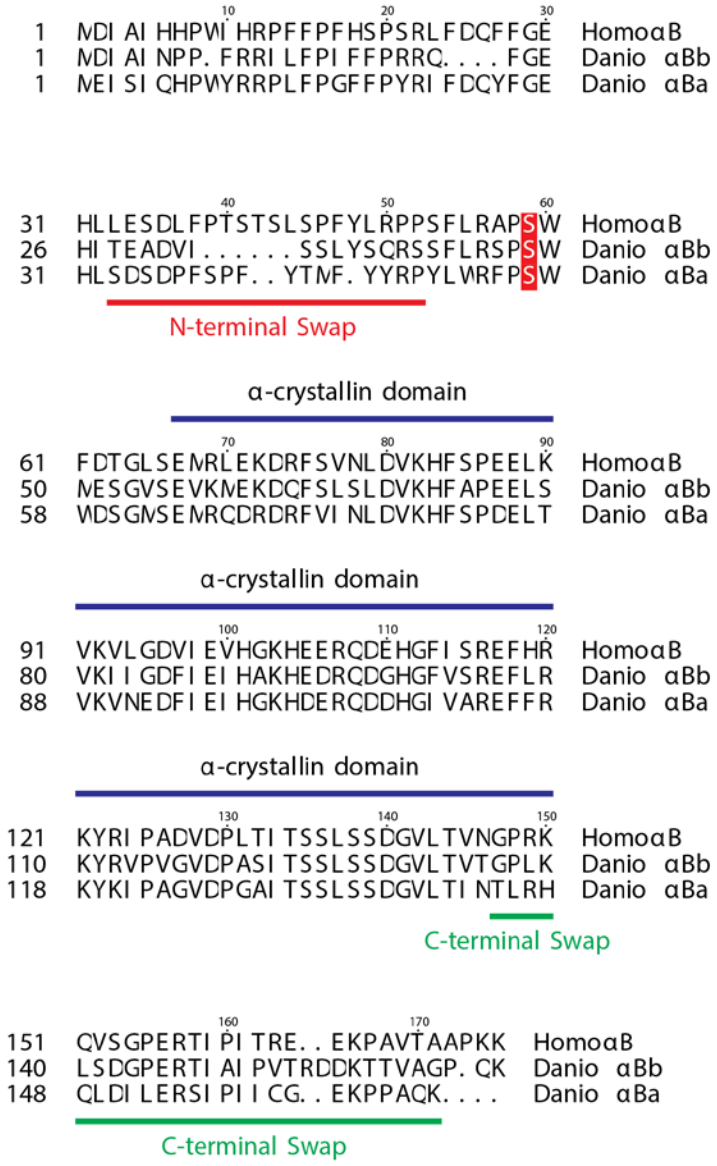

Figure 22: Sequence alignment between human and zebrafish αB crystallins.

Highly conserved Ser residue is marked in red. The α-crystallin domain is labeled as predicted by Conserved Domain Database (CDD) webserver maintained by NCBI.

By evaluating the role of sequence from evolutionary divergent but homologous αB and αBa, we aimed to learn about the mechanism that underlies the constitutively higher chaperone-like activity pf αBa-crystallin. Our hypothesis was that the elevated chaperone-like activity of αBa-crystallin stems from higher oligomeric state, which can be altered through sequence manipulation. Thus in this study, we studied the role of the N- and C-terminal regions of αBa-crystallin, by mimicking the role of evolutionary sequence diversity, in the formation of oligomers and chaperone activity of engineered αBa-crystallin mutants.

The second aim of our study was to establish the role of zebrafish αB-crystallin homologs in the lens. While αB-crystallin is relatively a minor constituent of the vertebrate lens proteome, several αB-crystallin mutations are implicated in mammalian autosomal cataracts (Graw, 2004, Graw, 2009, Andley, 2007). It is as yet unclear what role αB plays in the lens given αB knockout mice did not develop cataract, although αB was the predominant protein in the inclusion bodies of cataract in αA knockout mice (Brady et al., 1997, Brady and Wawrousek, 1997, Wawrousek and Brady, 1997). While confounding the effect αB in these knockout mice was the inadvertent disruption of the adjacent HSPB2 gene, the mice indeed suffered with degenerated skeletal muscles and developed severe fatal phenotype late in life (Brady and Wawrousek, 1997). Zebrafish with a conserved role for αA-crystallin in the maintenance of transparency in lens (Zou et al., 2015), and with a lens predominant αBa-crystallin paralog expressing distinct from the ubiquitous αBb-crystallin, both homologous to human αB-crystallin (Posner et al., 1999, Posner et al., 2005, Smith et al., 2006) is an attractive model system to assess the role of αB-crystallin *in vivo*. As a fast growing vertebrate, zebrafish can help us understand the role of αB-crystallins in the proteostasis of organs of long living cells with high proteostatic demand, such as eye lens and heart. Our hypothesis for this work was that both αBa and αBb-crystallins are required to maintain the zebrafish lens transparency, and we aimed

to test whether disruption in αBa- and αBb-crystallin expression would lead to cataract like phenotypes in zebrafish.

These studies can lead to establish zebrafish models to study the progression of cataract, to use zebrafish for screening of potential pharmacological compounds to develop drugs that can reverse cataract; and towards a better understanding of the role of αB-crystallin in particular and sHSPs in general in chaperonopathies.

CHAPTER II

ROLE OF THE N-TERMINUS IN THE OLIGOMERIZATION AND THE CHAPERONE ACTIVITY OF THE αBa Crystallin

Introduction

αB-crystallin (*cryab*/HSPB5) is a prominent member of the human sHSP repertory. Although most abundantly present in the eye lens, it is also expressed throughout the body, most noticeably in heart and brain tissues (Lowe et al., 1992, Iwaki et al., 1989, Iwaki et al., 1990). At the whole organismal level, αB-crystallin is the 818th most abundant protein (Figure 23) (Wang et al., 2015).

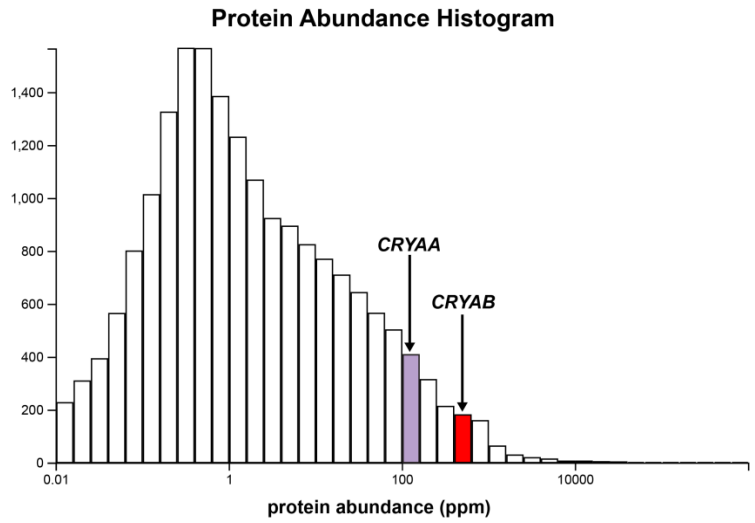

Figure 23: The abundance of αA and αB in human proteome.

The protein abundance, in parts per million (ppm), is aggregated by the Protein Abundance Database - PaxDb (https://pax-db.org/). Each protein is enumerated relative to all others in the proteome.

In most vertebrate eye lenses, αB-crystallin is expressed in a ~3:1 ratio with αA-crystallin (cryaa/HSPB4) and the two crystallins make up almost 40% of the total lens protein (Berzelius, 1842, Thomson and Augusteyn, 1985). As a typical molecular chaperone, αB-crystallin can bind partially unfolded proteins *in vitro* and strongly inhibits the aggregation of a variety of model targets (Basha et al., 2012, Hilton et al., 2013, McHaourab et al., 2009, Ecroyd and Carver, 2009, Mishra et al., 2012). *In vivo*, αB-crystallin is found associated with protein aggregates in several neurodegenerative disorders such as in Rosenthal fibers in Alexander's disease, amyloid fibers in Alzheimer's disease, Lewy bodies in Parkinson's disease, and glial cytoplasmic inclusions in multiple system atrophy (Ecroyd and Carver, 2009, Tomokane et al., 1991, Pountney et al., 2005). Similarly, inclusion bodies that form in cataracts of αA-crystallin knock-out mice contain αB-crystallin (Brady et al., 1997, Brady and Wawrousek, 1997, Wawrousek and Brady, 1997). αB-crystallin is also directly implicated in several degenerative myofibrillar myopathies, such as desmin-related cardiomyopathy, and dilated cardiomyopathy which are characterized by disintegrating Z-disk, accumulation of myofibrillar degradation products and insoluble protein deposits (Selcen, 2011, Boncoraglio et al., 2012). However, whether co-localization of αB-crystallin and other sHSPs in pathognomonic lesions is a cause or response to protein perturbations is not clear (Tanguay and Hightower, 2015).

Essential to the molecular chaperone function of αB-crystallin is its dynamic quaternary structure, similar to other active mammalian sHSPs such as αA-crystallin and Hsp27 (Delbecq and Klevit, 2013, Hochberg and Benesch, 2014, Spector, 1965, Baldwin et al., 2011). αB-crystallin forms a spectrum of poorly resolved, interconverting oligomeric states (van den Oetelaar et al., 1990, Haslbeck et al., 2016). Thus, the association number and corresponding quaternary structure of αB-crystallin is an average of a dynamically fluctuating oligomeric landscape (Thomson and Augusteyn, 1989, van den Oetelaar et al., 1990). While the

methodological consensus is that the αB-crystallin oligomers averages around ~600 kDa, the oligomeric ensemble ranges from 10-mers to 40-mers (Aquilina et al., 2003, Haley et al., 2000, Horwitz, 2009). The often described 24-mer of αB-crystallin may represent only about 5% of the multimeric species (Aquilina et al., 2003). A 32-mer coexistent with multiple assemblies of highly variable quaternary structures was resolved as an asymmetric structure with a large central cavity (Haley et al., 2000). Another 24-mer assembly was resolved as a spherical, symmetric protein shell with fenestrations (Peschek et al., 2009, Peschek et al., 2013). The continuum of iso-energetic subspecies of αB-crystallin arises from the dimer as the building block under physiological conditions, although monomeric units can be populated and can be incorporated in the αB oligomers at lower pH (Baldwin et al., 2011, Jehle et al., 2011, Braun et al., 2011, Peschek et al., 2009). It is possible that αB exists as a distribution of oligomeric species that are built of dimers, hexamers, and multiples of hexamers as building subunits (Delbecq and Klevit, 2013). Subtle changes in conditions, such as a stress or a chemical modification such as phosphorylation, alter the equilibrium between the oligomeric states of αB-crystallin (Ito et al., 2001, Ito et al., 1997, Bakthisaran et al., 2016, Baldwin et al., 2011).

Conforming to the tripartite architecture of a canonical sHSP, αB-crystallin consists of a 90 residues long highly conserved ACD flanked by a 60 residues long N-terminal domain (NTD) and a 25 residues long C-terminal domain (CTD) (Jehle et al., 2011, de Jong et al., 1998). The excised ACD domain of αB-crystallin self-assembles into a dimer as the basic building block of the larger αB-crystallin assembly. The dimer is held together by an extensive ionic interaction network across the dimer interface (Clark et al., 2011). The flexible ACD dimer interface can adopt different strand registers, highlighting that the dynamic behavior central to the polydispersity of oligomers is allowed by the ACD region (Bagneris et al., 2009, Jehle et al., 2010, Clark et al., 2011, Laganowsky et al., 2010, Koteiche and McHaourab, 1999). The

excised ACD dimers of αB-crystallin had reduced chaperone activity similar to HSPB6, which only forms dimers in solution (Weeks et al., 2014, Feil et al., 2001).

The heterogeneity of the oligomeric states of αB-crystallin (and other sHSPs) is aided by the highly flexible NTD and CTD sequences flanking the ACD (Jehle et al., 2011, Carver et al., 1992, Meehan et al., 2007). The CTD of αB contains a highly conserved IxI motif (90% of sHSPs), defined by two Ile (or Val) residues separated by one residue, which binds the hydrophobic grooves of ACD (Jehle et al., 2011, Baldwin et al., 2011, Jehle et al., 2010, Delbecq et al., 2012). Deletion or introduction of hydrophobic residues within CTD decrease the chaperone activity (Treweek et al., 2007)and swapping the CTD of αA-crystallin to αB-crystallin enhanced the chaperone activity (Pasta et al., 2002). Although deleting the CTD or mutations in the IxI motif cause loss of higher order oligomeric structure in several sHSPs including αB-crystallin (Studer et al., 2002, Hayes et al., 2008, Pasta et al., 2004), CTD alone is not sufficient to define or to maintain the oligomer geometry of sHSP (Basha et al., 2012).

The NTD emerges from the proximal side of the ACD beta sandwich and is believed to hold the sHSP oligomer together; however its exact placement is poorly resolved in available structures (Haley et al., 2000, van Montfort et al., 2001b). The NTD was buried inside the oligomeric shell in the Archean Hsp16.5, and has been only observed in an ordered state for half of the chains in 24-mers of yeast Hsp26 and 12-mer of wheat Hsp16.9 (van Montfort et al., 2001b, Haley et al., 2000, White et al., 2006). However, solid-state NMR studies and modeling of related structures suggested two β-strands in the αB-crystallin NTD that exist in multiple structural environments (Jehle et al., 2011). This suggests that the NTD of αB-crystallin provides a conformational switch for multimerization and structural heterogeneity (Jehle et al., 2011). For most sHSPs, deletion of all or part of the NTD disrupts the oligomers resulting in smaller oligomers, mostly dimers. (Ohto-Fujita et al., 2007, Peschek et al., 2013, Mainz et al., 2015,

Lelj-Garolla and Mauk, 2012, Moutaoufik et al., 2017, Berengian et al., 1999, Bova et al., 1997, McDonald et al., 2012).

Humans have 10 paralogous sHSPs, and orthologs can be identified in other vertebrates including in zebrafish (Kappe et al., 2010, Franck et al., 2004, Kappe et al., 2003, Elicker et al., 2007, Elicker and Hutson, 2007, Marvin et al., 2008). However, unique among vertebrates, zebrafish express two paralogs of αB-crystallin (genes called *cryaba* and *cryabb*; the proteins conventionally called αBa- and αBb-crystallin) (Smith et al., 2006). The αBa- and αBb-crystallins share ~50% amino-acid identity, and αBb is more similar to human αB (58% identity) than to its paralog αBa (Posner et al., 2005, Smith et al., 2006) (Figure 22). However, αBa-crystallin displays a substantially enhanced chaperone activity *in vitro* relative to other α-crystallins, while forming distinctly bigger oligomers (Koteiche et al., 2015). The activity of αBa-crystallin approached that of biochemically activated phophomimetic mutant of αB which suggests that constitutively higher chaperone-like activity of αBa-crystallin might be related to the expanded oligomeric ensemble, supported by an evolutionary diverse sequence in the NTD. Thus, the sequence divergence among taxonomically related sHSPs and the species-specific chaperones may represent an evolutionary strategy to tune the chaperone function by reshaping the sHSP oligomer ensemble dynamics and consequently, the chaperone activity as defined by binding affinity and capacity.

To test the hypothesis whether the sequences flanking the ACD of zebrafish αBa-crystallin encode for an activated chaperone, we generated chimeric αB-crystallin by sequence-guided domain swaps which mimic the evolutionary divergence between the homologous αB and αBa-crystallins. We assessed the consequences of the sequence changes on the oligomeric distribution by Size Exclusion Chromatogrophy (SEC), light scattering, and analytical centrifugation. Furthermore, we determined the chaperone activity of the chimeric mutants

through equilibrium binding assays using a destabilized model substrate, T4-Lysozyme. Our results show that the NTD of αBa promotes an expanded sHSP oligomer and the expanded oligomers display higher chaperone-like activity towards client protein. These results support a model that expansion of the oligomer is an alternate mechanism to enhance the chaperone activity of sHSPs by increasing accessibility to substrate binding sites in the NTD that are otherwise secluded within the confines of the oligomer.

Material and Methods

Cloning and mutagenesis of αBa variants

The cDNA of αBa was a gift from Dr. Mason Posner, Ashland University. The coding sequence was cloned in a pET20 vector between NdeI and BamHI sites. Chimeric αB constructs between human αB and αBa were generated by overlap extension polymerase chain reaction (Figure 24). Briefly, 5' → 3' primers were designed complementary to the desired sequence, with a ~21 bp overlapping region. The pairs of downstream and T7 promoter primers, and upstream and T7 terminator primers were used to amplify the region of interest from the cDNA, and the gel purified segments were further extended by amplifying with the T7 promoter and terminator primers. The amplified segment DNA was purified after running on agarose gel, digested with NdeI and XhoI restriction enzymes, and ligated into the vector backbone cut with the same enzymes. The ligation products were transformed into Escherichia coli *XL1 Blue cells* and sequences were confirmed after isolating DNA by MiniPrep (Qiagen).

The C-terminal domain flanking the ACD of αBa crystallin was swapped with αB sequence, such that Swap2 contained the wild type αBa^{1-143}, followed by $\alpha B^{147-175}$. The N-terminal domain immediately flanking the ACD of αBa-crystallin was swapped with αB sequence, such that the Swap3 and Swap4 contained progressively larger human αB sequences (αB^{41-52} in Swap3, and

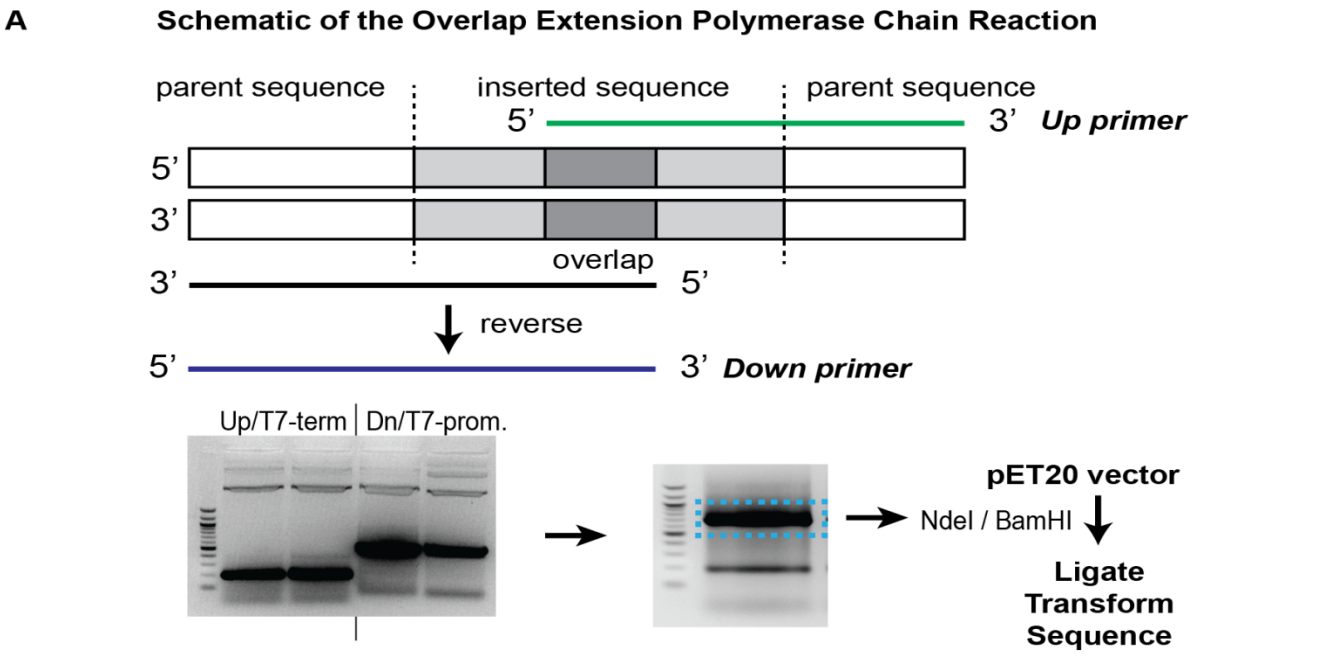

B

αB variants generated

Hs αB	33	LESDLFPTST SLSPFYLRPP	53		146	GPRKQVSGP ERTIPITREE KPAVTAAPKK	175
Dr αBa	33	SDSD--PFSP FYTMFYYR-P	50		143	TLRHQLDIL ERSIPIICGE KPPAQK----	168
Swap2		SDSD--PFSP FYTMFYYR-P				GPRKQVSGP ERTIPITREE KPAVTAAPKK	
Swap3		SDSD--PFST SLSPFYLRPP		α-Cry Domain		TLRHQLDIL ERSIPIICGE KPPAQK----	
Swap4		LESDLFPTST SLSPFYLRPP				TLRHQLDIL ERSIPIICGE KPPAQK----	

Figure 24: Schematic of the overlap extension PCR

(A) Primers shown by green and blue lines were designed complementary to the wild type and to-be inserted sequence, such that they overlap. After PCR amplification, the amplified arms were gel purified, annealed and amplified the second round, which were then ligated into the pET20 vector; and transformed into *E. coli* bacteria. (B) Protein sequences of the human αB (in red), zebrafish αBa (in red); and theSwap2, Swap3, and Swap4 variants.

αB^{33-52} in Swap4) placed between the remainder of wild type αBa sequences.

Over-expression and purification of αB-crystallin

Human αB-crystallin was cloned in pET20 expression vector was expressed in *Escherichia coli* BL21/DE3 cells and was purified as previously described (Koteiche and McHaourab, 2003, Horwitz et al., 1998). Briefly, overnight seeds from a single colony were used to inoculate LB cultures (supplemented with Ampicillin), and the cultures were grown to mid-log phase (OD600 ~ 1.0) at 37 °C by shaking. The over-expression was induced by the addition of 0.4mM isopropyl-1-thio-β-D-galactopyranoside after cooling the cultures to 34 °C. The induction was continued for 3h at 32 ºC, the cells were harvested by centrifugation and resuspended in cold lysis buffer (20 mM Tris, 25 mM NaCl, 0.1 mM EDTA, 0.02% NaN3, 10 mM dithiothreitol, pH 8.0). The resuspended cells were disrupted by sonication, and the DNA was precipitated by the addition of 0.017% polyethyleneimine. The lysate were centrifuged at 15,000 ×g for 20 min. The αB-crystallin was purified by anion exchange chromatography followed by size exclusion chromatography in the SEC buffer (9mM MOPS, 6mM Tris, pH 7.2).

Expression and purification of αBa-crystallin variants

The chimeric αB-crystallins constructs and the wild type zebrafish αBa proteins were over-expressed in Escherichia coli BL21/DE3 cells at 32 °C for 3 h after induction at mid-Log phase (OD600 ~ 1) by 400 mM isopropyl β-d-thiogalactopyranoside (IPTG) (Figure 25). The proteins were purified in 3-stages as shown in Figure 25. Briefly, the pelleted cells were lysed in the lysis buffer A (20mM Tris, 1mM EDTA, 0.02% (w/v) sodium azide; pH 8), supplemented with DTT, and the homogenate was cleared by centrifugation after precipitation of chromatin by polyethyleneimine. The crude protein extracts were eluted through HiTrap Q-column (GE Healthcare Life Sciences), which binds the αBa-S fraction while the αBb-L fraction did not bind

the column. The column-bound αBa-S protein form was eluted by a linear NaCl gradient (4 to 40%), after washing the column with buffer containing 4% NaCl. Both the zf-αBa-S and the zf-αBb-L protein fractions were further purified by reverse phase hydrophobic interaction chromatography (HIC) on a phenyl-Sepharose column 6 (GE Healthcare Life Sciences) after adding ammonium sulfate (0.5M). Proteins were eluted from the column through linear gradient of ammonium sulfate (from 0.5 to 0 M). Finally, all proteins were purified by size exclusion chromatography (SEC) on Superose 6 column, eluted in the SEC buffer (9mM MOPS, 6mM Tris, pH 7.2). The αBa-L oligomer eluted from the SEC at ~8ml, while αBb-S oligomer eluted at ~12ml (Figure 25).

The purity of the protein preparations were assessed by running them on denaturing polyacrylamide gels and the bands on SDS-PAGE were visualized by Coomasie-R staining (Figure 26). Protein concentrations were determined from absorbance at 280nm based on extinction coefficients predicted by ExPASy server359 (33920 $M^{-1}cm^{-1}$ for αBa, swap1 and swap2; 30940 M^{-1} cm^{-1} for swap3 and swap).

Expression, purification, and labelling of T4-Lysozyme

T4L-L46A mutant was expressed, purified, and labelled with monobromobimane as described previously (Claxton et al., 2008, McHaourab et al., 1996, McHaourab et al., 2002). Briefly, *Escherichia coli* cultures inoculated from overnight seeds were grown by shaking at 37°C until OD600 ~ 1 and induced by 0.4 mM isopropyl-β-D-thiogalactopyranoside (IPTG). After 3 hr induction at 30°C, the cells were harvested by centrifugation, resuspended into the lysis buffer (25mM MOPS, 25mM Tris, pH 7.6; 1mM EDTA, 0.02% (w/v) NaN_3, 10 mM DTT), disrupted by sonication and centrifuged (15000 xg). T4L protein was purified by cation exchange on Resource S column (Pharmacia) by eluting with linear gradient of 1M NaCl. The eluted protein

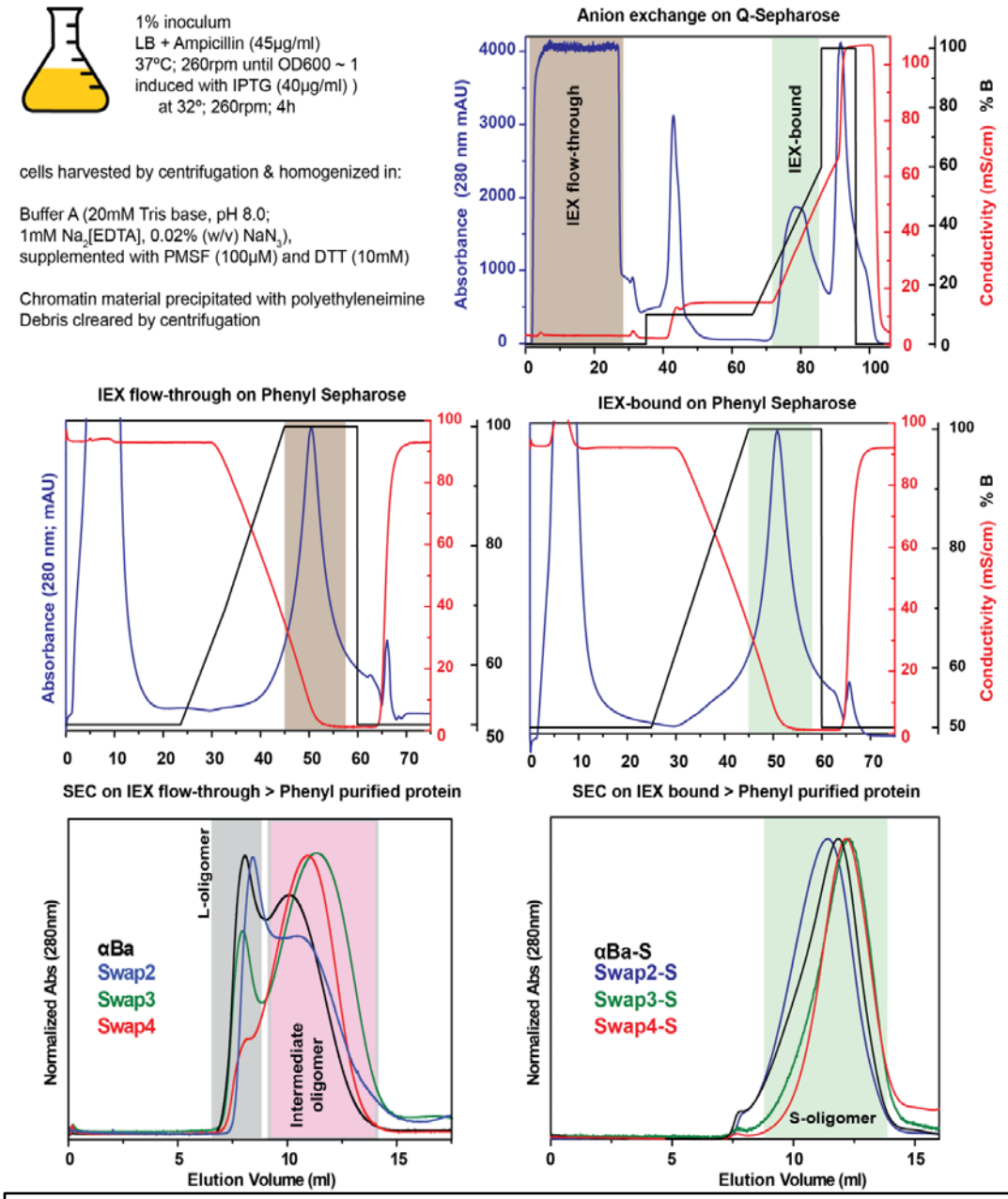

Figure 25: Purification scheme of Zf-αBa and swapped variants

The proteins were expressed in *E. coli* cells and were purified after cell lysis and centrifugation by sequential anion exchange, hydrophobic interaction and size exclusion chromatography. Protein fractions not bound by the Sepharose-Q column yielded larger oligomers, than the fractions bound by the Q-column.

was incubated with 10-fold excess of monobromobimane for two hours at room temperature, followed by overnight incubation at 4°C. Unbound label was removed in the subsequent size exclusion chromatography (SEC) on a Superdex 75 10/300 GL column (GE Healthcare Life Sciences) eluted in SEC buffer (9mM MOPS, 6mM Tris, pH 7.2).

Analytical size exclusion chromatography

Analytical SEC on purified proteins was performed on Superose 6, 10/300 GL column (GE Healthcare Life Sciences) equilibrated in the SEC buffer (9mM MOPS, 6mM Tris, pH 7.2) in an HP1100 HPLC system (Agilent). Elution profiles of the proteins were monitored by absorption at 280nm wavelength using a UV detector and by the tryptophan fluorescence (Excitation: 295nm; Emission 330nm) using a fluorescence detector. Proteins were injected from a 100µl loop at the indicated concentrations at an isocratic flow rate of 0.5ml/min.

Molar mass determination by multi-angle light scattering

Molar mass of the proteins were determined by the multi-angle laser light-scattering detector (Wyatt Technologies) connected in-tandem to a refractive Index (RI) detector (Agilent). 100µl of each protein at 1mg/ml concentrations was injected by an Agilent HP1100 HPLC system on a Superose 6 column equilibrated in the SEC buffer at the isocratic flow rate of 0.5ml/min. The elution of the proteins was also monitored by an absorbance detector. The molar mass of the proteins were calculated by the Astra software (Wyatt) from the concentration of proteins derived from the RI signal based on constant dn/dc (0.185 ml/g).

Oligomer size assessment by *analytical ultracentrifugation*

Molar mass of the proteins were also determined by the sedimentation velocity experiments conducted with Optima XLA Ultracentrifuge coupled to an interference optical system

(Beckman-Coulter). 397µl protein samples (OD280 ~ 0.3) and 400µl SEC buffer as reference were loaded into quartz windows double sector cells with Epon charcoal-filled centerpieces (path length 12mm). The AUC experiments were conducted at 4°C in a four-hole An-60 Ti rotor (Beckman) spun at 25,000 rpm (~50 *xg*); R_{min} = 5.8, and R_{max} = 7.3. At least 150 absorbance scans were collected for each experiment and the concentration profiles were obtained at 280nm. Partial specific volumes and molecular masses for αB-variants were calculated using the program SednTerp from the amino acid compositions (Lebowitz et al., 2002) and the velocity scans were analyzed with the program SEDFIT (Schuck, 2000, Lebowitz et al., 2002). The experimental parameters were validated by running BSA (Sigma) and T4-Lysozyme.

Negative stain transmission electron microscopy

5µl droplets of proteins at 10 nM monomeric concentrations were applied for three minutes to freshly glow discharged solid carbon support on copper 400 lines/inch square mesh TEM grids (Electron Microscopy Sciences). The drops were air dried and were washed twice with deionized water. Excess water was blotted away and replaced with pH neutralized 0.75% (w/v) uranyl formate solution, then allowed to air dry (Booth et al., 2011). Prepared grids were visualized at a nominal magnification of 14,000x on an FEI Morgagni operating at 100 kV. Digital images were captured by Images were recorded on an ATM 1Kx1K CCD camera.

Equilibrium binding assay of T4L-L46A to the αBa variants

Solutions of monobromobimane-labelled T4L-L46A at final concentration of 3µM with increasing molar excess of αBa variants diluted in the SEC buffer were incubated at 37 ºC for 2 h. The fluorescence anisotropy was measured in a SynergyH4 microplate reader (BioTek) at 37 ºC. The monobromobimane label was excited by 380nm filter (bandpass 20nm) and the emission fluorescence intensities in the perpendicular ($\perp$) and parallel ($\parallel$) polarizations were read by

460nm filter (bandpass 40nm). The steady state anisotropy (r) was calculated by the equation: $r = \frac{(I_{\parallel} - I_{\perp})}{(I_{\parallel} - 2I_{\perp})}$. Binding isotherms were generated by plotting bimane anisotropy as a function of the $\frac{[\alpha Ba]}{[T4L]}$ ratio. The binding isotherms were analyzed by Origin 8 (OriginLab Corporation, Northampton, MA) using the nonlinear least-squares fit by the Levenberg– Marquardt method (Marquardt, 1963). The K_D is reported with ± the standard deviation (s.d.) of the fit error.

Results

αBa and variants segregate into two distinct oligomeric ensembles

In contrast to the human αB-crystallin, zebrafish αBa and its engineered variants formed two distinct protein populations that present distinctly different electrostatic surfaces under the experimental conditions. The two populations of αBa and the engineered variants eluted at different ionic strengths from the anion exchange column (Figure 25). One population, hereafter referred to as αBa-S, bound the Q Sepharose resin at pH 8 and purified under similar conditions as human αB or the zebrafish αA and αBb (Koteiche et al., 2015). The other population, referred to as αBa-L, was excluded by the Q Sepharose resin at pH 8.0. While both the populations were have identical behavior on the hydrophobic interaction chromatography (HIC), subsequent size exclusion chromatography revealed distinct elution patterns in which the αBa-S ensemble eluted ~5.5 mL after the αBa-L ensemble suggesting either a larger hydrodynamic volume or a larger oligomeric size for the αBa-L compared to αBa-S. As shown by the denaturing SDS-PAGE in Figure 26 and confirmed by the mass spectrometry, the two oligomeric populations of the αBa- and variants originate from same ~20kDa monomeric protein of identical amino acid sequences. The oligomeric populations were stable so far as the SEC profiles of the isolated S- and the L-oligomers did not change after incubation in the buffers at pH 6.0, pH 7.2, or pH 8.2 at room temperature as shown in the Figure 27.

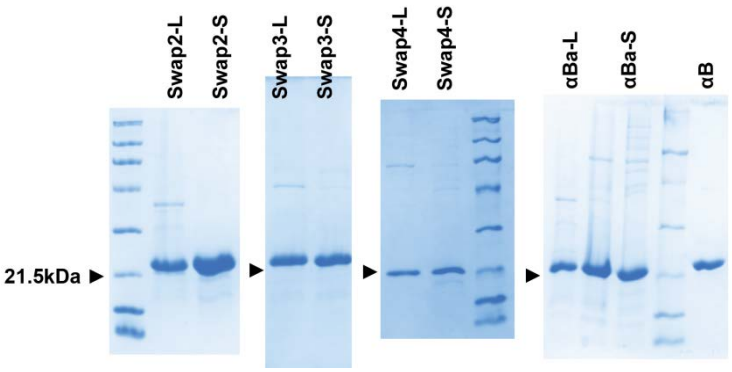

Figure 26: SDS-PAGE of αBa and its engineered variants.

The S- and the L- oligomers of the αBa- and variants originate from identical monomers. The arrowheads point to the position of the 21.5kDa protein ladder (BioRad). All proteins ran at a larger apparent molar mass than calculated monomeric weights (αBa = 18692, Swap2 = 20263, Swap3 = 19870, Swap4 = 20124 g^{-1} mol^{-1})

The L- and the S- oligomers of αBa have different oligomer assembly

Since the elution profile on SEC correspond to a fairly large molecular size for the αBa oligomers, we utilized negative stain transmission Electron Microscopy to assess the polydispersity of the protein assembly, and to visualize the general shape of the solvent-excluded surface of the two αBa oligomeric species. αBa samples negatively stained with uranyl formate and air dried revealed a highly polydisperse assembly for both the αBa-S and the αBa-L form (Figure 28). The particles of both forms were very heterogenous, highly amorphous and lacked well-defined arrangements, preventing us from extracting structural information from the EM images. However, the EM images reveal a contrast in the subunit arrangement between the S- and the L-form. While the particles in the S-form approached a spherical arrangement, the particles of L-form appeared fibrillar with elongated and polymorphic assemblies resembling the

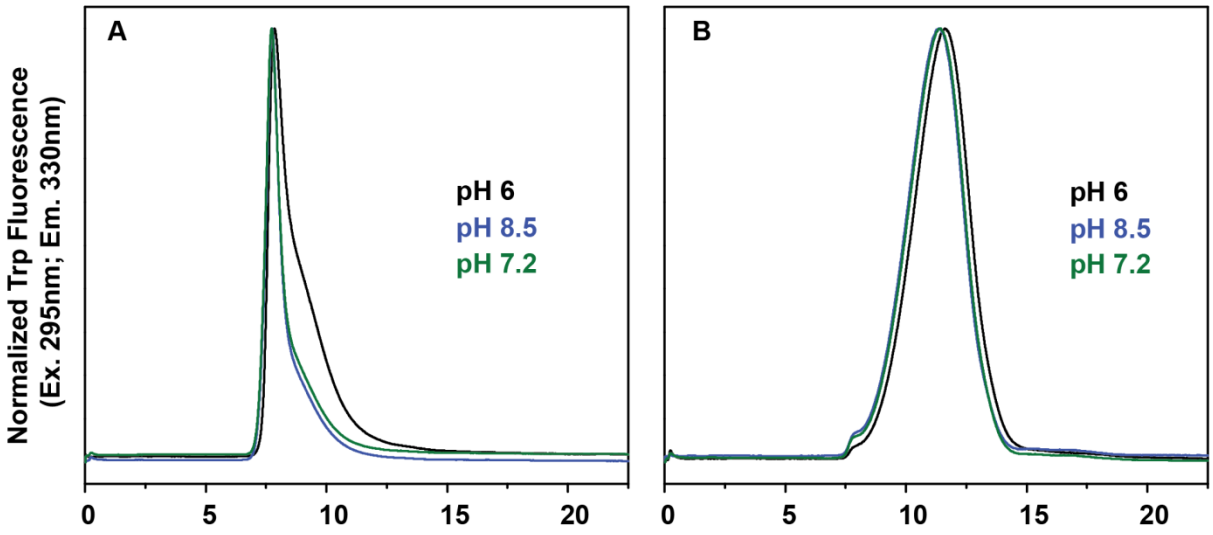

Figure 27: The effect of pH on the oligomeric forms of αBa

SEC profiles of the (A) L-form, and the (B) S-form, eluted from the Superose-6 column equilibrated in the buffer at pH 6 (Black trace), pH 7.2 (green trace); and pH 8.5 (Blue trace). The proteins purified in SEC buffer; pH 7.2 were diluted to 1mg/ml in the respective elution buffers: pH 6 buffer (15mM MES, 50mM NaCl, 0.1mM EDTA, 0.02% sodium azide); pH 7.2 buffer (9mM Tris, 6mM MES, 50mM NaCl, 0.1mM EDTA, 0.02% sodium azide); and pH 8.5 buffer (10mM Tris, 5 mM MES, 50mM NaCl, 0.1mM EDTA, 0.02% sodium azide) . 100µl proteins were injected in each run.

αB particles previously described to form under destabilizing conditions (Meehan et al., 2007, Meehan et al., 2004).

N-terminal domain of αBa promotes formation of larger oligomers

To evaluate the role of residues flanking the ACD in the atypical assembly of the αBa oligomers, we compared the relative distribution of the S- and the L-form oligomers of the engineered NTD and the CTD variants of αBa (Figure 29 A).

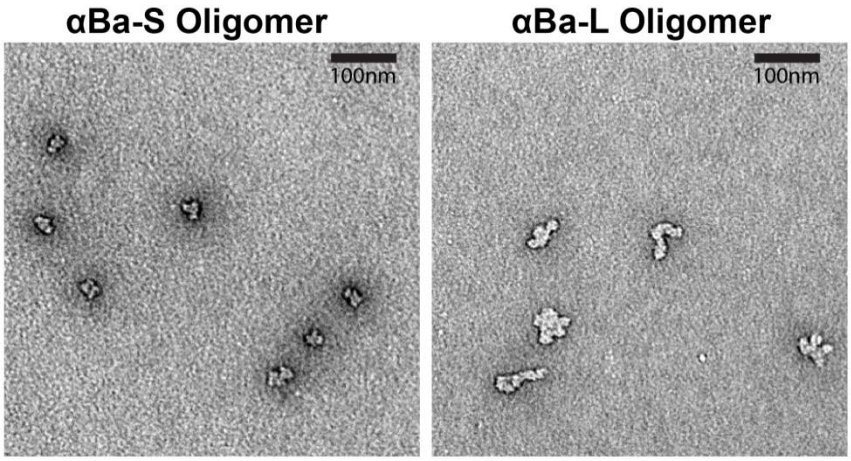

Figure 28: Electron microscopy image of S- and L- oligomers of αBa

Transmission electron microscopy image of the negative stained particles of αBa-S and αBa-L particles showing polydisperse and very different arrangement of the subunits in the two forms.

Since swapping of the zebrafish sequences with the human sequences did not affect the *in vitro* expression of the proteins, we normalized the yields between the variants to compare the relative oligomeric populations. While swapping the entire CTD (amino acids 144-168) of the αBa with αB sequence (148-175) in Swap2 enhanced the relative yield of the L-form (Figure 29 B and E), swapping of the NTD had the opposite effect (Figure 29 C and E) in a length dependent manner. With the increased contribution of the αB sequence in Swap4 compared to Swap3 (Figure 29 A), the relative yield of the L-form was reduced to 6.7±2.5% of the total protein as compared to 30.3±6.8% in wild type αBa.

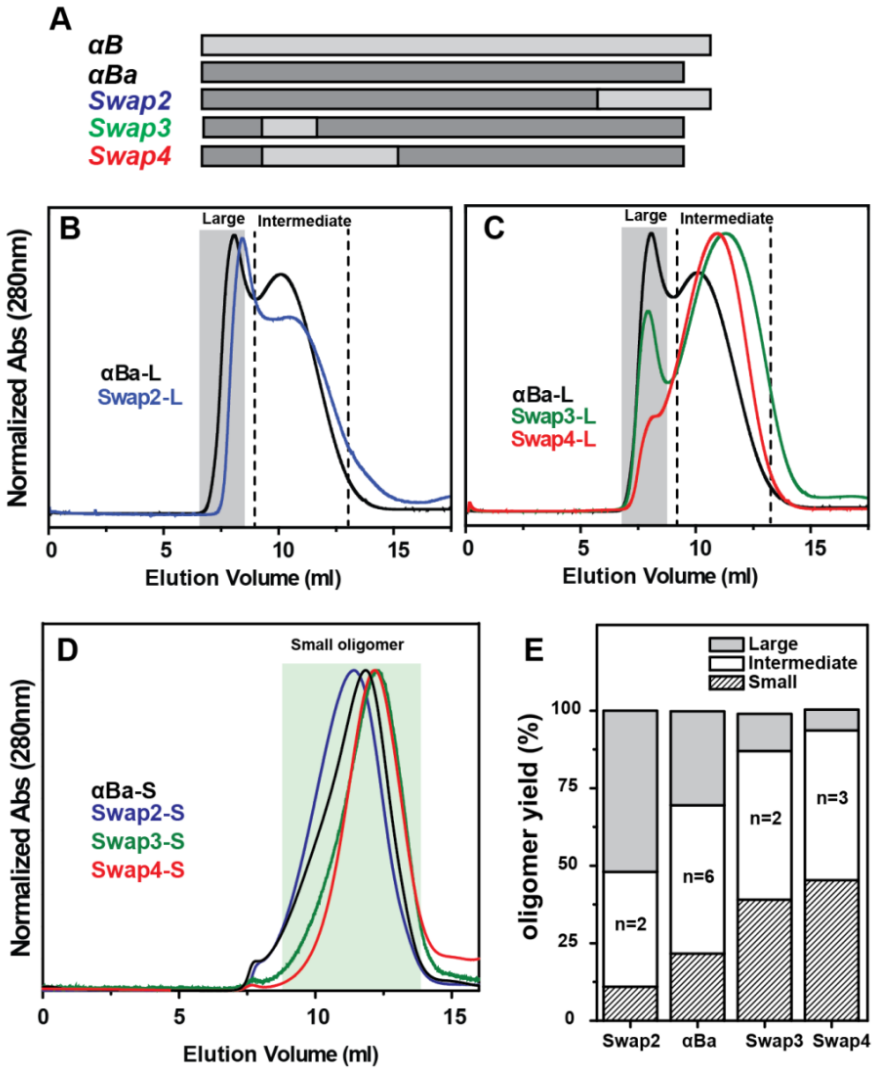

Figure 29: Relative yields of the oligomers upon swapping the C- and N- domains

(A) The schematic of the variants: αB sequence (light gray), αBa (dark gray); (B) the SEC profiles of the L- oligomers of αBa and Swap2 showing enhancement in the relative yield of the L-form; (C) the SEC profiles of the L-oligomers of αBa, Swap3 and Swap4 showing diminishing relative yield of the L-form with decreasing contribution of the zebrafish αBa NTD (αBa > Swap3 > Swap4); (D) SEC profiles of the S- oligomers showing similar elution pattern of the proteins; (E) relative oligomeric yields of each variants calculated by 100x(oliogomer/total) concentration (in mg)

Accordingly, the relative proportion of the S-form in Swap4 increased from 21.7±9.8% to 45.3±13% in the wild type αBa. However, the swapping of the NTD did not change the heterogeneity or the appearance of the particles of the Swap4-L and the Swap4-S forms relative to the wild type oligomers, as visualized by the negative stain electron microscopy.

The NTD influences the polydispersity of αBa oligomers

The Electron Microscopy of the negatively stained particles of αBa revealed a highly heterogenous assembly for both the S- and the L- oligomeric forms of αBa. Prompted by this, we evaluated the influence of the C- and the N- terminal domains on the polydispersity of the αBa and its variants by multi angle static light scattering (MALS) as the purified proteins eluted from a tandem SEC (Figure 30 A and B). From MALS the molecular weights of oligomeric protein particles were calculated independent of the amino acid sequence variations based on the approximation that all proteins have the same refractive index increment (dn/dc) (Wyatt, 2014, Zhao et al., 2011a). The shape of the distribution of molecular weights deduced from the angular distribution of the intensity of the light scattering reflects the polydispersity of the sample. As shown in Figure 30(A) and Figure 30(B) by the scatterplot of the molecular weights (left Y-axis) overlaid on the SEC profiles (right Y-axis), swapping of the NTD in the Swap3 (green points and traces) and Swap4 (red points and traces) enhanced the polydispersity of both the L-form (Figure 30 A) and the S-form (Figure 30 B). In the S-form, progressively diminishing the contribution of the NTD of αBa sequence by homologous αB NTD sequence (αBa > Swap3 > Swap4) reduced the average molar mass of the oligomer from 1.03×10^6 g/mol for αBa to 0.97×10^6 g/mol for Swap3 and to 0.83×10^6 g/mol for Swap4. In comparison, swapping of the CTD did not qualitatively affect the polydispersity of either form, although it had opposite effect on the oligomeric size of the Swap2 L-form versus the S-form. The molar mass of the S-form of Swap2 was 0.82×10^6 g/mol.

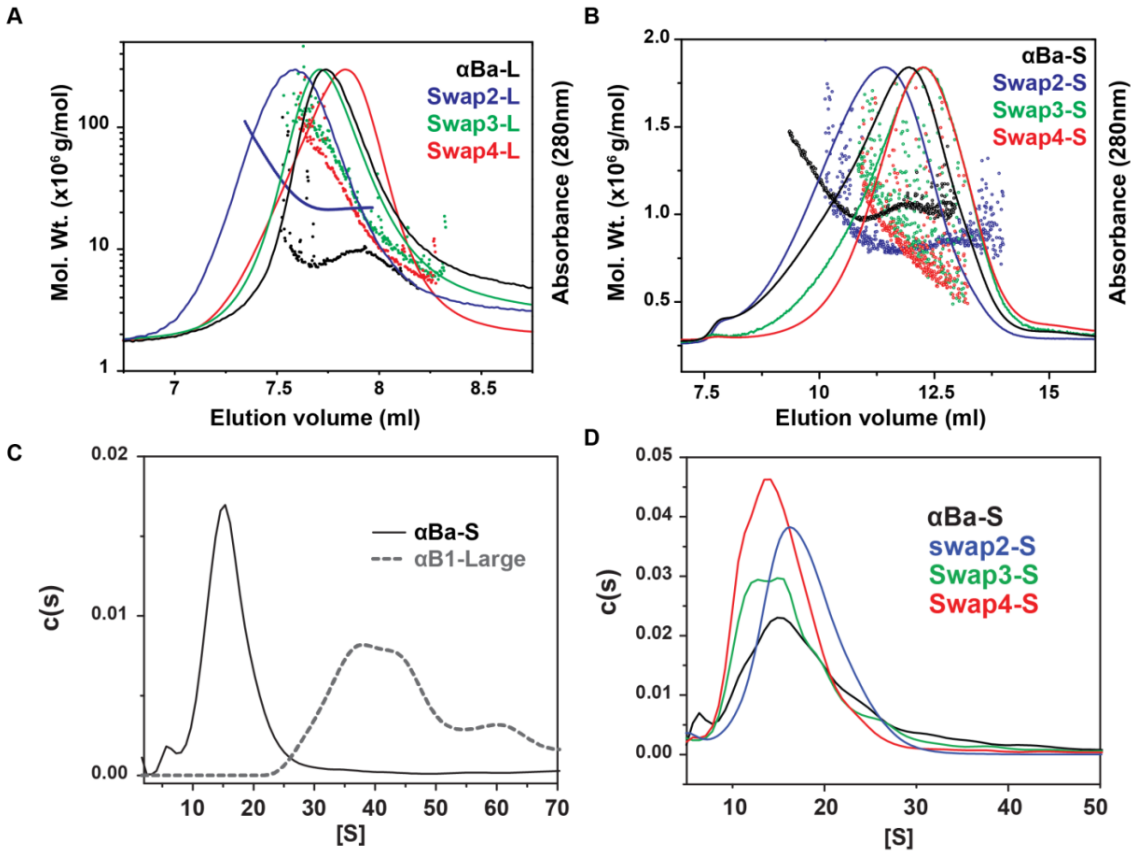

Figure 30: The distribution of molar mass of the oligomeric forms of αBa and variants

A and B: SEC profile (right Y axis) overlaid with molar mass (left Y-axis) calculated from light scattering as the proteins: αBa-S (black), Swap2 –S (blue), Swap3-S (green) and Swap4-S (red)) eluted from the SEC column (X-axis) (A) the L-forms; (B) the S-forms; C and D: normalized c(s) distribution curves calculated from the sedimentation velocity AUC experiments for (C) αBa-S (black line), αBa-L (gray dotted line); (D) αBa-S (black), Swap2 –S (blue), Swap3-S (green) and Swap4-S (red).

In a population of polydisperse non-spherical oligomers, such as the L-form of αBa, the molar masses measured by MALS may be overestimated by a small fraction of substantially large particles (Li et al., 2011). Therefore, to confirm that the L-form of αBa was indeed a larger oligomeric assembly, we chose sedimentation velocity experiments by analytical ultracentrifugation (AUC), where the oligomers can be better separated and analyzed. We centrifuged equal monomer concentration of the oligomeric forms at 25,000 rpm, and from the progression of the protein boundary, the sedimentation curves were fitted to a continuous sedimentation coefficient distribution, c(s) model. As shown in Figure 30(C), αBa-L boundary moved at a larger sedimentation coefficient than the αBa-S form. Also, αBa-L sedimentation profile resolved into a multimodal distribution of populations that further attested to the high polydispersity detected by the transmission electron microscopy and the light scattering. In agreement with the light scattering, the analytical ultracentrifugation Figure 30(D) showed that c(s) profiles of Swap3-S and Swap4-S shifted towards lower sedimentation coefficients (*S*) confirming their smaller average oligomeric sizes compared to αBa.

Substrate affinity of αBa corresponds to the oligomeric assembly

We compared the zebrafish αBa oligomeric subpopulations for their affinity towards an established model substrate, a destabilized mutant of T4L where Leu46 is mutated to Ala, by monitoring complex formation by anisotropy binding isotherms between increasing molar concentrations of the α-crystallin and the fixed concentration of the fluorescently label T4L-L46A at 37 °C (Koteiche et al., 2015, Claxton et al., 2008). From the nonlinear least squares fits to the binding curves, the binding capacity (*n*) or the affinity (K_D) of the chaperone can be deduced. As shown in the Figure 31, the L-form oligomers demonstrated highly elevated binding affinity to the T4L-L46A substrate relative to the S- form oligomers.

That swapping the NTD had no effect on the chaperone-like activity of Swap4 as compared to the αBa is consonant with their similar molar mass distribution, as measured by light scattering analysis (Figure 30 A). Further, the change in the oligomeric distribution of the S-form, caused by the swapping of the NTD, as in Swap3 and Swap4 led to lower affinity of the chaperones towards the model substrate T4L-L46A as shown in the in Figure 31(A) and summarized in the Table 2.

Table 2: Affinity of αBa-S oligomers for T4L-L46A mutant

(T4L-L46A was 3μM, and the data was fitted with *n*=0.25)

sHSP	K_D ± SE (μM)
αBa-S	6.37 ± 0.79
Swap2-S	8.72 ± 2.47
Swap3-S	11.50 ± 1.78
Swap4-S	10.19 ± 1.85

In agreement with the similar molar mass distributions of αBa-S and Swap2-S, their substrate affinities (K_D) are comparable; while a downward trend in the molar masses of the oligomers between αBa > Swap3 > Swap4 is reflected in the decreasing trend in their substrate affinities (K_D).

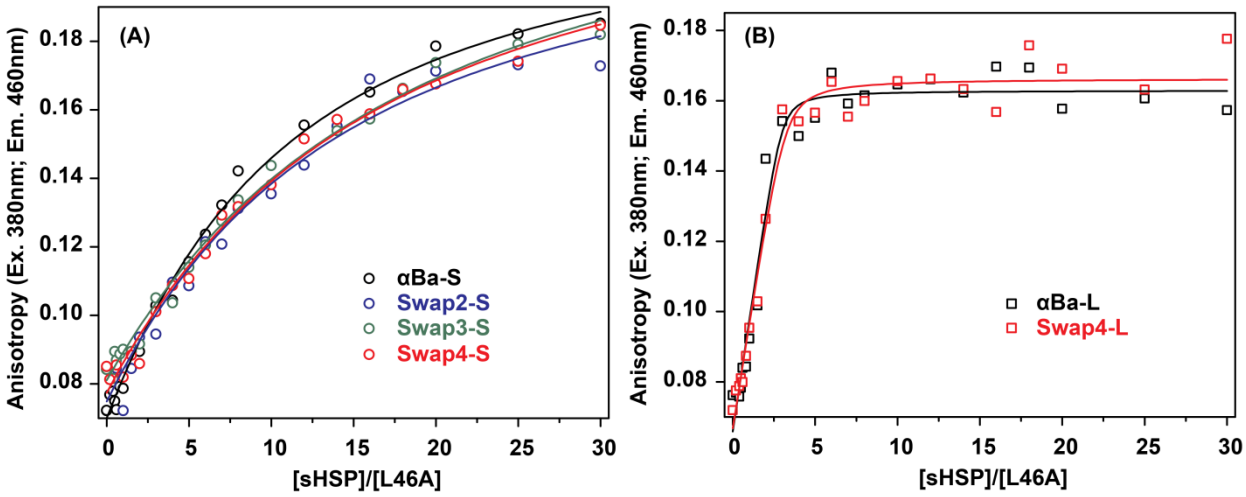

Figure 31: Binding isotherms for the S- and the L-forms of αBa and swap variants.

Molar excess of the sHSP, as indicated on the X-axis, were incubated at 37 ºC for 2 h with monobromobimane-labelled T4L-L46A (3 μM) in the SEC buffer (pH 7.2). The anisotropy of the fluorescence of the bound label (Y-axis) was measured. The solid lines are nonlinear least-squares fits to the data. (A) Binding isotherms of the S-form of αBa (black line), Swap2 (blue), Swap3 (green) and Swap4 (red); (B) Binding isotherms of the L-form of αBa (black line) and Swap4 (red).

Discussion

αB-crystallin plays an important role in the diverse physiological functions and the polydispersity of the oligomeric distribution of αB is critically important for its biochemical role (Benesch et al., 2008). Perturbations of the oligomeric distribution of αB by biochemical modification, such as phosphorylation or truncation affect its chaperone activity (Thornell and Aquilina, 2015, Ecroyd et al., 2007, Aquilina et al., 2003). The zebrafish orthologs αBa and αBb display a much higher chaperone-like activity compared to the human αB-crystallin and even among the paralogs, αBa displayed an order of magnitude higher affinity with greater capacity towards the substrate

(Koteiche et al., 2015, Sathish et al., 2003). sHSPs display two forms of activity: a low affinity state and a high affinity state (Claxton et al., 2008, Haslbeck et al., 2005). While low affinity binding recognizes substantially unfolded proteins, the high affinity binding mode recognizes compact states, likely early in the unfolding pathway which have not undergone global unfolding (Sathish et al., 2003). CryoEM and EPR studies of the Hsp16.5-WT with T4L complexes have uncovered that the high affinity binding, more relevant to the physiological role of the sHSPs, requires an oligomeric expansion although the low affinity mode of binding that occurs on the outer surface of the sHSP oligomer can occur without a significant oligomeric reorganization (Shi et al., 2013, Shi et al., 2006a). The N-terminal region plays a central role in the substrate recognition which can induce the oligomeric reorganization. A transition between the two binding affinity forms, different in oligomeric packing is an elegant mechanism of regulating the chaperone activity of sHSPs (Claxton et al., 2008, Haslbeck et al., 2005, Benesch et al., 2008).

sHSP oligomers expanded by protein engineering have been shown to have enhanced *in vitro* chaperone like activity and such expansion *in vivo* can be a physiologically relevant mechanism of high affinity substrate surveillance in the finely balanced crowded lens environment (Shi et al., 2013, Shi et al., 2006a, Mishra et al., 2018). Segregation of αBa into oligomeric populations with very different affinities towards the same substrate, as shown in this and a previous work could represent a mechanism of self-regulating chaperone activity of αBa without dependence on an external biochemical modification, such as phosphorylation (Koteiche et al., 2015). In fact, αBa-S binds substrates with affinities that approach other sHSPs only after biochemical activation, such as the mutation mimicking the triply phosphorylated state (S19D/S45D/S59D) of αB-crystallin (referred to as αB-D3), and the triply phosphorylated mimic (S15D/S78D/S82D) of Hsp27 (referred to as Hsp27-D3) (Koteiche et al., 2015). This suggests that zebrafish αBa is a chaperone that operates in a highly activated state, facilitated by an

expanded oligomer, and provides a possible example of the sHSP activation by the expansion of the oligomer different from the phosphorylation-induced activation by dissociation (Figure 32) (Peschek et al., 2013, Koteiche and McHaourab, 2003, Ecroyd et al., 2007).

Both, the expansion or the dissociation can structurally provide access of the substrate

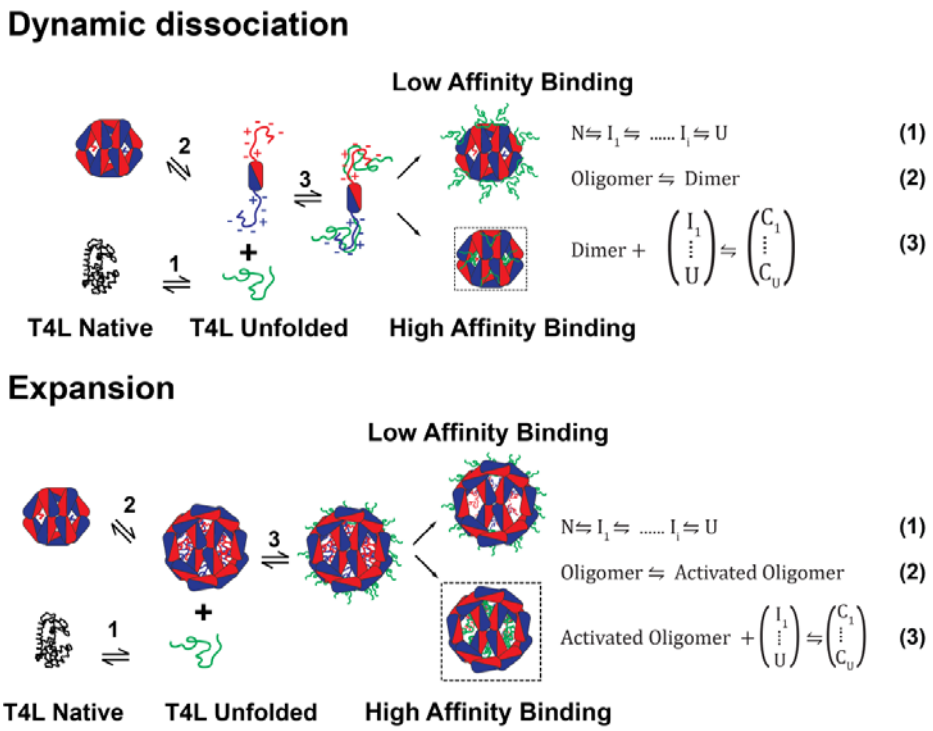

Figure 32: Expansion of the oligomer as a mechanism of the activation of sHSP.

In the dynamic dissociation, the equation 1 describes substrate unfolding on a pathway that might involve intermediate states. Equation 2 demonstrates that sHSP oligomeric structures are conformationally flexible. Phosphorylation activates substrate binding by shifting the equilibrium between oligomers and protomers. Alternatively, N-terminal region accessibility can be increased by oligomer expansion. In expansion, the equation 2 describes equilibrium between resting and active sHsp. In both mechanisms, the equation 3 describes complex formation between sHsp and substrate in low and high affinity binding.

to the NTD and thereby increase the affinity of the sHSP resulting in the enhanced chaperone activity. Polydispersity of sHSP oligomers is a mechanism for regulation of binding affinity and capacity. While the dynamic dissociation of oligomers exposes a highly flexible NTD containing putative substrate interaction sites which are otherwise inaccessible; expansion of the sHSP oligomers also increases the accessibility of the N-terminal region (Shi et al., 2013, McDonald et al., 2012). Thus, the energetic threshold for substrate binding is also determined by accessibility of the sHSP binding regions, expressed in eq. 2, in the schematic given in Figure 32 as equilibrium between resting and active sHsp.

Do the similar affinities of Swap3 and Swap4 indicate that the shared NTD sequence elements removed from αBa in these variants is the primary facilitator or determinant of binding and/or oligomer properties? The work presented here did not address whether the S- and the L-forms represent the resting or the active forms *per se*. But, this work illustrates that the oligomeric distribution of αBa is affected by the immediate sequences flanking the ACD. Since the oligomeric states could be altered by the homologous sequence, a change in the presentation of the sequences buried between protomeric assemblies could possibly represent a mechanism of allosteric self-regulation of αBa chaperone activity, whereby the substrate interaction could alter the oligomeric equilibrium and thereby regulate the activity of the chaperone. That the affinity of the S-form of αBa could be modulated by swapping the NTD of the orthologous αB sequences reemphasizes the role of the sequences flanking the ACD in the sHSP. The flanking sequences, especially the NTD play a critical role in the recognition of the substrate by the sHSP and have been shown to affect the oligomeric distribution (McDonald et al., 2012, Bova et al., 2000, Bova et al., 1997, Basha et al., 2006, Jehle et al., 2011, Jehle et al., 2010).

Therefore, it can be hypothesized that the high degree of evolutionary divergence in the flanking sequences, coupled with their role in modulating the oligomeric distribution and thereby changing the substrate binding activity of the sHSP ensemble reflects an evolutionary optimization of the proteostatic need of the organism. As has been shown elsewhere by expansion of a highly monodisperse symmetrical Archean Hsp16.5–P1, and by further change in the oligomeric distribution of the expanded oligomer by sequential alteration of the inserted peptide, the NTD has the ability encoded in its sequence to re-sculpture the oligomeric structure of sHSPS across taxa (Mishra et al., 2018, Shi et al., 2013, McHaourab et al., 2011a, Shi et al., 2006a). This plasticity in the oligomeric organization of the sHSPs, supported by the sequence elements could be of critical importance in the response of sHSPs towards the need of sequestering an array of structurally diverse client proteins and in the performance of the sHSPs in preventing the collapse of a proteome under stress.

CHAPTER III

LOSS OF αB-CRYSTALLIN FUNCTION IN ZEBRAFISH REVEALS CRITICAL ROLES IN THE DEVELOPMENT OF THE LENS AND STRESS RESISTANCE OF THE HEART

Introduction

αB-crystallin (*Cryab* or *HspB5*), expressed constitutively in multiple tissues and organs including the lens, heart and skeletal muscles (Boelens, 2014, Arrigo et al., 2007), can be transcriptionally induced by stress through the binding of heat shock transcription factor 1 (Hsf1) to a heat shock element in its promoter (Akerfelt et al., 2010). While initially characterized by its function as a molecular chaperone (Horwitz, 1992, Jakob et al., 1993, Muchowski et al., 1997, Koteiche and McHaourab, 2003), αB-crystallin appears to have physiological roles that transcend the non-specific binding of destabilized proteins (Reddy and Reddy, 2015, Mymrikov et al., 2017). For example, it has been associated with the integrity of Desmin, implicated in binding of Titin in the heart and intermediate filaments in the lens (Bullard et al., 2004, Bennardini et al., 1992, Nicholl and Quinlan, 1994), and more recently in direct regulation of Argonaute2 (Neppl et al., 2014).

The diversity of its molecular targets endows αB-crystallin with a pivotal role in the physiology of the heart and transparency of the lens (Boelens, 2014, Clark, 2016). Indeed, a number of mutations in αB-crystallin have been associated with severe pathologies of the lens, heart and skeletal muscles (Selcen and Engel, 2003, Simon et al., 2007, Forrest et al., 2011), including the R120G mutation, which is associated with Desmin-related myopathy in humans (Vicart et al., 1998). While the detailed mechanisms by which these mutations lead to pathology are not fully delineated, they collectively suggest a critical role for this protein in signaling networks that safeguard and maintain cellular proteostasis (Boelens, 2014).

While a role of αB-crystallin in the proteostasis network is well established and its involvement in the physiology and homeostasis of multiple tissues is supported by direct evidence, a detailed understanding of the molecular mechanisms underlying these roles is yet to emerge. An attempt to generate a knockout mouse line was confounded by the inadvertent knockout of HspB2, another sHSP with a presumed role in the development of muscle tissues (Brady et al., 2001). Although the knockout mice developed progressive myopathy into adulthood (Brady et al., 2001), disentangling the contributions of the two sHSP has proven challenging (Pinz et al., 2008, Benjamin et al., 2007).

Here we capitalized on the intrinsic advantages of the zebrafish as a vertebrate model system to carry out a detailed investigation of the consequences of αB-crystallin loss of function on lens and heart development. We find that whereas disruption of the two αB-crystallin genes leads to lens defects, they are not essential for cardiac development under normal rearing conditions. Rather, a novel role of αB-crystallins is uncovered under stress conditions, specifically in response to glucocorticoid receptor (GR) signaling. Zebrafish lines deficient in either αBa or αBb develop cardiac edema when embryos are subjected to crowding conditions or challenged with GR agonists. Together, our results provide novel insights on the physiological roles of vertebrate αB-crystallins.

Material and Methods

Zebrafish maintenance and breeding

AB wild-type strain zebrafish (*Danio rerio*) were used. The embryos were obtained by natural spawning and raised at 28.5°C on a 14/10 hour light/dark cycle in 0.3x Danieau water containing 0.003% 1-phenyl 2-thiourea (PTU) (w/v) to prevent pigment formation. Embryos were staged according to their ages (days post-fertilization, dpf). Following mutant and transgenic fish

lines were used: *cryaa*^{vu532} (Zou et al., 2015), *cryaba*^{vu537} (*αBa*^{35bpDEL}), *cryabb*^{vu538} (*αBb*^{10bpDEL}), Tg(*cryaa*:*cryabb*,*myl7*:TagRFP)^{vu539Tg} (Tg[*cryabb*]). All animal procedures were approved by the Vanderbilt University Institutional Animal Care and Use Committee.

Generation of Cryab mutants with CRISPR/Cas9 system

To establish zebrafish mutant lines of *Cryaba* and *Cryabb*, gRNAs targeting the first exons of *Cryaba* and *Cryabb* genes were designed and screened to induce indels by injection with Cas9 mRNA in zebrafish. Several mutant lines were established using four designed gRNAs for each gene (Table 3). Used gRNA target sequences are presented in Table 6. Each *Cryab* mutant allele was outcrossed to AB for at least two generations, then in-crossed to generate homozygous mutants, which were analyzed for phenotypes. Each clutch was carefully examined to rule out any unusual phenotypes arising due to possible off-target effects of CRISPR.

Zebrafish transgenesis

To establish the transgenic zebrafish expressing zebrafish *cryabb* gene specifically in the lens, Tg(*cryaa*:*cryabb*,*myl7*:TagRFP) was constructed by MultiSite Gateway (Invitrogen) assembly reactions using protocols established previously (Tol2kit; (Kwan et al., 2007). Briefly, entry vectors, p5E-Cryaa (Hayes et al., 2012) and p3E-polyA were assembled with pME-Cryabb and recombined into pDestTol2CR2 vector for microinjections. Tol2-mediated transgenesis were performed as previously descried (Zou et al., 2015).

Morpholino knockdown

Translation-blocking morpholino antisense oligo (MO) against the potential alternative start site of *cryaba*^{35bpDEL} allele was designed and synthesized by Gene Tools (5’-

GGACGATAGTAAAACATGGTGTAGA-3'; Philomath, OR). 5ng MO was injected into the yolk of 1-2 cell stage zygotes, which were the progenies from *cryaba*$^{-/-}$ incross.

Crowding and drug treatments

For crowding stress, 1dpf embryos were manually dechorined and 75 embryos were placed in one well of a 6-well plate (polystyrene, tissue culture grade) with 5ml of 0.3x Danieau water. For control, 15 embryos per well were used as non-stressed condition. To mimic the effect of glucocorticoid stress, we used pharmacological stimulation by treating embryos with 50μM dexamethasone (Sigma, D1756) and 50μM hydrocortisone (Sigma, H2270) diluted in 0.3x Danieau water (24-well plate, 10embyos/well) from 1dpf until 4dpf to examine the cardiac phenotypes. The optimal dosage of dexamethasone and hydrocortisone were determined after dose-response analysis.

Western analysis

Both lenses of each adult zebrafish (WT and *Cryab* mutants) were excised, washed and homogenized in the lysis buffer (20mM Tris HCl pH 7.6, 100mM NaCl, 1mM NaN_3, 1mM EDTA) (Horwitz, 1992) supplemented with 1mM PMSF and C0mplete protease cocktail (Roche). The homogenates were centrifuged at 15,000 *xg* at 4 ºC to separate water-soluble and water-insoluble fractions. After adding 2x Laemmli sample buffer supplemented with DTT, both fractions were heated in water bath for 5 min, and spun at 15,000 *xg* to clear the solutions. Protein concentrations were measured by RcDc protein assay kit (BioRad). 10μg total proteins separated by 12% SDS-PAGE were blotted to nitrocellulose membrane in Towbin buffer, and probed with custom Anti-αA and Anti-αBa polyclonal antibodies (Vanderbilt Antibody and Protein Resource Core), which were generated by injecting full-length αA and αBa proteins, purified from bacterial expression system, as described previously (Koteiche et al., 2015), in

rabbits. Antisera from two rabbits each, for both proteins were tested for titre and after booster shots, antibodies were affinity purified from the final bleeds using purified proteins as antigens. The blots were visualized by Anti-HRP secondary antibody (Promega) using enhanced chemiluminescence. (HyGLO™ Quick Spray Chemiluminescent; Denville Scientific Inc.). The cDNA construct encoding the N-terminal truncated αBa protein (Δ1-43aa) was generated by PCR, cloned into pET-20b(+) bacterial expression vector (Novagen), and expressed in *E. coli* as described in Chapter 2.

Whole-mount in situ hybridization (WMISH)

Linearized full-length coding sequence of *cryaba* and *cryabb*, with added T7 polymerase site was PCR amplified from the cDNA clones (obtained from Mason Posner (Ashland University, Ashland, Ohio). The Digoxigenin-labeled ISH probes were generated by transcribing with T7 RNA polymerase (NEB) and DIG RNA Labeling Mix (Roche). Subsequently, RNA probes were purified after Trizol precipitation using Direct-zol MiniPrep Kit (Zymo Research) and confirmed for purity and length (507bp for *cryaba*, 498bp for *cryabb*) by agarose gel electrophoresis. The whole-mount in situ hybridization on 2dpf embryos was performed according to the established protocol (Thisse and Thisse, 2014).

Quantitative RT-PCR

Total RNAs were isolated from embryos at desired stages by using Trizol Reagent (Invitrogen), followed by DNase treatment (Ambion). cDNA synthesis and qPCR using SYBR green were performed according to manufacturer's protocol (Bio-Rad). Three samples at indicated stages were collected and reactions were performed at least twice on each sample to determine ΔCT. The primers used in this study are listed in Table 9.

Cell death assays

Embryos were fixed overnight at 4°C in 4% paraformaldehyde in Phosphate Buffer Saline (PBS), dehydrated with 100% methanol and stored in -20°C. The procedures of TUNEL staining were carried out following the manufacturer's suggested protocol (In Situ Cell Death Detection Kit, TMR red - Sigma-Aldrich#12156792910).

Immunohistochemistry

Embryos were fixed overnight at 4°C in 4% paraformaldehyde in PBS and the anti-MF20 (ventricle) and anti-S46 (atrium) (Developmental Studies Hybridoma Bank) staining of the heart were performed as described (Yelon et al., 1999). The secondary antibodies used were anti-IgG2b-Alexa 568 (for MF20; Invitrogen) and the anti-IgG1-Alexa 488 (for S46; Invitrogen).

Heart Imaging and cardiac function measurements

Videos taken of the zebrafish hearts *in vivo* (Zeiss AxioZoom.V16 microscope) were used to calculate shortening fraction [calculate the shortening fraction (%) for the ventricle: (100) X (width at diastole–width at systole)/(width at diastole)] and heart rate (count the number of beats in 15 sec, then multiply the number of beats counted as beats/min), following the established protocol (Hoage et al., 2012)

Microscopy and image processing

Lenses of live embryos in 0.3x Daneau water with PTU/tricaine methanesulfonate were analyzed by bright field microscopy (Zeiss Axiovert 200) at 4dpf and graded into three classes depending on the severity of lens defects as defined in our previous study (Zou et al., 2015). Briefly, the phenotypic features appeared as either round, shiny crystal-like droplets spread across the lens that were classified as "Minor" defects, or large irregular protuberances located in the center of the lens classified as "Major" defects (Figure 33). Fluorescence images were taken with Zeiss AxioZoom.V16 microscope.

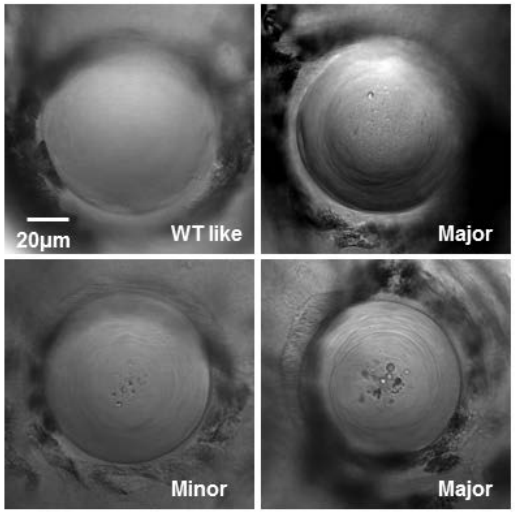

Figure 33: Three classes of lens phenotypes

The lens phenotype was graded into WT-like, minor lens defects; and major lens defects depending on the severity of lens defects. (Modified from (Zou et al., 2015)

iTRAQ quantification of protein changes

To quantify protein expression changes in zebrafish lenses, one lens from 6 month old fish of each genotype (WT, *cryaba*$^{-/-}$, *cryabb*$^{-/-}$ and *cryaba*$^{-/-}$; *cryabb*$^{-/-}$) were homogenized in 50 mL homogenizing buffer (25 mM Tris, 150 mM NaCl, 1 mM PMSF, 5 mM EDTA, 10 mM NaF, pH 7.5). The samples were centrifuged at 20,000 *xg* for 20 mins and pellets were washed with another 50 mL of homogenizing buffer followed by centrifugation at 20,000 *xg*. The supernatants were pooled together as the water-soluble fraction (WSF). Protein concentrations for WSF were measured by Bradford assay (Thermo Scientific, Rockford, IL). The pellets were considered as the water-insoluble fraction (WIF). WIF was washed with water twice, suspended in 100 mL of water, and an aliquot was mixed with equal volume of 5% SDS for BCA assay

(Thermo Scientific, Rockford, IL). 80 mg of WSF from each lens was reduced with 50 mM TCEP (Tris-(2-carboxyethyl)phosphine) at 60 °C for 1 hour, alkylated with 200 mM MMTS (methyl methanethiosulfonate) at room temperature for 10 min, and digested with sequencing-grade trypsin overnight. 20µg of each WSF fraction was then labeled with iTRAQ reagents according to the manufacturer's instructions (AB Sciex, Foster City, CA) (114 for WT, 115 for *cryaba*$^{-/-}$, 116 for *cryabb*$^{-/-}$ and 117 for *cryaba*$^{-/-}$; *cryabb*$^{-/-}$). For WIF, the entire reconstituted pellet for each WIF sample was digested with trypsin, and 18µg protein was labeled with iTRAQ reagents. Reagents were reconstituted in ethanol such that each protein sample was iTRAQ-labeled at a final concentration of 90% ethanol, and labeling was performed for 2 hours.

The iTRAQ-labeled samples were mixed, acidified with TFA, and were subsequently desalted by a modified Stage-tip method prior to LC-MS/MS analysis. iTRAQ labeled samples were analyzed using MudPIT analysis with 13 salt pulse steps (0 mM, 25 mM, 50 mM, 75 mM, 100 mM, 150 mM, 200 mM, 250 mM, 300 mM, 500 mM, 1 M and 2 M ammonium acetate). Peptides were introduced via nano-electrospray into a Q Exactive HF mass spectrometer (Thermo Scientific, San Jose, CA). The Q Exactive was operated in data-dependent mode acquiring HCD MS/MS scans (R = 15,000) after each MS1 scan (R = 60,000) on the 15 most abundant ions using an MS1 ion target of 3×10^6 ions and an MS2 target of 1×10^5 ions. The HCD-normalized collision energy was set to 30, dynamic exclusion was set to 30s, and peptide match and isotope exclusion were enabled. For iTRAQ data analysis, mass spectra were processed using the Spectrum Mill software package (version B.04.00, Agilent Technologies). MS/MS spectra acquired on the same precursor m/z (±0.01m/z) within ± 1 s in retention time were merged. MS/MS spectra of poor quality which failed the quality filter by not having a sequence tag length >1 were excluded from searching. A minimum matched peak intensity requirement was set to 50%. For peptide identification, MS/MS spectra were searched against a

Uniprot zebrafish database (Jun 21, 2012). Additional search parameters included: trypsin enzyme specificity with a maximum of three missed cleavages, ± 20 ppm precursor mass tolerance, ± 20 ppm (HCD) product mass tolerance, and fixed modifications including MMTS alkylation of cysteines and iTRAQ labeling of lysines and peptide N-termini. Oxidation of methionine was allowed as a variable modification. Autovalidation was performed such that peptide assignments to mass spectra were designated as valid following an automated procedure during which score thresholds were optimized separately for each precursor charge state and the maximum target-decoy-based false-discovery rate (FDR) was set to 1.0% (53,60).

Statistics

Differences among groups were analyzed by Student's t-test. Data are shown as means ± standard error (SE). Statistical significance was accepted when $p < 0.05$.

For statistical analysis of iTRAQ protein ratios, Log_2 protein ratios were fit to the normal distribution using non-linear (least squares) regression. The mean and standard deviation values derived from the Gaussian fit were used to calculate *p*-values, using *Z* score statistics. A given log_2 iTRAQ protein ratio, with the calculated mean and standard deviation of the fitted data, was transformed to a standard normal variable ($z = (x-\mu)/\sigma$). Calculated *p*-values were subsequently corrected for multiple comparisons using the Benjamini-Hochberg method (Benjamini and Hochberg, 1995).

Results

Generation of αB-crystallin loss-of-function alleles by CRISPR/Cas9 system

With the goal of defining the physiological roles of αB-crystallin and linking them to its well-understood chaperone mechanism, we have taken advantage of the CRISPR/Cas9 technology (Hwang et al., 2013, Jao et al., 2013, Jinek et al., 2012) to generate zebrafish mutant lines where the two αB-crystallin orthologs, *cryaba* and *cryabb*, have been disrupted (hereafter, we use the nomenclature, "αBa" and "αBb", for simplicity). We successfully generated multiple alleles carrying various deletions or insertions for each gene (summarized in Table 3, see

details in Experimental Procedures) and a few alleles were subsequently propagated after confirmation of the mutations by DNA sequencing (Figure 34 A. For the rest of this study, we focussed only on the *αBa*^{35bpDEL} and *αBb*^{10bpDEL} mutant alleles (Figure 34 B), given that both are predicted to encode extremely truncated polypeptides and are expected to function as null alleles. Henceforth these deletion mutations, *αBa*^{35bpDEL} and *αBb*^{10bpDEL}, are referred to as *αBa*$^{-/-}$ and *αBb*$^{-/-}$.

To confirm the loss of the αB proteins in αB-crystallin mutant lines, we utilized iTRAQ-based proteomics to quantify the relative changes in the abundance of αB proteins in the adult lens of *αBa*$^{-/-}$ and *αBb*$^{-/-}$ (Wang et al., 2013). In both water-soluble (WSF) and -insoluble (WIF) fractions, we observed that compared to WT, the relative abundance of native αB peptides in each respective mutant was reduced significantly to a marginally-detectable level (Figure 34 D). Additionally, we generated polyclonal antibodies against purified zebrafish αA- and αBa-crystallin proteins, and probed crude protein extracts from the lens of mutant fish lines. While the level of αA-crystallin was not affected by the loss of either αBa or αBb (Figure 34C, Anti-αA), we confirmed the loss of αBa-crystallin in the lens of both *αBa*$^{-/-}$ and the double mutant, *αBa*$^{-/-}$; *αBb*$^{-/-}$ (both WSF and WIF; Figure 34 C).

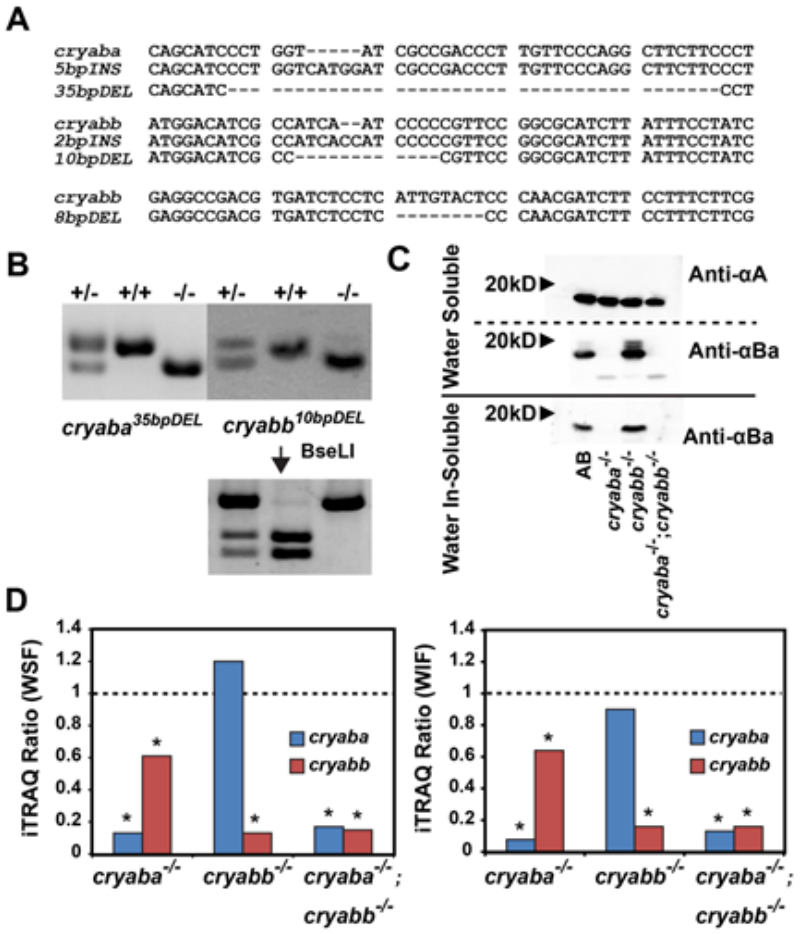

Figure 34: Generation of knock-out alleles of αB-crystallin genes by CRISPR/Cas9.

A, alignment of the DNA sequences of the mutant alleles of αBa and αBb. B, electrophoresis of the genomic DNA of the adult zebrafish amplified by PCR: αBa^{35bpDEL} on 3% agarose gel and αBb^{10bpDEL} on 4% agarose gel. The genotyping of αBb^{10bpDEL} allele was confirmed by digestion with restriction enzyme BseLI. C, Western immunoblot of the water-soluble and water in-soluble protein fraction of the excised lenses of the adult zebrafish. After transfer on nitrocellulose membrane, proteins were probed with polyclonal antibody against zebrafish *Cryaa* (αA) or zebrafish *Cryaba* (αBa). D, αB-crystallin iTRAQ ratios in the lens of both αBa$^{-/-}$ and αBb$^{-/-}$ adult fishes. The left panel shows iTRAQ ratios of αBa and αBb in mutant animals compared with wild-type animals in the lens WSF, and the right panel shows the same from the WIF.

Interestingly, using the αA western signal to normalize expression levels in the *αBb*$^{-/-}$ lens, we observed a slight increase of αBa protein in the WSF of the *αBb*$^{-/-}$ lens, which was in agreement with our iTRAQ data (Figure 34D), suggesting a possible compensatory response to the loss of αBb protein. Moreover, we observed mobility-shifts of the αBa band in the WSF (but not in WIF) of the lens (Anti-αBa; in WT and *αBb*$^{-/-}$) that could represent post-translational modifications, *e.g.* phosphorylation or acetylation (Thornell and Aquilina, 2015, Nahomi et al., 2013, Krishnamoorthy et al., 2013). These bands were particularly noticeable in *αBb*$^{-/-}$ lens, which might suggest an increase in the amount of post-translational modification of αBa-crystallin.

αB-crystallins are expressed in both the lens and heart during zebrafish embryogenesis

Previously we showed that both αBa and αBb are expressed in zebrafish embryos from as early as 2dpf (Zou et al., 2015). To determine their spatial expression pattern, we performed whole-mount RNA *in situ* hybridization (WMISH) for αBa and αBb on 2dpf embryos according to the established protocol (Thisse and Thisse, 2014). As expected, we observed the expression of αBa and αBb in the lens of 2dpf embryos as well as in the heart, albeit with lower staining signal (Figure 35 A; black arrows). In addition, both genes were broadly expressed in the brain region and showed particularly enriched expression in the otic vesicles (Figure 35 A, white arrowheads).

We explored whether compensatory transcriptional regulation exists between the two paralogs of αB genes in the reciprocal mutants, which is often found in duplicated genes. However, we observed no significant change (<1.6 cycle difference (Buhrdel et al., 2015)) of αBb expression in αBa mutant embryos and vice versa (Figure 35 B). On the other hand, we did not observe nonsense-mediated mRNA decay (NMD) for αBa or αBb mRNA transcripts that were derived from their respective mutant alleles, even though they are expected to behave as protein null

(Figure 35 B). Nonetheless, as shown in our western blot analysis, the retained αBa mRNA did not produce a detectable amount of αBa protein (Figure 34

details in Experimental Procedures) and a few alleles were subsequently propagated after confirmation of the mutations by DNA sequencing (Figure 34 A). For the rest of this study, we focussed only on the *αBa35bpDEL* and *αBb10bpDEL* mutant alleles (Figure 34B), given that both are predicted to encode extremely truncated polypeptides and are expected to function as null alleles. Henceforth these deletion mutations, *αBa35bpDEL* and *αBb10bpDEL,* are referred to as *αBa*$^{-/-}$ and *αBb*$^{-/-}$.

To confirm the loss of the αB proteins in αB-crystallin mutant lines, we utilized iTRAQ-based proteomics to quantify the relative changes in the abundance of αB proteins in the adult lens of *αBa*$^{-/-}$ and *αBb*$^{-/-}$ (Wang et al., 2013). In both water-soluble (WSF) and -insoluble (WIF) fractions, we observed that compared to WT, the relative abundance of native αB peptides in each respective mutant was reduced significantly to a marginally-detectable level (Figure 34 D). Additionally, we generated polyclonal antibodies against purified zebrafish αA- and αBa-crystallin proteins, and probed crude protein extracts from the lens of mutant fish lines. While the level of αA-crystallin was not affected by the loss of either αBa or αBb (**Figure 34**C, Anti-αA), we confirmed the loss of αBa-crystallin in the lens of both *αBa*$^{-/-}$ and the double mutant, *αBa*$^{-/-}$; *αBb*$^{-/-}$ (both WSF and WIF; Figure 34C) which further supported that the αBa mutation is a loss-of-function allele.

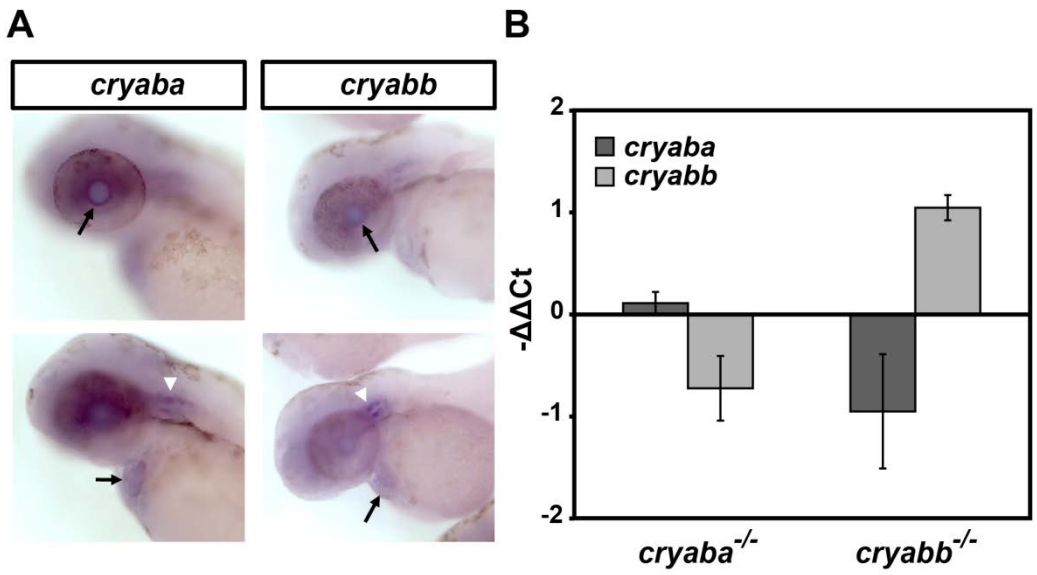

Figure 35: Expression profiles of αB-crystallin genes

A, expression pattern of αBa and αBb genes by whole-mount in situ hybridization. Black arrows indicate lens (top row) and heart (bottom row). White arrowheads indicate otic vesicles. B, relative expression changes of αBa and αBb genes in αBa and αBb homozygous mutants, as measured by qRT-PCR.

.***Loss-of-function of αB-crystallin causes lens defects in zebrafish***

Consistent with our previous demonstration that knockdown of *αBa* and *αBb* by morpholinos can perturb lens transparency in zebrafish (Zou et al., 2015), the loss of αB-crystallin function, either *αBa* or *αBb*, led to apparent abnormalities in the embryonic lens starting at 3dpf which became evident at 4dpf (Figure 36 A), while the overall morphology of the embryos remained normal. The nature of these lens defects were similar to those previously described for αB-crystallin morphants or αA-crystallin knockout lines ($\alpha A^{-/-}$) (Zou et al., 2015).

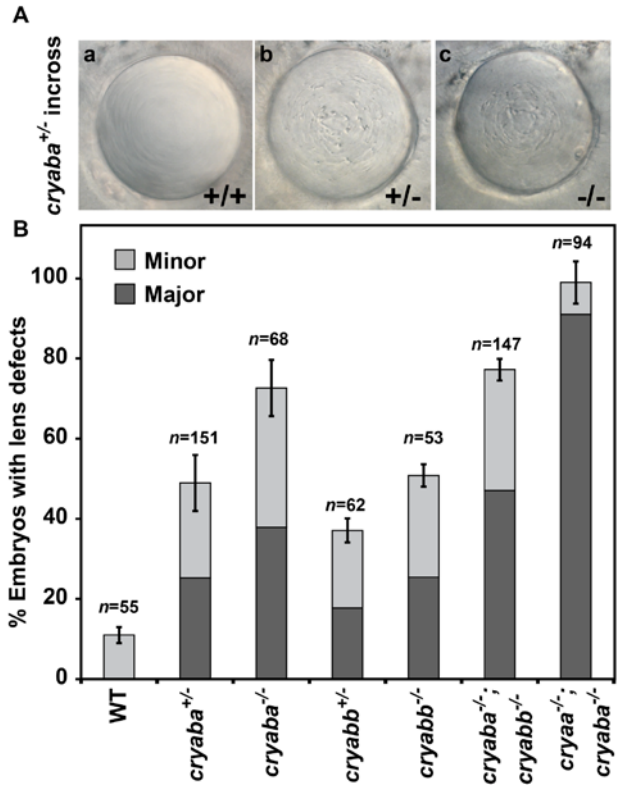

Figure 36: Lens defects in zebrafish αB-crystallin mutant embryos

A, representative images of lens phenotypes in WT and αBa homo-/heterozygotes. B, comparison of percentage of embryos showing lens defects between WT and αB-crystallin homo-/heterozygous mutants (αBa and αBb), as well as αB-crystallin double mutants and αA-/αB-crystallin double mutants.

Following the same classification system previously established, as shown in Figure 33, lens defects were categorized into three classes based on the severity: “Major” (Figure 36 Ab,c), “Minor” (not shown), and “WT-like” (Figure 36 Aa) (Zou et al., 2015). Initially, we noted that the incidence of lens defects in the offspring derived from heterozygote incrosses, both minor and major classes, occurred in a frequency inconsistent with the lens phenotype being strictly recessive (>25%). Genotyping of phenotypic embryos revealed that both the minor and major

phenotypes occur in heterozygous and homozygous mutants. Similar to *αA*$^{-/-}$ embryos, both *αBa*$^{-/-}$ and *αBb*$^{-/-}$ showed lens defects with a range of severity. Greater penetrance and severity of lens defects was observed in *αBa*$^{-/-}$ embryos. For *αBa*$^{-/-}$, ~75% of the total embryos presented lens defects and 38% were of the "major" class. ~50% of the *αBb*$^{-/-}$ embryos showed lens abnormalities and 25% were of the "major" class (Figure 36 B). These results suggested that *αBa* might play a more important role than *αBb* in the maintenance of zebrafish lens transparency. Interestingly, a gene dosage effect was observed in *αBa* and *αBb* genes. When we crossed homozygous *αBa* mutant adult with WT fish (*αBa*$^{-/-}$ x WT), the resulting heterozygous αBa mutant embryos (*αBa*$^{+/-}$) exhibited reduced lens defects (~48%), relative to *αBa*$^{-/-}$ embryos. A similar effect was observed for *αBb*$^{-/-}$ embryos, in which ~37% of them showed lens defects (Figure 36 B).

Because both *αBa* and *αBb* mutants were adult viable, we generated *αBa*/*αBb* double mutants (*αBa*$^{-/-}$; *αBb*$^{-/-}$) to determine if a higher penetrance of the lens phenotypes would be observed by complete elimination of αB-crystallin. Compared to the single mutant, particularly *αBa*$^{-/-}$, the frequency of major lens defects increased moderately in *αBa*/*αBb* double mutants (by about 10%), but the overall penetrance was not significantly changed, consistent with the conclusion that *αBa* plays a more prominent role in lens development than *αBb* (Figure 36 B).

While both *αA* and *αBa* appear critical for proper lens formation, the penetrance and severity of the phenotypes varies in the single knockout lines. Therefore, we generated a double loss-of-function line by crossing *αBa*$^{-/-}$ fish with the *αA*$^{-/-}$ line generated in our earlier work (Zou et al., 2015) and examined the occurrence of the lens defects. To avoid the protective effect of maternal *αA* expression (Zou et al., 2015), *αA*$^{-/-}$; *αBa*$^{-/-}$ embryos were derived from *αA*$^{-/-}$; *αBb*$^{-/-}$ adults incross. As expected, they exhibited an almost complete penetrance (~99%), with approximately 90% of lens defects belonging to the major class (Figure 36 B).

αB-crystallin mutants showed stress-induced cardiac phenotypes

In addition to its role in the lens, αB-crystallin has been implicated in the cellular integrity of the cardiomyocytes through interactions with Titin and Desmin (Bennardini et al., 1992, Vicart et al., 1998, Inagaki et al., 2006). Therefore we examined if *αBa* mutants exhibited abnormalities in heart development by incrossing either $\alpha Ba^{+/-}$ or $\alpha Ba^{-/-}$. The resulting embryos from both crosses displayed morphologically normal hearts (Figure 37Aa-b) under routine collection and regular embryo rearing conditions (28.5 °C, in 35mm petri dish, up to 5-6 dpf). Similar results were observed in *αBb* mutants (both $\alpha Bb^{+/-}$ and $\alpha Bb^{-/-}$). These results contradict a previous study reporting that knocking-down *αBa* and *αBb* genes by morpholinos would lead to heart failure and skeletal muscle defects in zebrafish embryos (Buhrdel et al., 2015).

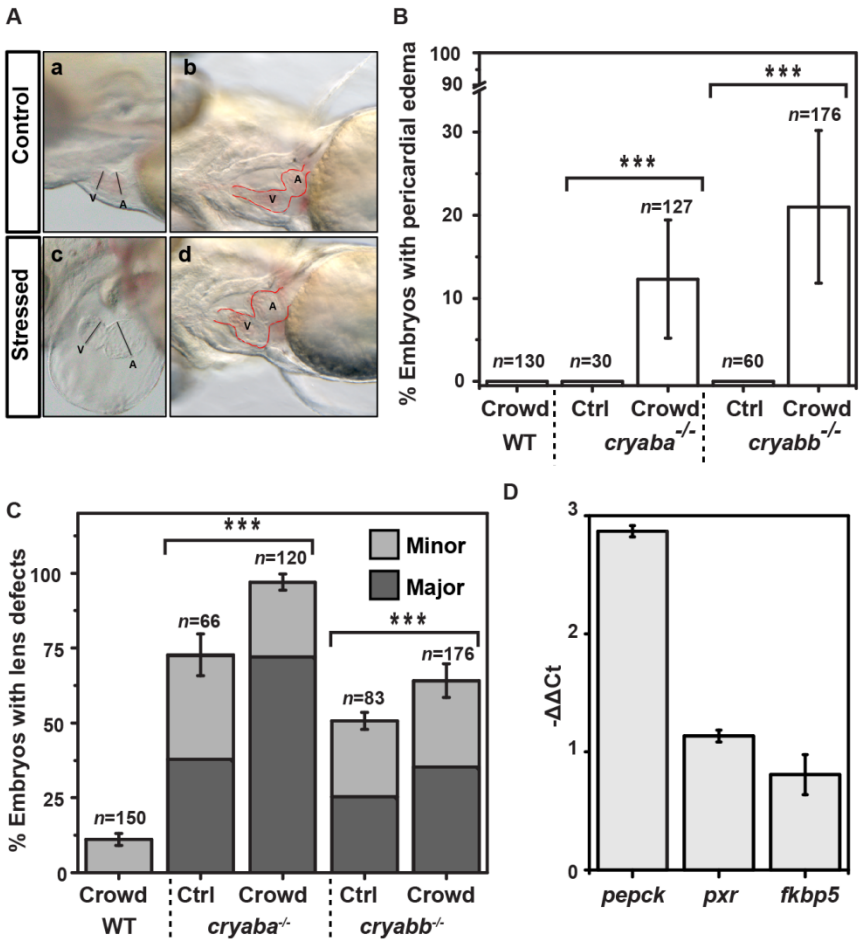

Figure 37**:** Stress-induced cardiac phenotypes in αB-crystallin mutant embryos.

A, representative images of cardiac phenotypes in αB-crystallin mutant embryos: panels a and b, control/non-stressed; panels c and d, subjected to crowding stress. A, atrium; V, ventricle. Red dotted line demarcates the heart morphology. B, percentage of αB-crystallin mutant embryos showing pericardial edema under crowding stress. C, percentage of embryos showing lens defects in αB-crystallin mutants (αBa$^{-/-}$ and αBb$^{-/-}$) was influenced by the crowding stress. D, relative expression changes of GR signaling target genes (*pepck*, *pxr*, and *fkbp5*) in 3-dpf WT embryos after being raised in crowding conditions for 2 days (from 1 to 3 dpf), as measured by qRT-PCR.

Given the prevalent non-specific effects and the reported unreliability of using morpholino to interfere with gene functions (Kok et al., 2015), we conclude that αB-crystallin genes are largely dispensable for muscle and heart development during embryogenesis. Indeed, αB-crystallin double mutant fishes (*αBa*$^{-/-}$; *αBb*$^{-/-}$) are viable and fertile as adults. Raising the progenies derived from *αBa*$^{+/-}$ or *αBb*$^{+/-}$ adult incross, we found that the ratio of either *αBa*$^{-/-}$ or *αBb*$^{-/-}$ progeny that survived to adulthood (>3 month old) was in accordance with Mendelian ratio (Table 5). Moreover, the *αBa*$^{-/-}$ and *αBb*$^{-/-}$ adults did not exhibit lower survival rate compared to siblings under normal housing conditions for at least 10 months (Table 5). This data further suggested that neither αB-crystallin gene is essential for zebrafish overall viability.

While αB-crystallin deficient embryos showed no apparent cardiac phenotype under the normal rearing conditions described above, we examined if αB-crystallin is involved in the stress tolerance of the zebrafish developing heart. As a member of sHsps, αB-crystallin has been shown to be inducible by various cellular stresses, including oxidative, genotoxic and heat shock stresses (Head et al., 1994, Ito et al., 1997, Djabali et al., 1997, Bakthisaran et al., 2016). Therefore, we raised 1dpf αB-crystallin mutant (*αBa*$^{-/-}$ and *αBb*$^{-/-}$) embryos in high density (75 embryos per well of a 6-well plate; see Experimental Procedures for detail) to simulate a "stressed" condition or a non-permissive condition induced by crowding, while controls from the same clutch were stocked at normal/non-stressed density (15 embryos per well of a 6-well plate). The gross morphology and heart development of the embryos was monitored daily until 5dpf. Compared to the control embryos, the αB-crystallin mutant embryos subjected to crowding stress progressively developed pericardial edema with moderate penetrance (Figure 37A,B; *αBb*$^{-/-}$ shown here but similar phenotypes were observed in *αBa*$^{-/-}$), which becomes more evident at 4dpf (Figure 37Ac-d). In contrast, no such cardiac phenotype was detectable in the control (non-stressed) αB-crystallin mutant embryos (Figure 37Aa-b). These cardiac phenotypes were

very similar to what has been described previously in embryonic lethal mutants that developed cardiomyopathy, such as *titin* mutants (Xu et al., 2002). The stress-induced pericardial edema in αB-crystallin mutants was not reversible, as we were unable to raise those *αBa*$^{-/-}$ and *αBb*$^{-/-}$ embryos showing cardiac phenotypes to adulthood (none survived before reaching the juvenile stage).

Interestingly, in addition to cardiac phenotypes, the lens defects shown in both *αBa*$^{-/-}$ and *αBb*$^{-/-}$ embryos were also influenced by crowding stress (Figure 37C). Compared to the non-stressed condition (control), we observed higher penetrance of overall lens defects in αBa$^{-/-}$ (~20% increase) and *αBb*$^{-/-}$ (~12% increase) under the crowded rearing conditions.

The sensitivity of αB-crystallin mutants to crowding stress is mediated by glucocorticoid levels

Based on the observation that crowding causes phenotypic enhancement in two distinct tissues, we hypothesized that the underlying stress may be mediated by a systemic and intrinsic factor. Crowding stress of adult zebrafish has been shown to increase the body cortisol level (Ramsay et al., 2006, Sallin and Jazwinska, 2016). We examined the changes of the expression of known GR signaling downstream genes (*fkbp5*, *pxr*, and *pepck*) (Chen et al., 2016) in embryos raised under crowding conditions for two days. We found that although all three genes showed trends of increased expression, only *pepck* was significantly upregulated (Figure 37D), which was consistent with the finding that *pepck* is a more sensitive GR signaling reporter gene during embryonic stages (Chen et al., 2016).

Earlier reports have shown that the cardiac performance of zebrafish embryos declined when exposed to elevated cortisol level (Nesan and Vijayan, 2012). Therefore, we tested if the αB-crystallin mutants lower the tolerance of the heart to cortisol, which is the main glucocorticoid

stress hormone. For this purpose, the αB-crystallin mutant embryos were challenged with two different synthetic glucocorticoids, dexamethasone and hydrocortisone, to mimic the elevation of stress hormone level and overactivation of glucocorticoid receptor (GR) signaling. The αB-crystallin mutants (*αBa*$^{-/-}$, *αBb*$^{-/-}$ and *αBa*$^{-/-}$; *αBb*$^{-/-}$) treated with both GR agonists from 1dpf to 4dpf under normal rearing conditions developed pericardial edema and dilated cardiac chambers (Figure 38A and Figure 38Ce-f), similar to the phenotypes under the crowding stress (Figure 37A). In contrast, non-treated αB-crystallin mutants (DMSO control) or WT embryos subjected to the same regimen of synthetic glucocorticoids mostly remained normal (Figure 38B). As expected, the αA-crystallin mutant did not exhibit cardiac abnormality when subjected to the crowding stress and dexamethasone treatment (Figure 38D), which emphasize the distinct involvement of αB-crystallin in the maintenance of cardiac function. Together, these results clearly suggested that without the presence of αB-crystallin (*i.e.* loss-of-function), the embryonic heart is more vulnerable to development of cardiac abnormalities mediated by GR signaling activity.

Early cardiac development is unperturbed but cardiac functions appear compromised in αB-crystallin mutants when challenged with stress

We examined if the heart phenotypes were a result of failures of cell fate specification by immunostaining of the ventricle and atrium. Compared to WT, both non-stressed *αBb*$^{-/-}$ embryos (and *αBa*$^{-/-}$) at 2dpf showed largely normal specification and partition of the cardiac chambers (Figure 38Ca-b), consistent with the notion that αB-crystallin genes are not required for early cardiac development. Since cell death/apoptosis has been implicated in the αB-crystallin-associated cardiomyopathy, we performed TUNEL assay on both *αBb*$^{-/-}$ and *αBa*$^{-/-}$ embryos at 2dpf and found no evidence of increased cell death in the heart, which suggested

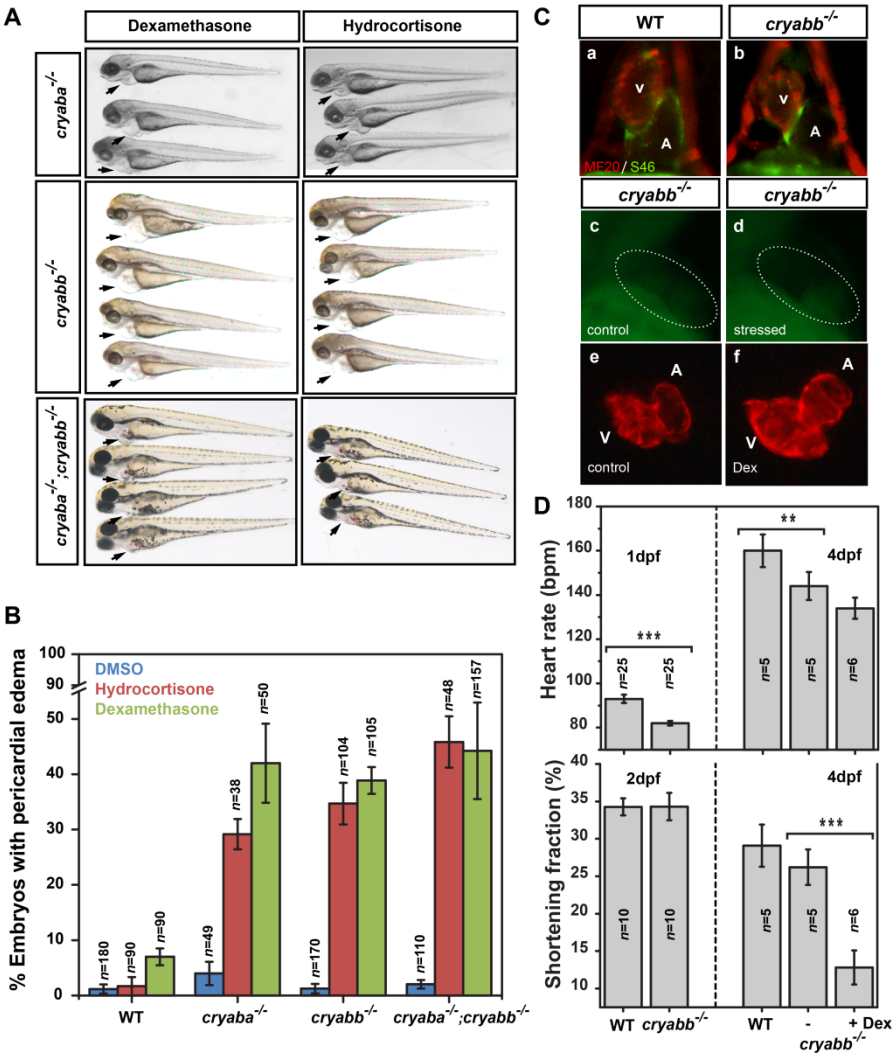

Figure 38**:** Overactivation of GR signaling induced cardiac phenotypes in αB-mutants.

A, αBb$^{-/-}$ embryos showed pericardial edema when treated with GR agonists, dexamethasone (50 μM) and hydrocortisone (50 μM). B, percentage of αBb$^{-/-}$ embryos showing pericardial edema when treated with GR agonists. C, immunofluorescence with MF20 and S46 antibodies visualized the ventricle (red) and atrium (green) in WT and αBb$^{-/-}$ embryos at 2 dpf (panels a and b). The TUNEL staining revealed no significant increase of apoptosis in the heart (dotted circle area) of 2-dpf αBb$^{-/-}$ embryos subjected to crowding compared with control αBb$^{-/-}$ embryos (panels c and d). The cardiac chambers of 4 dpf αBb$^{-/-}$embryos were dilated after treating with dexamethasone (Dex) (panels e and f). D, upper panel, heart rates of WT, αBb$^{-/-}$ embryos (1 and 4 dpf), and αBb$^{-/-}$ embryos treated with dexamethasone (4 dpf). Lower panel, ventricular shortening fraction of WT, αBb$^{-/-}$ embryos (2 and 4 dpf), and αBb$^{-/-}$ embryos treated with dexamethasone (4 dpf).

that apoptosis is not involved in the stress-induced heart phenotypes described above (Figure 38Cc-d).

Even though the early heart development appeared to be unaffected in αB-crystallin mutants, taking advantage of the embryos optical transparency, we performed time-lapse imaging to monitor the heart rate and contraction dynamics of *αBb* mutants, without stress. We found that, compared to the WT, *αBb* homozygotes exhibited slower heart rate (~10% decrease) at 1dpf, which persisted at 4dpf (Figure 38D). The ventricular shortening fraction, which can be used as an estimate of myocardial contractility, was not affected at 2dpf (Figure 38D (lower pannel)). However, at 4dpf, a small reduction of shortening fraction was observed in *αBb* mutants, albeit not significant, compared to WT (Figure 38D). This marginally affected cardiac performance maybe be offset by compensatory mechanisms, given the fact that the αB-crystallin mutants survive to adulthood.

In contrast, treatment with dexamethasone significantly reduced (~50%) the ventricular shortening fraction of the *αBb* mutants when compared to non-treated *αBb* mutants (Figure 38D, lower pannel), while the heart rate of *αBb* mutants was not further affected (Figure 38D, upper pannel). Also, compared to non-treated *αBb* mutants, apparent abnormality in cardiac contraction could be observed in dexamethasone-treated *αBb* mutants. This result strongly highlights the contribution of αB-crystallin to the stress tolerance of the heart, in this case, for cortisol stress. Further detailed experiments are needed to examine the molecular/cellular mechanisms underlying the hyper-susceptibility of cardiac tissues towards GR signaling activation in αB-crystallin mutants.

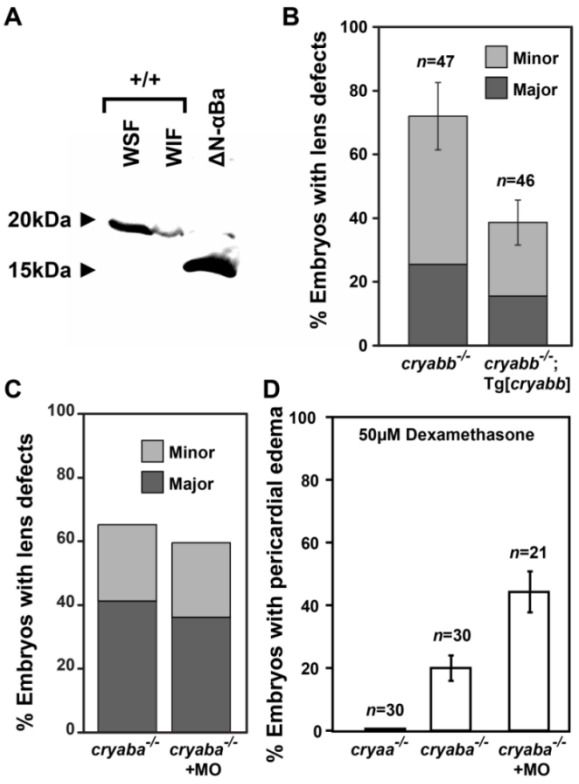

Figure 39: αB-crystallin mutations function as loss-of-function alleles.

A, purified N-terminal truncated (Δ1–43 amino acids) αBa protein (from bacterial expression) was detectable by anti-αBa polyclonal antibody. The WSF and WIF protein fractions of the excised lenses of the wild-type adult zebrafish served as controls, Western blotted for full-length αBa protein. B, transgenic expression of zebrafish αBb (Tg[cryabb]) in the lens of αBb$^{-/-}$embryos showed suppression for its lens defects, compared with non-transgenic siblings (αBb−/−). C, percentage of embryos with lens defects remained unchanged in αBa$^{-/-}$embryos injected a morpholino (MO) interfering with the alternative start site compared with control αBa$^{-/-}$embryos. D, GR activation-induced (50 μM dexamethasone) pericardial edema in αBa$^{-/-}$embryos was not suppressed by injecting morpholino interfering with the alternative start site. In addition, αA$^{-/-}$embryos showed no heart edema when treated with dexamethasone.

The phenotypes of αB-crystallin mutants result from haploinsufficiency instead of a toxic gain-of-function effect

The lack of NMD and the persistent mRNA (B) described above raised a concern that the observed lens and heart defects in αB-crystallin mutants could be due to the dominant (or toxic) effects (i.e. gain-of-function) of residual N-terminal truncated αB-crystallin protein possibly resulting from an alternative translation even though such a possible N-terminal truncated (Δ1-43aa) mutant αBa protein should be detectable by our anti-αBa antibody (Figure 39A). To further exclude this possibility, we injected a morpholino specifically targeting a possible alternative initiation site into αBa mutants and examined if the phenotypes could be suppressed. As shown in Figure 39C and Figure 39D, there was no suppression of lens and heart phenotypes by morpholino knockdown, which argued against the αBa mutant allele functioning as dominant-negative alleles. Finally, lens-specific expression of zebrafish αBb (Tg[*cryabb*]) also partially alleviated the lens defects of αBb mutant embryos (Figure 6B), which further supports the loss-of-function and haploinsufficient nature of our αB-crystallin mutant alleles.

Discussion

αB-crystallin loss-of-function mutants reveal important physiological roles

To our knowledge, this work reports the first αB-crystallin specific loss-of-function lines in vertebrate animals. The previously described αB-crystallin knockout mouse was in fact a compounded mutant line that also contained disruptions in the adjacent Hspb2 gene (Brady et al., 2001) precluding a direct assessment of an exclusively αB-crystallin loss-of-function phenotype. The availability of the zebrafish model yielded novel insights into the role of αB-crystallin in the lens and cardiac muscle. While there has been evidence of transcriptional control by the glucocorticoid receptor (Aoyama et al., 1993, Kinyamu et al., 2008, Cheng et al.,

2013), our results tie this observation to a prominent role of αB-crystallin in the heart resistance to stress.

Unexpectedly, results from qRT-PCR suggested that the mRNAs encoded by the *αB* mutant alleles did not undergo significant NMD despite premature stop codons introduced in the first exons. This phenomenon of escaping NMD has been observed previously in first exon mutations (Neu-Yilik et al., 2011, Cain et al., 2017), which underscores the importance of selecting mutation target sites and confirming the mutations given the explosion of CRISPR/Cas9 genome editing techniques (Mou et al., 2017). Several lines of evidence support our contention that the *αB* alleles described in this study function as null alleles or at least strong hypomorphic alleles including the lack of stably expressed αBa protein as revealed by western blot analysis (Figure 34C) and quantitative proteomics by mass spectrometry (Figure 34D) of homozygous mutant (*αBa*$^{-/-}$, *αBb*$^{-/-}$, and *αBa*$^{-/-}$; *αBb*$^{-/-}$) lenses. Although it remains theoretically possible that an N-terminal truncated Cryab protein encoded by alternative downstream initiation sites could function as antimorphic (or neomorphic), dominant alleles (i.e. gain-of-function) and contribute to the phenotype. But we discounted this possibility not only because the N terminus of B-crystallin has been demonstrated critical for the oligomerization and its chaperone activity (Jehle et al., 2011, Bova et al., 2000, Santhoshkumar et al., 2009, Asomugha et al., 2011), but also based on the data from the alternative-translation blocking morpholino (Figure 39C-D), as well as by the rescue of lens defects by lens-specific expression of αBb (Figure 39B). Moreover, by western analysis we were able to detect the purified N-terminal truncated mutant αBa protein that expressed in the bacterial system (Figure 39A), which suggests that in *αBa* mutants, the amount of the alternatively translated αBa protein, if does exist, would be negligible (Figure 34C).

Unlike the lens in the mouse model (Brady et al., 2001), transparency of embryonic lens in zebrafish shows a dosage-dependence on αB-crystallin. Homozygous mutants of *αBa* and/or *αBb* develop lens abnormalities in the majority of the embryos, while heterozygous *αBa* and *αBb* mutants also showed lens defects albeit to a lesser extent (Figure 36). Furthermore, we found that *αBa* plays a more critical role in the maintenance of lens transparency compared to *αBb*, consistent with an elevated *in vitro* chaperone-like activity (Koteiche et al., 2015) (Figure 36). Similar to what we observed in αA-crystallin knockout mutants (Zou et al., 2015), this gene dosage effect (or haploinsufficiency) in αB-crystallin mutants may likely reflect the low abundance of overall α-crystallin proteins in the zebrafish embryonic lens, where a small change in the expression could cause a strong response in the proteostatic network. Although not frequently reported, cataract formation could be caused by haploinsufficiency of other ocular proteins such as monocarboxylate transporter, SLC16A12; and regulatory proteins PITX3 and PAX6 (Castorino et al., 2011, Bidinost et al., 2006, Glaser et al., 1994).

In contrast to previous reports (Posner et al., 1999, Elicker and Hutson, 2007, Marvin et al., 2008), we detected low-level expression of *αBa* and *αBb* in the lens and the heart during zebrafish embryogenesis (Figure 35) (Harding et al., 2008, Zou et al., 2015). Furthermore, we found no evidence of compromised skeletal muscle functions in both αB-crystallin mutants, unlike the severe muscular phenotypes shown in a previous study using morpholino knockdown strategies (Buhrdel et al., 2015). In addition to the notorious off-target effects of morpholino usage, it is also likely that other members of sHsp genes expressed in the myotomes, such as *hspb1*, *hspb7*, *hspb8* and *hspb9* (Mao and Shelden, 2006, Marvin et al., 2008) can compensate the loss of both αB-crystallin genes and maintain a functional proteostasis network in the muscle.

Cardiac phenotypes in zebrafish αB-crystallin mutant embryos

Several genetic evidences support the contribution of αB-crystallin to cardiac function, particularly R120G mutation (CRYAB R120G) leading to desmin-related cardiomyopathy (Vicart et al., 1998) as well as cardiomyopathy-associated CRYAB mutation, D109H (Sacconi et al., 2012). Hence, the lack of apparent phenotypes in the developing hearts of αB-crystallin homozygous mutants, including *αBa*$^{-/-}$; *αBb*$^{-/-}$ double mutants, was unexpected. However, the full effect of αB-crystallin deficiency may be masked or compensated by several sHsp chaperones that are robustly expressed in the developing heart tubes, such as the *hspb1*, *hspb7* and *hspb12* (Mao and Shelden, 2006, Marvin et al., 2008).

A major finding of this work is the emergent role of αB-crystallin under stress conditions. αB-crystallin mutants raised under crowding stress developed severe pericardial edema in a fraction of mutant embryos, even though the penetrance was low compared to the lens phenotypes (about 10~20%; Figure 37B). Interestingly, a difference in sensitivity to loss of αBa and αBb was also observed in the heart that is opposite to the lens phenotype (Figure 36B). This may be a consequence of the higher level of αBb compared to αBa in the cardiomyocytes at 4dpf embryos (Shih et al., 2015). While we did detect expression of both αB-crystallin genes in the heart of 2dpf embryos, the non-quantitative nature of the WMISH procedure precluded us from comparing the relative expression level between *αBa* and *αBb* genes. Additionally, differential substrate specificity or different post-translational modification of the two αB-crystallin paralogs may contribute to the variation of the gene dosage requirement in these tissues.

Similar to the lens phenotype, the cardiac phenotype does not appear to be due to a failure of specification of the cardiac tissue as both atrial and ventricular markers are normally expressed. In the non-stressed αB-crystallin mutants, we did observe a small decline of cardiac function such as slower heart rates (Figure 38D). Given the known association of αB-crystallin

with Desmin or Titin (Bullard et al., 2004, Bennardini et al., 1992, Nicholl and Quinlan, 1994), subtle changes may exist at the cellular level such as sarcomere integrity, which requires further detailed analyses. Our current hypothesis is that loss of αB-crystallin would only slightly weaken the myocardium but not enough to cause severe damage (i.e. become sensitized). However, exposure to stress (*e.g.* GR agonists) would exacerbate the phenotypes and lead to cardiac dysfunction, which is strongly supported by our observations (Figure 38D-E).

Stress-induced phenotypes in αB-crystallin mutants uncover a novel intersection between steroid signaling and proteostasis

Following up on the established link between crowding stress and activation of glucocorticoid signaling (Ramsay et al., 2006, Sallin and Jazwinska, 2016), we determined that the αB-crystallin mutants were highly sensitive to the treatment of GR signaling agonists, dexamethasone and hydrocortisone, and prone to develop pericardial edema (Figure 38A). This synergism may be explained by the transcriptional regulation by the GR of a particular proteostatic target that leads to phenotype enhancement. Although GR-mediated transcriptional activation of sHSPs, including αB-crystallin in cell culture systems, has been demonstrated (Aoyama et al., 1993, Kinyamu et al., 2008, Cheng et al., 2013), we did not detect changes in expression of *αBa* or *αBb*. In fact, the action of GR signaling agonists here is unlikely to be mediated through direct transcriptional activation of the αB genes as the αB protein levels in homozygote mutants would not be affected by increased αB transcripts.

Although the importance of GR signaling in cardiac function and maintenances has been repeatedly demonstrated, the exact roles remain controversial due to its intricate regulations and interactions (Rog-Zielinska et al., 2014, Roy et al., 2009, Sainte-Marie et al., 2007, Oakley and Cidlowski, 2015, Oakley et al., 2013). Here we provide additional wrinkles to this complex

signaling system in which the proteostatic state (i.e. loss of αB-crystallin) of the cells (in this case the cardiomyocytes) may alter the GR signaling activities and influence the cellular responses. Thus, further experiments are needed to delineate the interactions between GR signaling and αB-crystallin.

It has been well established that prolonged corticosteroid therapy is a major risk factor for the formation of steroid-induced posterior subcapsular cataracts (PSCs), which account for approximately 15% of all cataracts (Leske et al., 1997, McCarty et al., 2000, Renfro and Snow, 1992, Veenstra et al., 1999, Costagliola et al., 1989). Although the pathoetiology and the mechanism of glucocorticoid action in the lens remain unresolved (James, 2007), two main underlying mechanisms have been examined and debated: glucocorticoid-induced gene transcription events and glucocorticoid-lens protein adduct formation (James, 2007). Only steroids with glucocorticoid activity are associated with steroid-induced PSC (Urban and Cotlier, 1986), strongly suggesting involvement of the GR (Dickerson et al., 1997).

Our result suggests that a compromised proteostatic system in the lens may contribute to the occurrence of steroid-induced cataracts. Indeed, the formation of PSC is quite heterogeneous and its dose-dependence on steroid use is also controversial (Skalka and Prchal, 1980, Donshik et al., 1981, Brocklebank et al., 1982). Thus, we propose that individual susceptibility, which reflects the difference in genetic predisposition (such as polymorphisms in αB-crystallin gene) that impacts the lens proteostatic capacity, play a critical role in the development of PSC. Under this assumption, instead of a “determining factor”, the steroid use acts as an “environmental factor” that would facilitate the PSC formation via interactions with αB-crystallin (or other resident proteostatic factors).

The physiological responses of GR signaling activation are notoriously diverse and often exhibit profound variability in specificity or sensitivity between different tissues and individuals, partly due to its heterogeneity and complex regulation (Oakley and Cidlowski, 2013). Thus, the novel intersection uncovered in this study between GR signaling and proteostasis in the lens and the heart is likely tissue- or context-dependent. With gene profiling studies revealing a vast array of downstream target genes of GR signaling, further experiments utilizing genetic tools in zebrafish are set up to decipher this new interaction with potentially significant clinical relevance.

Table 3: Mutation alleles of αB-crystallin genes generated by CRISPR/Cas9

Genotype	Predicted polypeptide sequence	Predicted polypeptide length
αBa^{5bpINS}	MEISIQHPWS WIADPCSQAS SLIEFLISIL ESIYLTVTLF HLSTPCFTIV LICGAFQAGG TVACRR	66
αBa^{15bpDEL}	Δ^{10}YRRPL^{14}	163
αBa^{35bpDEL}	MEISIQHPLS NF	12
αBb^{2bpDEL}	MDIAITIPRS GASYFLSSFP AGNLGSILLR PM	32
αBb^{10bpDEL}	MDIARSGASY FLSSFPAGNL GSILLRPT	28
αBb^{8bpDEL}	MDIAINPPFR RILFPIFFPR RQFGEHITEA DVISSPTIFL SSQSKLDGKR SF	52
αBb^{3bpDEL}	MDIAINPPFR RILFPIFFPR RQFGEHITEA DVISSLSQRS SFLRSPSWME SGVSEVSYKK LVFSGF	66

The native residues are underlined.

Table 4: Summary of αB-crystallin iTRAQ data

Genotype	Sample	Protein	Fold change	*p* value	Significant?
cryaba$^{-/-}$	WSF	Cryaba	0.138	7.18E-13	Yes
cryaba$^{-/-}$	WSF	Cryabb	0.610	0.039	No
cryabb$^{-/-}$	WSF	Cryaba	1.200	0.027	No
cryabb$^{-/-}$	WSF	Cryabb	0.136	5E-96	Yes
cryaba$^{-/-}$; *cryabb*$^{-/-}$	WSF	Cryaba	0.166	2.24E-11	Yes
cryaba$^{-/-}$; *cryabb*$^{-/-}$	WSF	Cryabb	0.147	1.14E-12	Yes
cryaba$^{-/-}$	WIF	Cryaba	0.077	1.28E-23	Yes
cryaba$^{-/-}$	WIF	Cryabb	0.638	0.041	No
cryabb$^{-/-}$	WIF	Cryaba	0.897	0.179	No
cryabb$^{-/-}$	WIF	Cryabb	0.161	1.13E-60	Yes
cryaba$^{-/-}$; *cryabb*$^{-/-}$	WIF	Cryaba	0.130	1.31E-10	Yes
cryaba$^{-/-}$; *cryabb*$^{-/-}$	WIF	Cryabb	0.158	5.79E-9	Yes

- Significance based on Benjamini-Hochberg correction for multiple comparisons.

Table 5: Survival analysis of the progeny from incross of αB-crystallin heterozygotes

	Cryaba^{35bpDEL}			**Cryabb^{10bpDEL}**		
	Homozygote (−/−)	**Heterozygote (−/+)**	**WT (+/+)**	**Homozygote (−/−)**	**Heterozygote (−/+)**	**WT (+/+)**
% per genotype (expected: 25:50:25%)	24%	49%	27%	22%	51%	27%
Survival rate (%) At 10 months	96%	90%	89%	88%	86%	75%

Table 6: Target sequence for designing gRNA for knock-out of *cryaba* and *cryabb*

Gene	**Primer**	**Targeted Sequence**
cryaba	T01	GGCGCTTTCCAAGCTGGT
	T02	GTAAAACATGGTGTAGAA
	T03	CTGATCAAAAATTCGATA
	T04	ACAAGGGTCGGCGATACC
cryabb	T01	GCCGGAACGGGGGATTGA
	T02	CTCCCCAAATTGCCGGCG
	T03	ATCGTTGGGAGTACAATG
	T04	TTCGCAGTCCAAGCTGGA

Table 7: Primer sequence for initial screening of KO in *cryaba* and *cryabb*

Gene		Primer Sequence
cryaba	Forward	AATGAGCCAGAGGGGAAGAG
	Reverse	TGTGAAAATGTCCTTGCATCA
cryabb	Forward	GGAAGGGGAGAACACAGTGG
	Reverse	ACGCGTGACTCCTCAACTTT

Table 8: Primer sequence for PCR amplification to genotype alleles of *cryaba* and *cryabb*

Gene	Allele		Primer Sequence (5' → 3')
cryaba	αBa^{5bpINS}	Forward	AGCCCAGCATTTGAGACTCTATG
		Reverse	GTGTAGAAAGGTGAAAAAGGGTC
cryaba	αBa^{35bpDEL}	Forward	ATAGATCAGTGGCTGACACGAGG
		Reverse	CATGCCACTGTCCCACCAGC
cryabb	αBa^{10bpDEL}	Forward	GGAAGGGGAGAACACAGTGG
	αBa^{8bpDEL}	Reverse	ACGCGTGACTCCTCAACTTT

Table 9: Primer sequences for qPCR

Gene		Primer Sequence (5'→3')
cryaa	Forward	AGGGCAAGCATGGAGAAAG
	Reverse	GCAGACAGTGTGCAGGTGAT
cryaba	Forward	GCATGTCGGAGATGAGACAG
	Reverse	CTGCCGTTCATCATGTTTTC
cryabb	Forward	TCTTCCTTTCTTCGCAGTCC
	Reverse	TGATAGCTCCTCTGGTGCAA
ßactin	Forward	CGAGCTGTCTTCCCATCCA
	Reverse	TCACCAACGTAGCTGTCTTTCTG
pepck	Forward	AACTCCAGGTTTTGTGCCCC
	Reverse	TACACCAAAGGCACACCTTCT
pxr	Forward	ATGAAGTGACGGGAATTTGGG
	Reverse	GATGGTGCTGAAAACCAGCTC
fkbp5	Forward	GTCGACTGTTTGATTCGCGG
	Reverse	AGGCGTACTTGGGCTTTAGG

CHAPTER IV

PERSPECTIVES ON FUTURE DIRECTIONS

Mapping the N-terminus of αB for its role in oligomerization

The work presented in this dissertation illustrates the role of the C-terminal (147-175) and the N-terminal sequence (33-52) flanking the ACD of αBa in modulating the oligomerization and thereby affecting the chaperone activity. In the N-terminus, our studied region overlaps with a previously identified “recognition sequence” which has been shown to be involved in interaction among crystallins and substrate proteins (Ghosh et al., 2006, Sreelakshmi et al., 2004). Deletion of the residues 41-58 has been shown to form oligomers larger and more polydisperse than the wild-type αB-crystallin while staying equally chaperone active (Ghosh et al., 2006). Our results of swapping αB residues 33-52 are also consonant with high resolution studies which show that residues 45–68 of αB form β_1-loop-β_2 structure which adopts different environments in the EM density maps affecting the higher-order multimers of αB (Jehle et al., 2011). Thus our study adds to the consensus that the sequences intercalating the proximal N-terminus of sHSP with the ACD have an important role in the upward transition of the oligomeric assembly.

However, this work did not extend further up the N-terminus; therefore, it is not clear what role the rest of the NTD of αBa plays in the formation of the large oligomers seen here. A conserved sequence motif (SXXFD) is found in some mammalian sHSPs, including αB-crystallin, just before the peptides swapped in this work, which aligns with the hydrophobic residues of ACD (van Montfort et al., 2001b, Bagneris et al., 2009). Removal of the sequence ^{21}SRLFDQFFG^{29} from the NTD has been shown for human α-crystallins to result in a smaller assembly with increased chaperone activity (Pasta et al., 2003). Zebrafish αBa has weak homology to this mammalian NTD motif, while αBb completely lacks it (Figure 22). For Hsp27, it

has been shown that deleting the entire NTD consisting of residues 2 through 87 (referred to as Hsp27-trunc) restricted the assembly to a tetramer, while still maintaining the concentration-dependent equilibrium between the monomer and the tetramer (Berengian et al., 1997, Bova et al., 2000, Bova et al., 1997). The NTD deficient Hsp27-trunc mutant was chaperone inactive, illustrating its critical role in the interaction with the substrate (McDonald et al., 2012). Similarly, it has been shown that while truncation of the first 19 residues from N- or the C-terminus of αA-crystallin did not significantly change the size of oligomers but deletion of the entire N-terminal (63 residues) of αA-crystallin reduced the assembly to just dimers or tetramers (Merck et al., 1992, Bova et al., 2000). Thus, the sequence elements between the proximal and the distal NTD of αB-crystallin, especially α_2-loop-β_1 (residues 23–37) can play a critical role in affecting the placement of the $\beta 1/\beta_2$ to form the oligomers bigger than the often-resolved simplest 24-mer species. Since there are significant differences in the sequences between the two zebrafish αB paralogs, in the region upstream to the region studied in this work, swapping the peptides between them will highlight the role of that domain in oligomeric assembly and chaperone activity.

In the work presented here, we only engineered N- and C-terminal swapped variants of αBa, and we did not extend the homology directed swapping to test the effect on the swapped αB variants. Our hypothesis was that the constitutively higher chaperone-like activity of αBa arises from the properties of the higher oligomeric ensemble supported by the NTD. A corollary to this hypothesis is that reverse swapping the NTD of human αB with homologous NTD of zebrafish αBa should shift the equilibrium of the engineered αB towards higher oligomeric size, with increase the chaperone activity. Without measuring an engineered αB, it is not confirmed yet whether the reduction in the αBa-L form in the Swap4 variant compared to the WT; and the

reduction in the chaperone activity shown in the present work were not artifacts of the protein modification.

While the *in vitro* expression of the cloned proteins is very effective in studying the effects of the sequence manipulation on oligomer dynamics, it does not illustrate the oligomeric state of the proteins *in vivo*. As shown here, zebrafish αBa seems unique among the vertebrate αB-crystallins studied so far, in that it forms two distinct oligomeric ensembles. However, our work did not establish that the very large oligomers shown *in vitro* are physiologically relevant such that they exist *in vivo*. The state of the αBa oligomers needs to be studied in the proteins isolated from the fish lenses. Since this work has now produced polyclonal antibodies raised against the *in vitro* expressed αBa protein, which can detect αBa in the crude adult lens homogenate as shown in the details in Experimental Procedures, it should now be possible to isolate αBa protein enough for the biochemical characterizations, from a sufficiently large number of excised adult zebrafish lenses. Using the already established methods of isolating the α-crystallins from the vertebrate lens, a future work should attempt to isolate αBa crystallin from the adult zebrafish lenses, and then measure its oligomeric status and the chaperone activity.

Measuring subunit exchange rate in the αB oligomer by Fluorescence Resonance Energy Transfer (FRET)

The work presented here illustrates that swapping the sequences of the flanking regions of αBa with αB-crystallin affect oligomer polydispersity. However it did not determine whether the change in polydispersity correlated with a faster exchange rate in the subunits of αBa. Also, we did not study whether the two oligomeric ensembles differ in the subunit exchange rate, besides the size of the oligomeric assembly. It is well established that the chaperone properties of αB-

crystallin and other sHSPs rely on the dynamic equilibrium between their oligomeric and protomeric states. *In vitro*, subunit exchange has thermal dependence, and the ionic and structural conditions provided by the N- and C-terminal flanking regions could tune the exchange rate *in vivo*, making sub-oligomeric forms available for substrate binding. Transitions away from energetically stable oligomers expose hydrophobic patches in the functional regions of the sHsp monomer, which then interact with the hydrophobic core of the substrate proteins.

Förster resonance energy transfer (FRET) is the non-radiative energy transfer from an excited fluorescent donor molecule directly to an acceptor molecule through the dipole-dipole coupling mechanism. Calculation of FRET efficiency is an elegant molecular ruler, which has been employed *in vitro* and *in vivo* to measure nanometer-scale proximities between two fluorescently labeled proteins (Zheng, 2010, dos Remedios and Moens, 1995). FRET has been used to calculate subunit exchange rates between homo- and hetero-oligomers of sHSPs such as αA and Hsp27 (Bova et al., 2000, Raju et al., 2012).

To extend the work presented here, labeled αBa engineered variants with donor and acceptor fluorescent dye pairs, such as 4-Acetamido-4-isothiocyanatostilbene-2-2-disulfonic acid (AIAS) and Lucifer yellow iodoacetamide (LYI), could be used to measure subunit exchange rates by monitoring time dependent quenching of fluorescence intensity of the donor AIAS after mixing αB samples labeled with each dye. The decreased AIAS fluorescence would reflect enhanced FRET efficiency, which in turn should originate from the exchange reaction that brings the labeled αBa subunits closer. Confirmation that subunit exchange is reversible can be shown by monitoring the time-course of recovery of AIAS signal following the mixing with unlabeled αBa.

Elucidation of the folding pattern and subunit interface in the oligomer by Site Directed Spin Labeling (SDSL) and Electron Paramagnetic Resonance (EPR) spectroscopy

Electron Paramagnetic Resonance (EPR) is a spectroscopy technique which probes spin properties of unpaired electrons in the presence of an externally applied static magnetic field. While most proteins are natively EPR silent, a nitroxide free radical spin label can be attached to the proteins as an EPR reporter group (McHaourab et al., 2011b, Hubbell et al., 1996, McHaourab et al., 1996). The EPR spectrum of the label reports its conformational mobility which is representative of the immediate environment of the spin label. From the EPR spectra by the site directed spin labelling (SDSL), detailed structural properties of the proteins such as backbone dynamics, secondary structure, tertiary contacts and inter-residue distances can be inferred (Claxton et al., 2015). In this approach, proteins are labeled with SDSL at either a native cysteine residue or at an introduced cysteine mutant of a non-conserved site by traditional PCR based methods of amino acid mutation on a Cys-less mutant background. Protein is reacted with a thiol-specific, methylthiosulphonate (MTSSL) spin label and the unreacted excess label is removed by SEC. Our lab has used this approach to investigate quaternary interactions along conserved sequences in the ACD of αA, Hsp27 and Hsp16.3 (Koteiche et al., 1998, Koteiche and McHaourab, 1999, Koteiche and McHaourab, 2002, Koteiche and McHaourab, 2003, Koteiche and Mchaourab, 2004, Koteiche et al., 2005, Koteiche and McHaourab, 2006, Koteiche et al., 2007, Kumar et al., 2009, McHaourab et al., 1997, McHaourab et al., 2002, Mchaourab et al., 2005, McHaourab et al., 2007, McHaourab et al., 2008, Murthy et al., 2004, Sathish et al., 2004, Shashidharamurthy et al., 2005, Shi et al., 2006a, Shi et al., 2013). The anti-parallel orientation of the ß-sheets in the ACD of sHSPs was first reflected by the periodic pattern in the accessibility towards polar NiEDDA and apolar O_2 and in site-specific changes of amplitude and width of the EPR spectra in cysteine scanning

experiments (Koteiche and McHaourab, 1999). Using EPR spectroscopy, in a future work, it could be studied whether the two oligomeric ensembles differ in the placement of their terminal regions in the oligomeric organization. Previous studies in our lab using EPR analyses have illustrated that environment, and/or accessibility of the NTD of Hsp27 change upon transition from the large oligomers to the dimer (McDonald et al., 2012). While the EPR line shapes from spin labels placed in the NTD in Hsp27 were consistent with buried location and extensive subunit contacts, the activated triply phosphorylated mimic Hsp27-D3 ($Hsp27^{S15D/S78D/S82D}$) showed less restricted spin-label motion capturing the structural rearrangements indicative of oligomer dissociation (McDonald et al., 2012). Extending a similar study in the αBa would be useful in understanding whether the terminal regions of αBa-S and αBa-L oligomers differ distinctly in their placement, and whether particular residues are responsible in maintaining distinct oligomeric ensembles uniquely observed in αBa.

Role of αB crystallins in the maintenance of lens transparency

The work presented here demonstrates the critical role of αB-crystallins in the maintenance of zebrafish lens transparency and complements previous studies in mouse and zebrafish that established the essentiality of αA crystallin for a similar role (Zou et al., 2015, Brady et al., 1997, Brady and Wawrousek, 1997, Wawrousek and Brady, 1997, Brady et al., 2001). However we did not follow the temporal progression of the cataractous aggregations and their effect on the lens and heart proteome. Since the lens proteome is fine-tuned for minimal light scattering, a future work utilizing the αBa and αBb knockout mutants can be used to establish a timeline of the perturbation in the soluble lens proteome. It has previously been shown that modulation of α-crystallin levels can overcome some crystallin aggregation, confirming their putative role *in vivo* as a chaperone (Goishi et al., 2006, Wu et al., 2016). However, it has not been shown if there are early events in the inter-crystallin interaction that begin the cascade of cataractous

aggregation. Lens fiber cells must maintain a regulated network of molecular components and cellular pathways to assure proteostasis and avoid cataract. Therefore, a perturbation in the lens proteome, either due to aging or due to mutations in lens proteins, should lead to a delicate rebalancing of the protein distribution (Morimoto and Cuervo, 2014). The work presented here did not find evidence that the absence of αBa or αBb is compensated by a reciprocal over-expression of the other α-crystallins. However, we did not address whether the cataractous lens modulates α-crystallin activity (by phosphorylation or by attenuating oligomeric composition) in response to the cataractous aggregations.

A future work can utilize the robust approach of proteomics, such as 2D-gel electrophoresis and mass spectrometry to follow up on the limitations of the present work. Studying the expression of the entire proteome during cataractogenesis will provide a holistic view of the cellular processes that maintain transparency in healthy lens. It will also help identify the early events before the proteostatic collapse leads to aggregate formation clouding the lens.

Two-dimensional polyacrylamide gel electrophoresis (2D-PAGE) using pH dependent isoelectric focusing (IEF) followed by monomeric size dependent SDS–PAGE is an effective, relatively fast technique to simultaneously separate and visualize proteins from tissue homogenates (Welman et al., 2006, Mandal et al., 2009). Time dependent 2D-PAGE can analyze global changes in the gene expression and protein modification as the lens undergoes the proteostatic stress (Harrington et al., 2007). Difference Gel Electrophoresis (DIGE) is a modified 2D-PAGE, where proteins are labeled with fluorescent dyes (CyDyes: Cy2, Cy3, and Cy5) prior to IEF allowing statistically valid quantification of a dynamic range of protein concentrations with high sensitivity (Tannu and Hemby, 2006, Santhoshkumar et al., 2014, Andley et al., 2014).

To identify lenticular proteins that change in abundance and to follow the change with time and progression of cataract upon proteostatic perturbation, proteins from the lenses of the WT and the α-crystallin KO zebrafish can be isolated at different ages and under different stress conditions. Following the procedure outlined in Chapter III, the water-soluble (WSF) and water-insoluble (WIS) fractions can be separated from the lens homogenates, by centrifugation (12,000× *g* for 50 min at 4 °C), and the proteins in the supernatant (WSF) and pellet (WIS) can be determined using Bradford reagent. Normalized amount of proteins can then be visualized by 2D-PAGE and the protein distributions can be estimated by densitometry against purified reference proteins as loading and staining control. This would identify and visualize the proteins which change in the relative expression upon cataract. The gel spots identified by differential expression in mutants vs. wild type control can then be selected for further MS analysis.

Difference gel electrophoresis (DIGE) is a modification of 2D-PAGE that circumvents the reproducibility problems associated with comparing two different 2D gels, by requiring a single gel to reproducibly detect differences between two protein samples (Conrads et al., 2003). For DIGE, the water-soluble and -insoluble proteins will be labeled with two fluorescent dyes, such as 1-(5-carboxypentyl)-1′-propylindocarbocyanine halide (Cy3) N-hydroxysuccinimidyl ester and 1-(5-carboxypentyl)-1′-methylindodicarbocyanine halide (Cy5) N-hydroxysuccinimidyl ester, respectively. The labeled proteins will be mixed and separated in the same 2D gel by the established protocols of 2D-DIGE (Andley et al., 2014, Santhoshkumar et al., 2014). Samples will be imaged using wavelengths specific for each dye, and will be normalized to the control samples labeled with fluorescent dyes and run on the same 2D gels. The differential expressions between WT and mutant lenses among the samples will be assessed and the individual protein spots showing differential intensities will be excised from the gel and will be

analyzed by mass spectrometry. Multi-gel analyses will ensure significance in changes in temporal protein abundance between WT and knockout zebrafish lenses.

Since α-crystallins can be partially enriched from the lens homogenates by SEC, we can use this fraction to monitor change in the chaperone activity by our well-established assay. We can measure the change in the chaperone activity as function of age, the cataract severity, and the proteome. Our hypothesis is that cataractous puncta seen in the zebrafish lens are aggregated proteins. Using fluorescently tagged crystallin mutant lines, a future work can attempt to compare the extent of the aggregation in the cataractous lenses microscopically *in situ* and chromatographically *ex situ*. From the excised lenses that show cataract, we can isolate proteins which partition between the WSF and WIF. From the fractionation of the proteins, it can be studied whether a correlation exists between the intensity or the distribution of the fluorescent puncta; and the perturbing factor (thermodynamic instability of the substrate, compromise of the chaperone activity of the α-crystallin, or the combination).

For monitoring the association of substrate proteins with the α-crystallin pool, we can use transgenic lenses that express fluorescent reporter protein (RFP or CFP) tagged with cataractogenic heterologous γD or homologous γMx crystallins. We can excise such lenses, homogenize them in buffer, separate the WSF by centrifugation and monitor the fluorescent proteins coeluting with the α-crystallin pool in SEC, using an HPLC (Agilent HP1100) fitted with both UV absorbance and Fluorescence detectors. We can also monitor changes in the water soluble protein elution profiles as a function of aging and cataract severity.

For the system that shows the most severe phenotypes, we can further analyze change in the lens proteome relative to the wild type by a multiplex Isobaric tags for relative and absolute quantification (iTRAQ) mass spectrometry combined with 2D-LC-MS/MS. The large dynamic range of iTRAQ can identify and quantify relative expressions of a large number of

proteins in mutants or aged samples compared to the WT control, simultaneously and in a relatively short time (Wu et al., 2016). In conjunction with 2D-DIGE, iTRAQ will identify the networks and the steps involved in the failure of lens proteostasis.

A future work should evaluate whether αBa and/or αBb deficiency in lens accentuates the cataract phenotype in the already established fish mutants, where heterologous expression of aggregation-prone γD crystallin mutants chronically perturbs the lens proteostasis (Mishra et al., 2012, Wu et al., 2016). We should also compare the chaperone efficacy of αBa and αBb in restoring the cataract in the zebrafish lenses by genetically enhancing the expressing of αBa or αBb in the γD transgenic lines.

REFERENCES

2012. *Ageing in the Twenty-First Century: A Celebration and A Challenge* United Nations Population Fund (UNFPA), New York, and HelpAge International, London

A, W., RB, W., MCCOY MA & TEUTSCH SM 2016. *Making eye health a population health imperative: Vision for tomorrow,* Washington, DC, The National Academies Press.

AEVERMANN, B. D. & WATERS, E. R. 2008. A comparative genomic analysis of the small heat shock proteins in Caenorhabditis elegans and briggsae. *Genetica,* 133**,** 307-19.

AGUILANIU, H., GUSTAFSSON, L., RIGOULET, M. & NYSTROM, T. 2003. Asymmetric inheritance of oxidatively damaged proteins during cytokinesis. *Science,* 299**,** 1751-3.

AHMAD, N., ASLAM, M., MUENSTER, D., HORSCH, M., KHAN, M. A., CARLSSON, P., BECKERS, J. & GRAW, J. 2013. Pitx3 directly regulates Foxe3 during early lens development. *Int J Dev Biol,* 57**,** 741-51.

AIZENBERG, J., SUNDAR, V. C., YABLON, A. D., WEAVER, J. C. & CHEN, G. 2004. Biological glass fibers: correlation between optical and structural properties. *Proc Natl Acad Sci U S A,* 101**,** 3358-63.

AKERFELT, M., MORIMOTO, R. I. & SISTONEN, L. 2010. Heat shock factors: integrators of cell stress, development and lifespan. *Nat Rev Mol Cell Biol,* 11**,** 545-55.

ALSOP, D. & VIJAYAN, M. M. 2009. Molecular programming of the corticosteroid stress axis during zebrafish development. *Comp Biochem Physiol A Mol Integr Physiol,* 153**,** 49-54.

ANDLEY, U. P. 2007. Crystallins in the eye: Function and pathology. *Prog Retin Eye Res,* 26**,** 78-98.

ANDLEY, U. P., MALONE, J. P. & TOWNSEND, R. R. 2014. In vivo substrates of the lens molecular chaperones alphaA-crystallin and alphaB-crystallin. *PLoS One,* 9**,** e95507.

ANFINSEN, C. B. 1973. Principles that govern the folding of protein chains. *Science,* 181**,** 223-30.

ANFINSEN, C. B., HABER, E., SELA, M. & WHITE, F. H., JR. 1961. The kinetics of formation of native ribonuclease during oxidation of the reduced polypeptide chain. *Proc Natl Acad Sci U S A,* 47**,** 1309-14.

AOYAMA, A., FROHLI, E., SCHAFER, R. & KLEMENZ, R. 1993. Alpha B-crystallin expression in mouse NIH 3T3 fibroblasts: glucocorticoid responsiveness and involvement in thermal protection. *Mol Cell Biol,* 13**,** 1824-35.

AQUILINA, J. A., BENESCH, J. L., BATEMAN, O. A., SLINGSBY, C. & ROBINSON, C. V. 2003. Polydispersity of a mammalian chaperone: mass spectrometry reveals

the population of oligomers in alphaB-crystallin. *Proc Natl Acad Sci U S A,* 100**,** 10611-6.

ARRIGO, A. P., SIMON, S., GIBERT, B., KRETZ-REMY, C., NIVON, M., CZEKALLA, A., GUILLET, D., MOULIN, M., DIAZ-LATOUD, C. & VICART, P. 2007. Hsp27 (HspB1) and alphaB-crystallin (HspB5) as therapeutic targets. *FEBS Lett,* 581**,** 3665-74.

ASBELL, P. A., DUALAN, I., MINDEL, J., BROCKS, D., AHMAD, M. & EPSTEIN, S. 2005. Age-related cataract. *Lancet,* 365**,** 599-609.

ASHERIE, N. 2011. Blind attraction: the mechanism of an inherited congenital cataract. *Proc Natl Acad Sci U S A,* 108**,** 437-8.

ASOMUGHA, C. O., GUPTA, R. & SRIVASTAVA, O. P. 2011. Structural and functional properties of NH(2)-terminal domain, core domain, and COOH-terminal extension of alphaA- and alphaB-crystallins. *Mol Vis,* 17**,** 2356-67.

AUGUSTEYN, R. C. 2004. alpha-crystallin: a review of its structure and function. *Clin Exp Optom,* 87**,** 356-66.

BAASE, W. A., LIU, L., TRONRUD, D. E. & MATTHEWS, B. W. 2010. Lessons from the lysozyme of phage T4. *Protein Sci,* 19**,** 631-41.

BAGNERIS, C., BATEMAN, O. A., NAYLOR, C. E., CRONIN, N., BOELENS, W. C., KEEP, N. H. & SLINGSBY, C. 2009. Crystal structures of alpha-crystallin domain dimers of alphaB-crystallin and Hsp20. *J Mol Biol,* 392**,** 1242-52.

BAKKERS, J. 2011. Zebrafish as a model to study cardiac development and human cardiac disease. *Cardiovasc Res,* 91**,** 279-88.

BAKTHISARAN, R., AKULA, K. K., TANGIRALA, R. & RAO CH, M. 2016. Phosphorylation of alphaB-crystallin: Role in stress, aging and patho-physiological conditions. *Biochim Biophys Acta,* 1860**,** 167-82.

BALCH, W. E., MORIMOTO, R. I., DILLIN, A. & KELLY, J. W. 2008. Adapting proteostasis for disease intervention. *Science,* 319**,** 916-9.

BALDWIN, A. J., LIOE, H., ROBINSON, C. V., KAY, L. E. & BENESCH, J. L. 2011. alphaB-crystallin polydispersity is a consequence of unbiased quaternary dynamics. *J Mol Biol,* 413**,** 297-309.

BALTUSSEN, R., SYLLA, M. & MARIOTTI, S. P. 2004. Cost-effectiveness analysis of cataract surgery: a global and regional analysis. *Bull World Health Organ,* 82**,** 338-45.

BAMBERGER, C. M., BAMBERGER, A. M., DE CASTRO, M. & CHROUSOS, G. P. 1995. Glucocorticoid receptor beta, a potential endogenous inhibitor of glucocorticoid action in humans. *J Clin Invest,* 95**,** 2435-41.

BANERJEE, P. R., PANDE, A., PATROSZ, J., THURSTON, G. M. & PANDE, J. 2011. Cataract-associated mutant E107A of human gammaD-crystallin shows increased attraction to alpha-crystallin and enhanced light scattering. *Proc Natl Acad Sci U S A,* 108**,** 574-9.

BANERJEE, P. R., PANDE, A., THURSTON, G. & PANDE, J. 2010. Thermodynamic Studies on the Cataract-Associated Mutant, E107a, of Human Gamma-D Crystallin: Molecular Basis for Cataract Formation. *Biophysical Journal,* 98**,** 44a-44a.

BASHA, E., FRIEDRICH, K. L. & VIERLING, E. 2006. The N-terminal arm of small heat shock proteins is important for both chaperone activity and substrate specificity. *J Biol Chem,* 281**,** 39943-52.

BASHA, E., O'NEILL, H. & VIERLING, E. 2012. Small heat shock proteins and alpha-crystallins: dynamic proteins with flexible functions. *Trends Biochem Sci,* 37**,** 106-17.

BASSNETT, S., SHI, Y. & VRENSEN, G. F. 2011. Biological glass: structural determinants of eye lens transparency. *Philos Trans R Soc Lond B Biol Sci,* 366**,** 1250-64.

BEMPORAD, F., GSPONER, J., HOPEARUOHO, H. I., PLAKOUTSI, G., STATI, G., STEFANI, M., TADDEI, N., VENDRUSCOLO, M. & CHITI, F. 2008. Biological function in a non-native partially folded state of a protein. *EMBO J,* 27**,** 1525-35.

BENEDEK, G. B. 1971. Theory of transparency of the eye. *Appl Opt,* 10**,** 459-73.

BENESCH, J. L., AYOUB, M., ROBINSON, C. V. & AQUILINA, J. A. 2008. Small heat shock protein activity is regulated by variable oligomeric substructure. *J Biol Chem,* 283**,** 28513-7.

BENJAMIN, I. J., GUO, Y., SRINIVASAN, S., BOUDINA, S., TAYLOR, R. P., RAJASEKARAN, N. S., GOTTLIEB, R., WAWROUSEK, E. F., ABEL, E. D. & BOLLI, R. 2007. CRYAB and HSPB2 deficiency alters cardiac metabolism and paradoxically confers protection against myocardial ischemia in aging mice. *Am J Physiol Heart Circ Physiol,* 293**,** H3201-9.

BENJAMINI, Y. & HOCHBERG, Y. 1995. Controlling the False Discovery Rate - a Practical and Powerful Approach to Multiple Testing. *Journal of the Royal Statistical Society Series B-Methodological,* 57**,** 289-300.

BENNARDINI, F., WRZOSEK, A. & CHIESI, M. 1992. Alpha B-crystallin in cardiac tissue. Association with actin and desmin filaments. *Circ Res,* 71**,** 288-94.

BERENGIAN, A. R., BOVA, M. P. & MCHAOURAB, H. S. 1997. Structure and function of the conserved domain in alphaA-crystallin. Site-directed spin labeling identifies a beta-strand located near a subunit interface. *Biochemistry,* 36**,** 9951-7.

BERENGIAN, A. R., PARFENOVA, M. & MCHAOURAB, H. S. 1999. Site-directed Spin Labeling Study of Subunit Interactions in the α-Crystallin Domain of Small Heat-shock Proteins. *Journal of Biological Chemistry,* 274**,** 6305-6314.

BERGMANN, O., BHARDWAJ, R. D., BERNARD, S., ZDUNEK, S., BARNABE-HEIDER, F., WALSH, S., ZUPICICH, J., ALKASS, K., BUCHHOLZ, B. A., DRUID, H., JOVINGE, S. & FRISEN, J. 2009. Evidence for cardiomyocyte renewal in humans. *Science,* 324**,** 98-102.

BERNHARD, D. & LAUFER, G. 2008. The aging cardiomyocyte: a mini-review. *Gerontology,* 54**,** 24-31.

BERZELIUS, J. N. J. 1842. Jahres-Bericht über die Fortschritte der Chemie und Mineralogie. *Jahres-Bericht über die Fortschritte der Chemie und Mineralogie*.

BHAT, S. P., HORWITZ, J., SRINIVASAN, A. & DING, L. 1991. Alpha B-crystallin exists as an independent protein in the heart and in the lens. *Eur J Biochem,* 202**,** 775-81.

BHATTACHARYYA, J., PADMANABHA UDUPA, E. G., WANG, J. & SHARMA, K. K. 2006. Mini-alphaB-crystallin: a functional element of alphaB-crystallin with chaperone-like activity. *Biochemistry,* 45**,** 3069-76.

BIANCONI, E., PIOVESAN, A., FACCHIN, F., BERAUDI, A., CASADEI, R., FRABETTI, F., VITALE, L., PELLERI, M. C., TASSANI, S., PIVA, F., PEREZ-AMODIO, S., STRIPPOLI, P. & CANAIDER, S. 2013. An estimation of the number of cells in the human body. *Ann Hum Biol,* 40**,** 463-71.

BIDINOST, C., MATSUMOTO, M., CHUNG, D., SALEM, N., ZHANG, K., STOCKTON, D. W., KHOURY, A., MEGARBANE, A., BEJJANI, B. A. & TRABOULSI, E. I. 2006. Heterozygous and homozygous mutations in PITX3 in a large Lebanese family with posterior polar cataracts and neurodevelopmental abnormalities. *Invest Ophthalmol Vis Sci,* 47**,** 1274-80.

BLACK, R. L., OGLESBY, R. B., VON SALLMANN, L. & BUNIM, J. J. 1960. Posterior subcapsular cataracts induced by corticosteroids in patients with rheumatoid arthritis. *JAMA,* 174**,** 166-71.

BOELENS, W. C. 2014. Cell biological roles of alphaB-crystallin. *Prog Biophys Mol Biol,* 115**,** 3-10.

BONCORAGLIO, A., MINOIA, M. & CARRA, S. 2012. The family of mammalian small heat shock proteins (HSPBs): implications in protein deposit diseases and motor neuropathies. *Int J Biochem Cell Biol,* 44**,** 1657-69.

BOOTH, D. S., AVILA-SAKAR, A. & CHENG, Y. 2011. Visualizing proteins and macromolecular complexes by negative stain EM: from grid preparation to image acquisition. *J Vis Exp*.

BORCHMAN, D., STIMMELMAYR, R. & GEORGE, J. C. 2017. Whales, lifespan, phospholipids, and cataracts. *J Lipid Res,* 58**,** 2289-2298.

BOUDOULAS, K. D., BORER, J. S. & BOUDOULAS, H. 2015. Heart Rate, Life Expectancy and the Cardiovascular System: Therapeutic Considerations. *Cardiology,* 132**,** 199-212.

BOURNELE, D. & BEIS, D. 2016. Zebrafish models of cardiovascular disease. *Heart Fail Rev,* 21**,** 803-813.

BOUZAS, E. A., MASTORAKOS, G., FRIEDMAN, T. C., SCOTT, M. H., CHROUSOS, G. P. & KAISER-KUPFER, M. I. 1993. Posterior subcapsular cataract in endogenous Cushing syndrome: an uncommon manifestation. *Invest Ophthalmol Vis Sci,* 34**,** 3497-500.

BOVA, M. P., DING, L. L., HORWITZ, J. & FUNG, B. K. 1997. Subunit exchange of alphaA-crystallin. *J Biol Chem,* 272**,** 29511-7.

BOVA, M. P., MCHAOURAB, H. S., HAN, Y. & FUNG, B. K. 2000. Subunit exchange of small heat shock proteins. Analysis of oligomer formation of alphaA-crystallin and Hsp27 by fluorescence resonance energy transfer and site-directed truncations. *J Biol Chem,* 275**,** 1035-42.

BRADY, J. P., GARLAND, D., DUGLAS-TABOR, Y., ROBISON, W. G., JR., GROOME, A. & WAWROUSEK, E. F. 1997. Targeted disruption of the mouse alpha A-crystallin gene induces cataract and cytoplasmic inclusion bodies containing the small heat shock protein alpha B-crystallin. *Proc Natl Acad Sci U S A,* 94**,** 884-9.

BRADY, J. P., GARLAND, D. L., GREEN, D. E., TAMM, E. R., GIBLIN, F. J. & WAWROUSEK, E. F. 2001. AlphaB-crystallin in lens development and muscle integrity: a gene knockout approach. *Invest Ophthalmol Vis Sci,* 42**,** 2924-34.

BRADY, J. P. & WAWROUSEK, E. F. 1997. Targeted disruption of the mouse alpha beta-crystallin gene. *Investigative Ophthalmology & Visual Science,* 38**,** 4352-4352.

BRÄNDÉN, C.-I. & TOOZE, J. 1999. *Introduction to protein structure,* New York, Garland Pub.

BRAUN, N., ZACHARIAS, M., PESCHEK, J., KASTENMULLER, A., ZOU, J., HANZLIK, M., HASLBECK, M., RAPPSILBER, J., BUCHNER, J. & WEINKAUF, S. 2011. Multiple molecular architectures of the eye lens chaperone alphaB-crystallin elucidated by a triple hybrid approach. *Proc Natl Acad Sci U S A,* 108**,** 20491-6.

BREHME, M., VOISINE, C., ROLLAND, T., WACHI, S., SOPER, J. H., ZHU, Y., ORTON, K., VILLELLA, A., GARZA, D., VIDAL, M., GE, H. & MORIMOTO, R. I. 2014. A chaperome subnetwork safeguards proteostasis in aging and neurodegenerative disease. *Cell Rep,* 9**,** 1135-50.

BROADLEY, S. A. & HARTL, F. U. 2009. The role of molecular chaperones in human misfolding diseases. *FEBS Lett,* 583**,** 2647-53.

BROCCHIERI, L. & KARLIN, S. 2005. Protein length in eukaryotic and prokaryotic proteomes. *Nucleic Acids Res,* 33**,** 3390-400.

BROCKLEBANK, J. T., HARCOURT, R. B. & MEADOW, S. R. 1982. Corticosteroid-induced cataracts in idiopathic nephrotic syndrome. *Arch Dis Child,* 57**,** 30-4.

BRUNDEL, B. J., HENNING, R. H., KE, L., VAN GELDER, I. C., CRIJNS, H. J. & KAMPINGA, H. H. 2006. Heat shock protein upregulation protects against pacing-induced myolysis in HL-1 atrial myocytes and in human atrial fibrillation. *J Mol Cell Cardiol,* 41**,** 555-62.

BUHRDEL, J. B., HIRTH, S., KESSLER, M., WESTPHAL, S., FORSTER, M., MANTA, L., WICHE, G., SCHOSER, B., SCHESSL, J., SCHRODER, R., CLEMEN, C. S., EICHINGER, L., FURST, D. O., VAN DER VEN, P. F., ROTTBAUER, W. & JUST, S. 2015. In vivo characterization of human myofibrillar myopathy genes in zebrafish. *Biochem Biophys Res Commun,* 461**,** 217-23.

BULLARD, B., FERGUSON, C., MINAJEVA, A., LEAKE, M. C., GAUTEL, M., LABEIT, D., DING, L., LABEIT, S., HORWITZ, J., LEONARD, K. R. & LINKE, W. A. 2004. Association of the chaperone alphaB-crystallin with titin in heart muscle. *J Biol Chem,* 279**,** 7917-24.

BURNS, C. M. 2016. The History of Cortisone Discovery and Development. *Rheum Dis Clin North Am,* 42**,** 1-14, vii.

BURY, N. R. & STURM, A. 2007. Evolution of the corticosteroid receptor signalling pathway in fish. *Gen Comp Endocrinol,* 153**,** 47-56.

BUTTGEREIT, F., SEIBEL, M. J. H. & BIJLSMA, J. W. J. 2013. 87 - Glucocorticoids A2 - Rich, Robert R. *In:* FLEISHER, T. A., SHEARER, W. T., SCHROEDER, H. W., FREW, A. J. & WEYAND, C. M. (eds.) *Clinical Immunology (Fourth Edition).* London: Content Repository Only!

CAIN, J. T., KIM, D. I., QUAST, M., SHIVEGA, W. G., PATRICK, R. J., MOSER, C., REUTER, S., PEREZ, M., MYERS, A., WEIMER, J. M., ROUX, K. J. & LANDSVERK, M. 2017. Nonsense pathogenic variants in exon 1 of PHOX2B lead to translational reinitiation in congenital central hypoventilation syndrome. *Am J Med Genet A,* 173**,** 1200-1207.

CAPALDI, A. P., KLEANTHOUS, C. & RADFORD, S. E. 2002. Im7 folding mechanism: misfolding on a path to the native state. *Nat Struct Biol,* 9**,** 209-16.

CARLSON, B. M. 2014. Sense Organs. *Human Embryology and Developmental Biology.* Philadelphia: W.B. Saunders.

CARRA, S., ALBERTI, S., ARRIGO, P. A., BENESCH, J. L., BENJAMIN, I. J., BOELENS, W., BARTELT-KIRBACH, B., BRUNDEL, B., BUCHNER, J., BUKAU, B., CARVER, J. A., ECROYD, H., EMANUELSSON, C., FINET, S., GOLENHOFEN, N., GOLOUBINOFF, P., GUSEV, N., HASLBECK, M., HIGHTOWER, L. E., KAMPINGA, H. H., KLEVIT, R. E., LIBEREK, K., MCHAOURAB, H. S., MCMENIMEN, K. A., POLETTI, A., QUINLAN, R., STRELKOV, S. V., TOTH, M. E., VIERLING, E. & TANGUAY, R. M. 2017. The growing world of small heat shock proteins: from structure to functions. *Cell Stress Chaperones,* 22**,** 601-611.

CARVER, J. A., AQUILINA, J. A., TRUSCOTT, R. J. & RALSTON, G. B. 1992. Identification by 1H NMR spectroscopy of flexible C-terminal extensions in bovine lens alpha-crystallin. *FEBS Lett,* 311**,** 143-9.

CASTORINO, J. J., GALLAGHER-COLOMBO, S. M., LEVIN, A. V., FITZGERALD, P. G., POLISHOOK, J., KLOECKENER-GRUISSEM, B., OSTERTAG, E. & PHILP, N. J. 2011. Juvenile cataract-associated mutation of solute carrier SLC16A12 impairs trafficking of the protein to the plasma membrane. *Invest Ophthalmol Vis Sci,* 52**,** 6774-84.

CAVADAS, C., AVELEIRA, C. A., SOUZA, G. F. & VELLOSO, L. A. 2016. The pathophysiology of defective proteostasis in the hypothalamus - from obesity to ageing. *Nat Rev Endocrinol,* 12**,** 723-733.

CHARMPILAS, N., KYRIAKAKIS, E. & TAVERNARAKIS, N. 2017. Small heat shock proteins in ageing and age-related diseases. *Cell Stress Chaperones,* 22**,** 481-492.

CHAUDHURI, T. K. & PAUL, S. 2006. Protein-misfolding diseases and chaperone-based therapeutic approaches. *FEBS J,* 273**,** 1331-49.

CHEN, Q., JIA, A., SNYDER, S. A., GONG, Z. & LAM, S. H. 2016. Glucocorticoid activity detected by in vivo zebrafish assay and in vitro glucocorticoid receptor bioassay at environmental relevant concentrations. *Chemosphere,* 144**,** 1162-9.

CHENG, X., ZHAO, X., KHURANA, S., BRUGGEMAN, L. A. & KAO, H. Y. 2013. Microarray analyses of glucocorticoid and vitamin D3 target genes in differentiating cultured human podocytes. *PLoS One,* 8**,** e60213.

CHICO, T. J., INGHAM, P. W. & CROSSMAN, D. C. 2008. Modeling cardiovascular disease in the zebrafish. *Trends Cardiovasc Med,* 18**,** 150-5.

CHIESI, M. & BENNARDINI, F. 1992. Determination of alpha B crystallin aggregation: a new alternative method to assess ischemic damage of the heart. *Basic Res Cardiol,* 87**,** 38-46.
CHITI, F. & DOBSON, C. M. 2006. Protein misfolding, functional amyloid, and human disease. *Annu Rev Biochem,* 75**,** 333-66.
CHOW, R. L. & LANG, R. A. 2001. Early eye development in vertebrates. *Annu Rev Cell Dev Biol,* 17**,** 255-96.
CLARK, A. R., LUBSEN, N. H. & SLINGSBY, C. 2012. sHSP in the eye lens: crystallin mutations, cataract and proteostasis. *Int J Biochem Cell Biol,* 44**,** 1687-97.
CLARK, A. R., NAYLOR, C. E., BAGNERIS, C., KEEP, N. H. & SLINGSBY, C. 2011. Crystal structure of R120G disease mutant of human alphaB-crystallin domain dimer shows closure of a groove. *J Mol Biol,* 408**,** 118-34.
CLARK, J. I. 2016. Functional sequences in human alphaB crystallin. *Biochim Biophys Acta,* 1860**,** 240-5.
CLAXTON, D. P., KAZMIER, K., MISHRA, S. & MCHAOURAB, H. S. 2015. Navigating Membrane Protein Structure, Dynamics, and Energy Landscapes Using Spin Labeling and EPR Spectroscopy. *Methods Enzymol,* 564**,** 349-87.
CLAXTON, D. P., ZOU, P. & MCHAOURAB, H. S. 2008. Structure and orientation of T4 lysozyme bound to the small heat shock protein alpha-crystallin. *J Mol Biol,* 375**,** 1026-39.
COLE, T. J., BLENDY, J. A., MONAGHAN, A. P., KRIEGLSTEIN, K., SCHMID, W., AGUZZI, A., FANTUZZI, G., HUMMLER, E., UNSICKER, K. & SCHUTZ, G. 1995. Targeted disruption of the glucocorticoid receptor gene blocks adrenergic chromaffin cell development and severely retards lung maturation. *Genes Dev,* 9**,** 1608-21.
CONRADS, T. P., ISSAQ, H. J. & HOANG, V. M. 2003. Current Strategies for Quantitative Proteomics. *In:* SMITH, R. D. & VEENSTRA, T. D. (eds.) *Advances in Protein Chemistry.* Academic Press.
COSTAGLIOLA, C., CATI-GIOVANNELLI, B., PICCIRILLO, A. & DELFINO, M. 1989. Cataracts associated with long-term topical steroids. *Br J Dermatol,* 120**,** 472-3.
CVEKL, A. & ASHERY-PADAN, R. 2014. The cellular and molecular mechanisms of vertebrate lens development. *Development,* 141**,** 4432-47.
CVEKL, A. & DUNCAN, M. K. 2007. Genetic and epigenetic mechanisms of gene regulation during lens development. *Prog Retin Eye Res,* 26**,** 555-97.
CVEKL, A., ZHAO, Y., MCGREAL, R., XIE, Q., GU, X. & ZHENG, D. 2017. Evolutionary Origins of Pax6 Control of Crystallin Genes. *Genome Biol Evol,* 9**,** 2075-2092.
DA SILVA-FERRADA, E., RIBEIRO-RODRIGUES, T. M., RODRIGUEZ, M. S. & GIRAO, H. 2016. Proteostasis and SUMO in the heart. *Int J Biochem Cell Biol,* 79**,** 443-450.
DAHLMAN, J. M., MARGOT, K. L., DING, L. L., HORWITZ, J. & POSNER, M. 2005. Zebrafish alpha-crystallins: protein structure and chaperone-like activity compared to their mammalian orthologs. *Molecular Vision,* 11**,** 88-96.
DAHM, R. 1999. Lens Fibre Cell Differentiation – A Link with Apoptosis? *Ophthalmic Research,* 31**,** 163-183.

DAHM, R., SCHONTHALER, H. B., SOEHN, A. S., VAN MARLE, J. & VRENSEN, G. F. 2007. Development and adult morphology of the eye lens in the zebrafish. *Exp Eye Res,* 85**,** 74-89.

DAI, D. F., KARUNADHARMA, P. P., CHIAO, Y. A., BASISTY, N., CRISPIN, D., HSIEH, E. J., CHEN, T., GU, H., DJUKOVIC, D., RAFTERY, D., BEYER, R. P., MACCOSS, M. J. & RABINOVITCH, P. S. 2014. Altered proteome turnover and remodeling by short-term caloric restriction or rapamycin rejuvenate the aging heart. *Aging Cell,* 13**,** 529-39.

DAVSON, H. & PERKINS, E. S. 2017. Human eye. Available: https://www.britannica.com/science/human-eye.

DE CASTRO, M., ELLIOT, S., KINO, T., BAMBERGER, C., KARL, M., WEBSTER, E. & CHROUSOS, G. P. 1996. The non-ligand binding beta-isoform of the human glucocorticoid receptor (hGR beta): tissue levels, mechanism of action, and potential physiologic role. *Mol Med,* 2**,** 597-607.

DE JONG, W. W., CASPERS, G. J. & LEUNISSEN, J. A. 1998. Genealogy of the alpha-crystallin--small heat-shock protein superfamily. *Int J Biol Macromol,* 22**,** 151-62.

DELAYE, M. & TARDIEU, A. 1983. Short-range order of crystallin proteins accounts for eye lens transparency. *Nature,* 302**,** 415-7.

DELBECQ, S. P., JEHLE, S. & KLEVIT, R. 2012. Binding determinants of the small heat shock protein, alphaB-crystallin: recognition of the 'IxI' motif. *EMBO J,* 31**,** 4587-94.

DELBECQ, S. P. & KLEVIT, R. E. 2013. One size does not fit all: the oligomeric states of alphaB crystallin. *FEBS Lett,* 587**,** 1073-80.

DENG, M., CHEN, P. C., XIE, S., ZHAO, J., GONG, L., LIU, J., ZHANG, L., SUN, S., LIU, J., MA, H., BATRA, S. K. & LI, D. W. 2010. The small heat shock protein alphaA-crystallin is expressed in pancreas and acts as a negative regulator of carcinogenesis. *Biochim Biophys Acta,* 1802**,** 621-31.

DEVAJA, O., KING, R. J., PAPADOPOULOS, A. & RAJU, K. S. 1997. Heat-shock protein 27 (HSP27) and its role in female reproductive organs. *Eur J Gynaecol Oncol,* 18**,** 16-22.

DICKERSON, J. E., JR., DOTZEL, E. & CLARK, A. F. 1997. Steroid-induced cataract: new perspective from in vitro and lens culture studies. *Exp Eye Res,* 65**,** 507-16.

DIOKMETZIDOU, A., SOUMAKA, E., KLOUKINA, I., TSIKITIS, M., MAKRIDAKIS, M., VARELA, A., DAVOS, C. H., GEORGOPOULOS, S., ANESTI, V., VLAHOU, A. & CAPETANAKI, Y. 2016. Desmin and alphaB-crystallin interplay in the maintenance of mitochondrial homeostasis and cardiomyocyte survival. *J Cell Sci,* 129**,** 3705-3720.

DJABALI, K., DE NECHAUD, B., LANDON, F. & PORTIER, M. M. 1997. AlphaB-crystallin interacts with intermediate filaments in response to stress. *J Cell Sci,* 110 (Pt 21)**,** 2759-69.

DONSHIK, P. C., CAVANAUGH, H. D., BORUCHOFF, S. A. & DOHLMAN, C. H. 1981. Posterior subcapsular cataracts induced by topical corticosteroids following keratoplasty for keratoconus. *Ann Ophthalmol,* 13**,** 29-32.

DOS REMEDIOS, C. G. & MOENS, P. D. 1995. Fluorescence resonance energy transfer spectroscopy is a reliable "ruler" for measuring structural changes in proteins. Dispelling the problem of the unknown orientation factor. *J Struct Biol,* 115**,** 175-85.

DOU, W., TIAN, Y., LIU, H., SHI, Y., SMAGGHE, G. & WANG, J. J. 2017. Characteristics of six small heat shock protein genes from Bactrocera dorsalis: Diverse expression under conditions of thermal stress and normal growth. *Comp Biochem Physiol B Biochem Mol Biol,* 213**,** 8-16.

EASTER, S. S., JR. & NICOLA, G. N. 1996. The development of vision in the zebrafish (Danio rerio). *Dev Biol,* 180**,** 646-63.

EASTER, S. S. & NICOLA, G. N. 1995. The Development of Vision and Eye-Movements in Zebrafish (Danio-Rerio). *Investigative Ophthalmology & Visual Science,* 36**,** S762-S762.

ECROYD, H. & CARVER, J. A. 2009. Crystallin proteins and amyloid fibrils. *Cell Mol Life Sci,* 66**,** 62-81.

ECROYD, H., MEEHAN, S., HORWITZ, J., AQUILINA, J. A., BENESCH, J. L., ROBINSON, C. V., MACPHEE, C. E. & CARVER, J. A. 2007. Mimicking phosphorylation of alphaB-crystallin affects its chaperone activity. *Biochem J,* 401**,** 129-41.

EHRNSPERGER, M., GRABER, S., GAESTEL, M. & BUCHNER, J. 1997. Binding of non-native protein to Hsp25 during heat shock creates a reservoir of folding intermediates for reactivation. *EMBO J,* 16**,** 221-9.

ELICKER, K. S. & HUTSON, L. D. 2007. Genome-wide analysis and expression profiling of the small heat shock proteins in zebrafish. *Gene,* 403**,** 60-9.

ELICKER, K. S., KURIHARA, T. & HUTSON, L. D. 2007. Characterization of the zebrafish small heat shock protein family. *Faseb Journal,* 21**,** A226-A226.

ELLIS, J. 1987. Proteins as molecular chaperones. *Nature,* 328**,** 378-9.

ELLIS, R. J. 1993. The general concept of molecular chaperones. *Philos Trans R Soc Lond B Biol Sci,* 339**,** 257-61.

ELLIS, R. J. 2001. Macromolecular crowding: obvious but underappreciated. *Trends Biochem Sci,* 26**,** 597-604.

ERICKSON, R. R., DUNNING, L. M. & HOLTZMAN, J. L. 2006. The effect of aging on the chaperone concentrations in the hepatic, endoplasmic reticulum of male rats: the possible role of protein misfolding due to the loss of chaperones in the decline in physiological function seen with age. *J Gerontol A Biol Sci Med Sci,* 61**,** 435-43.

FACCHINELLO, N., SKOBO, T., MENEGHETTI, G., COLLETTI, E., DINARELLO, A., TISO, N., COSTA, R., GIOACCHINI, G., CARNEVALI, O., ARGENTON, F., COLOMBO, L. & DALLA VALLE, L. 2017. nr3c1 null mutant zebrafish are viable and reveal DNA-binding-independent activities of the glucocorticoid receptor. *Sci Rep,* 7**,** 4371.

FADOOL, J. M. & DOWLING, J. E. 2008. Zebrafish: a model system for the study of eye genetics. *Prog Retin Eye Res,* 27**,** 89-110.

FAGERBERG, L., HALLSTROM, B. M., OKSVOLD, P., KAMPF, C., DJUREINOVIC, D., ODEBERG, J., HABUKA, M., TAHMASEBPOOR, S., DANIELSSON, A., EDLUND, K., ASPLUND, A., SJOSTEDT, E., LUNDBERG, E., SZIGYARTO, C. A., SKOGS, M., TAKANEN, J. O., BERLING, H., TEGEL, H., MULDER, J., NILSSON, P., SCHWENK, J. M., LINDSKOG, C., DANIELSSON, F., MARDINOGLU, A., SIVERTSSON, A., VON FEILITZEN, K., FORSBERG, M., ZWAHLEN, M., OLSSON, I., NAVANI, S., HUSS, M., NIELSEN, J., PONTEN, F. & UHLEN, M. 2014. Analysis of the human tissue-specific expression by genome-wide integration of transcriptomics and antibody-based proteomics. *Mol Cell Proteomics,* 13**,** 397-406.

FANG, N. N. & MAYOR, T. 2012. Hul5 ubiquitin ligase: good riddance to bad proteins. *Prion,* 6**,** 240-4.

FEIL, I. K., MALFOIS, M., HENDLE, J., VAN DER ZANDT, H. & SVERGUN, D. I. 2001. A novel quaternary structure of the dimeric alpha-crystallin domain with chaperone-like activity. *J Biol Chem,* 276**,** 12024-9.

FINKELSTEIN, A. V., BOGATYREVA, N. S. & GARBUZYNSKIY, S. O. 2013. Restrictions to protein folding determined by the protein size. *FEBS Lett,* 587**,** 1884-90.

FLECKENSTEIN, T., KASTENMULLER, A., STEIN, M. L., PETERS, C., DAAKE, M., KRAUSE, M., WEINFURTNER, D., HASLBECK, M., WEINKAUF, S., GROLL, M. & BUCHNER, J. 2015. The Chaperone Activity of the Developmental Small Heat Shock Protein Sip1 Is Regulated by pH-Dependent Conformational Changes. *Mol Cell,* 58**,** 1067-78.

FLEISCH, V. C. & NEUHAUSS, S. C. 2006. Visual behavior in zebrafish. *Zebrafish,* 3**,** 191-201.

FORREST, K. M., AL-SARRAJ, S., SEWRY, C., BUK, S., TAN, S. V., PITT, M., DURWARD, A., MCDOUGALL, M., IRVING, M., HANNA, M. G., MATTHEWS, E., SARKOZY, A., HUDSON, J., BARRESI, R., BUSHBY, K., JUNGBLUTH, H. & WRAIGE, E. 2011. Infantile onset myofibrillar myopathy due to recessive CRYAB mutations. *Neuromuscul Disord,* 21**,** 37-40.

FOSTER, A., GILBERT, C. & RAHI, J. 1997. Epidemiology of cataract in childhood: a global perspective. *J Cataract Refract Surg,* 23 Suppl 1**,** 601-4.

FOSTER, A. & RESNIKOFF, S. 2005. The impact of Vision 2020 on global blindness. *Eye (Lond),* 19**,** 1133-5.

FOWLER, W. A. 1987. The Age of the Observable Universe. *Quarterly Journal of the Royal Astronomical Society,* 28**,** 87-108.

FOWLER, W. A. 1989. The age of the observable universe - arguments for a short age,

11.0 +/- 1.6 GYr. *Annals of the New York Academy of Sciences,* 571**,** 68-78.

FRANCK, E., MADSEN, O., VAN RHEEDE, T., RICARD, G., HUYNEN, M. A. & DE JONG, W. W. 2004. Evolutionary diversity of vertebrate small heat shock proteins. *J Mol Evol,* 59**,** 792-805.

FUENSANTA, A. V.-D. & DOBLE, N. 2012. The Human Eye and Adaptive Optics. *In:* TYSON, R. K. (ed.) *Topics in Adaptive Optics.* Rijeka: InTech.

GARNER, W. H. & SPECTOR, A. 1978. Racemization in human lens: evidence of rapid insolubilization of specific polypeptides in cataract formation. *Proc Natl Acad Sci U S A,* 75**,** 3618-20.

GE, H., WANG, L., ZHU, Y., BAILEY, K., USECHE, F., BALCH, W., DILLIN, A., MORIMOTO, R., NEWMAN, W. & REINHART, P. 2010. The proteostasis network in age-associated neurodegenerative diseases. *Society for Neuroscience Abstract Viewer and Itinerary Planner,* 40.

GEORGE, J. C., BADA, J., ZEH, J., SCOTT, L., BROWN, S. E., O'HARA, T. & SUYDAM, R. 1999. Age and growth estimates of bowhead whales (Balaena mysticetus) via aspartic acid racemization. *Canadian Journal of Zoology,* 77**,** 571-580.

GESTRI, G., LINK, B. A. & NEUHAUSS, S. C. 2012. The visual system of zebrafish and its use to model human ocular diseases. *Dev Neurobiol,* 72**,** 302-27.

GHOSH, J. G. & CLARK, J. I. 2005. Insights into the domains required for dimerization and assembly of human alphaB crystallin. *Protein Sci,* 14**,** 684-95.

GHOSH, J. G., SHENOY, A. K., JR. & CLARK, J. I. 2006. N- and C-Terminal motifs in human alphaB crystallin play an important role in the recognition, selection, and solubilization of substrates. *Biochemistry,* 45**,** 13847-54.

GIDALEVITZ, T., BEN-ZVI, A., HO, K. H., BRIGNULL, H. R. & MORIMOTO, R. I. 2006. Progressive disruption of cellular protein folding in models of polyglutamine diseases. *Science,* 311**,** 1471-4.

GIESE, K. C. & VIERLING, E. 2002. Changes in oligomerization are essential for the chaperone activity of a small heat shock protein in vivo and in vitro. *J Biol Chem,* 277**,** 46310-8.

GILBERT, S. F. 2003. *Developmental biology,* Sunderland, Mass., Sinauer Associates.

GLASER, T., JEPEAL, L., EDWARDS, J. G., YOUNG, S. R., FAVOR, J. & MAAS, R. L. 1994. PAX6 gene dosage effect in a family with congenital cataracts, aniridia, anophthalmia and central nervous system defects. *Nat Genet,* 7**,** 463-71.

GOGATE, P., GILBERT, C. & ZIN, A. 2011. Severe visual impairment and blindness in infants: causes and opportunities for control. *Middle East Afr J Ophthalmol,* 18**,** 109-14.

GOGATE, P., KALUA, K. & COURTRIGHT, P. 2009. Blindness in childhood in developing countries: time for a reassessment? *PLoS Med,* 6**,** e1000177.

GOISHI, K., SHIMIZU, A., NAJARRO, G., WATANABE, S., ROGERS, R., ZON, L. I. & KLAGSBRUN, M. 2006. AlphaA-crystallin expression prevents gamma-crystallin insolubility and cataract formation in the zebrafish cloche mutant lens. *Development,* 133**,** 2585-93.

GOLENHOFEN, N., ARBEITER, A., KOOB, R. & DRENCKHAHN, D. 2002. Ischemia-induced association of the stress protein alpha B-crystallin with I-band portion of cardiac titin. *J Mol Cell Cardiol,* 34**,** 309-19.

GOLENHOFEN, N., PERNG, M. D., QUINLAN, R. A. & DRENCKHAHN, D. 2004. Comparison of the small heat shock proteins alphaB-crystallin, MKBP, HSP25, HSP20, and cvHSP in heart and skeletal muscle. *Histochem Cell Biol,* 122**,** 415-25.

GORDON, B. L. 1935. The problem of the crystalline lens. *Archives of Ophthalmology,* 14**,** 774-788.
GRANZIER, H. L. & LABEIT, S. 2004. The giant protein titin: a major player in myocardial mechanics, signaling, and disease. *Circ Res,* 94**,** 284-95.
GRAW, J. 2004. Congenital hereditary cataracts. *Int J Dev Biol,* 48**,** 1031-44.
GRAW, J. 2009. Genetics of crystallins: cataract and beyond. *Exp Eye Res,* 88**,** 173-89.
GREILING, T. M., AOSE, M. & CLARK, J. I. 2010. Cell fate and differentiation of the developing ocular lens. *Invest Ophthalmol Vis Sci,* 51**,** 1540-6.
GUPTA, V. & WAGNER, B. J. 2009. Search for a functional glucocorticoid receptor in the mammalian lens. *Exp Eye Res,* 88**,** 248-56.
GUTTE, B. & MERRIFIELD, R. B. 1969. The total synthesis of an enzyme with ribonuclease A activity. *J Am Chem Soc,* 91**,** 501-2.
HALDER, G., CALLAERTS, P. & GEHRING, W. J. 1995. Induction of ectopic eyes by targeted expression of the eyeless gene in Drosophila. *Science,* 267**,** 1788-92.
HALEY, D. A., BOVA, M. P., HUANG, Q. L., MCHAOURAB, H. S. & STEWART, P. L. 2000. Small heat-shock protein structures reveal a continuum from symmetric to variable assemblies. *J Mol Biol,* 298**,** 261-72.
HALSKAU, O., JR., PEREZ-JIMENEZ, R., IBARRA-MOLERO, B., UNDERHAUG, J., MUNOZ, V., MARTINEZ, A. & SANCHEZ-RUIZ, J. M. 2008. Large-scale modulation of thermodynamic protein folding barriers linked to electrostatics. *Proc Natl Acad Sci U S A,* 105**,** 8625-30.
HARDING, R. L., HOWLEY, S., BAKER, L. J., MURPHY, T. R., ARCHER, W. E., WISTOW, G., HYDE, D. R. & VIHTELIC, T. S. 2008. Lengsin expression and function during zebrafish lens formation. *Exp Eye Res,* 86**,** 807-18.
HARRINGTON, V., SRIVASTAVA, O. P. & KIRK, M. 2007. Proteomic analysis of water insoluble proteins from normal and cataractous human lenses. *Mol Vis,* 13**,** 1680-94.
HARTL, F. U. 1996. Molecular chaperones in cellular protein folding. *Nature,* 381**,** 571-9.
HARTL, F. U. 2017. Protein Misfolding Diseases. *Annu Rev Biochem,* 86**,** 21-26.
HARTL, F. U., BRACHER, A. & HAYER-HARTL, M. 2011. Molecular chaperones in protein folding and proteostasis. *Nature,* 475**,** 324-32.
HARTL, F. U. & HAYER-HARTL, M. 2002. Molecular chaperones in the cytosol: from nascent chain to folded protein. *Science,* 295**,** 1852-8.
HARTL, F. U. & HAYER-HARTL, M. 2009. Converging concepts of protein folding in vitro and in vivo. *Nat Struct Mol Biol,* 16**,** 574-81.
HASLBECK, M. 2002. sHsps and their role in the chaperone network. *Cell Mol Life Sci,* 59**,** 1649-57.
HASLBECK, M., BRAUN, N., STROMER, T., RICHTER, B., MODEL, N., WEINKAUF, S. & BUCHNER, J. 2004. Hsp42 is the general small heat shock protein in the cytosol of Saccharomyces cerevisiae. *EMBO J,* 23**,** 638-49.
HASLBECK, M., FRANZMANN, T., WEINFURTNER, D. & BUCHNER, J. 2005. Some like it hot: the structure and function of small heat-shock proteins. *Nature Structural & Molecular Biology,* 12**,** 842-846.

HASLBECK, M., PESCHEK, J., BUCHNER, J. & WEINKAUF, S. 2016. Structure and function of alpha-crystallins: Traversing from in vitro to in vivo. *Biochim Biophys Acta,* 1860**,** 149-66.

HASLBECK, M. & VIERLING, E. 2015. A first line of stress defense: small heat shock proteins and their function in protein homeostasis. *J Mol Biol,* 427**,** 1537-48.

HAYES, J. M., HARTSOCK, A., CLARK, B. S., NAPIER, H. R., LINK, B. A. & GROSS, J. M. 2012. Integrin alpha5/fibronectin1 and focal adhesion kinase are required for lens fiber morphogenesis in zebrafish. *Mol Biol Cell,* 23**,** 4725-38.

HAYES, V. H., DEVLIN, G. & QUINLAN, R. A. 2008. Truncation of alphaB-crystallin by the myopathy-causing Q151X mutation significantly destabilizes the protein leading to aggregate formation in transfected cells. *J Biol Chem,* 283**,** 10500-12.

HEAD, M. W., CORBIN, E. & GOLDMAN, J. E. 1994. Coordinate and independent regulation of alpha B-crystallin and hsp27 expression in response to physiological stress. *J Cell Physiol,* 159**,** 41-50.

HEJTMANCIK, J. F. 2008. Congenital cataracts and their molecular genetics. *Semin Cell Dev Biol,* 19**,** 134-49.

HELFMAN, P. M. & BADA, J. L. 1975. Aspartic acid racemization in tooth enamel from living humans. *Proc Natl Acad Sci U S A,* 72**,** 2891-4.

HENNING, R. H. & BRUNDEL, B. 2017. Proteostasis in cardiac health and disease. *Nat Rev Cardiol,* 14**,** 637-653.

HERSHBERGER, R. E., HEDGES, D. J. & MORALES, A. 2013. Dilated cardiomyopathy: the complexity of a diverse genetic architecture. *Nat Rev Cardiol,* 10**,** 531-47.

HIDALGO, C. & GRANZIER, H. 2013. Tuning the molecular giant titin through phosphorylation: role in health and disease. *Trends Cardiovasc Med,* 23**,** 165-71.

HIGUCHI-SANABRIA, R., FRANKINO, P. A., PAUL, J. W., 3RD, TRONNES, S. U. & DILLIN, A. 2018. A Futile Battle? Protein Quality Control and the Stress of Aging. *Dev Cell,* 44**,** 139-163.

HILTON, G., LIOE, H., STENGEL, F., BALDWIN, A. & BENESCH, J. P. 2013. Small Heat-Shock Proteins: Paramedics of the Cell. *In:* JACKSON, S. (ed.) *Molecular Chaperones.* Springer Berlin Heidelberg.

HIRSCH, H. R. 1978. The waste-product theory of aging: waste dilution by cell division. *Mech Ageing Dev,* 8**,** 51-62.

HO, H. Y., CHANG, K. H., NICHOLS, J. & LI, M. 2009. Homeodomain protein Pitx3 maintains the mitotic activity of lens epithelial cells. *Mech Dev,* 126**,** 18-29.

HOAGE, T., DING, Y. & XU, X. 2012. Quantifying cardiac functions in embryonic and adult zebrafish. *Methods Mol Biol,* 843**,** 11-20.

HOCHBERG, G. K. & BENESCH, J. L. 2014. Dynamical structure of alphaB-crystallin. *Prog Biophys Mol Biol,* 115**,** 11-20.

HOCHBERG, G. K. A., SHEPHERD, D. A., MARKLUND, E. G., SANTHANAGOPLAN, I., DEGIACOMI, M. T., LAGANOWSKY, A., ALLISON, T. M., BASHA, E., MARTY, M. T., GALPIN, M. R., STRUWE, W. B., BALDWIN, A. J., VIERLING, E. & BENESCH, J. L. P. 2018. Structural principles that enable oligomeric small heat-shock protein paralogs to evolve distinct functions. *Science,* 359**,** 930-935.

HOLLANDER, J. M., MARTIN, J. L., BELKE, D. D., SCOTT, B. T., SWANSON, E., KRISHNAMOORTHY, V. & DILLMANN, W. H. 2004. Overexpression of wild-type heat shock protein 27 and a nonphosphorylatable heat shock protein 27 mutant protects against ischemia/reperfusion injury in a transgenic mouse model. *Circulation,* 110**,** 3544-52.

HORWITZ, J. 1992. Alpha-crystallin can function as a molecular chaperone. *Proc Natl Acad Sci U S A,* 89**,** 10449-53.

HORWITZ, J. 2009. Alpha crystallin: the quest for a homogeneous quaternary structure. *Exp Eye Res,* 88**,** 190-4.

HORWITZ, J., HUANG, Q. L., DING, L. & BOVA, M. P. 1998. Lens alpha-crystallin: chaperone-like properties. *Methods Enzymol,* 290**,** 365-83.

HU, X., VAN MARION, D. M. S., WIERSMA, M., ZHANG, D. & BRUNDEL, B. 2017. The protective role of small heat shock proteins in cardiac diseases: key role in atrial fibrillation. *Cell Stress Chaperones,* 22**,** 665-674.

HUANG, L.-H., WANG, H.-S. & KANG, L. 2008. Different evolutionary lineages of large and small heat shock proteins in eukaryotes. *Cell Research,* 18**,** 1074.

HUBBELL, W. L., MCHAOURAB, H. S., ALTENBACH, C. & LIETZOW, M. A. 1996. Watching proteins move using site-directed spin labeling. *Structure,* 4**,** 779-83.

HWANG, W. Y., FU, Y., REYON, D., MAEDER, M. L., TSAI, S. Q., SANDER, J. D., PETERSON, R. T., YEH, J. R. & JOUNG, J. K. 2013. Efficient genome editing in zebrafish using a CRISPR-Cas system. *Nat Biotechnol,* 31**,** 227-9.

INAGAKI, N., HAYASHI, T., ARIMURA, T., KOGA, Y., TAKAHASHI, M., SHIBATA, H., TERAOKA, K., CHIKAMORI, T., YAMASHINA, A. & KIMURA, A. 2006. Alpha B-crystallin mutation in dilated cardiomyopathy. *Biochem Biophys Res Commun,* 342**,** 379-86.

IRELAND, R. C. & BERGER, E. M. 1982. Synthesis of low molecular weight heat shock peptides stimulated by ecdysterone in a cultured Drosophila cell line. *Proc Natl Acad Sci U S A,* 79**,** 855-9.

ITO, H., KAMEI, K., IWAMOTO, I., INAGUMA, Y., NOHARA, D. & KATO, K. 2001. Phosphorylation-induced change of the oligomerization state of alpha B-crystallin. *J Biol Chem,* 276**,** 5346-52.

ITO, H., OKAMOTO, K., NAKAYAMA, H., ISOBE, T. & KATO, K. 1997. Phosphorylation of alphaB-crystallin in response to various types of stress. *J Biol Chem,* 272**,** 29934-41.

IWAKI, T., KUME-IWAKI, A. & GOLDMAN, J. E. 1990. Cellular distribution of alpha B-crystallin in non-lenticular tissues. *J Histochem Cytochem,* 38**,** 31-9.

IWAKI, T., KUME-IWAKI, A., LIEM, R. K. H. & GOLDMAN, J. E. 1989. ±B-crystallin is expressed in non-lenticular tissues and accumulates in Alexander's disease brain. *Cell,* 57**,** 71-78.

JAENICKE, R. & SLINGSBY, C. 2001. Lens crystallins and their microbial homologs: structure, stability, and function. *Crit Rev Biochem Mol Biol,* 36**,** 435-99.

JAKOB, U., GAESTEL, M., ENGEL, K. & BUCHNER, J. 1993. Small heat shock proteins are molecular chaperones. *J Biol Chem,* 268**,** 1517-20.

JAMES, E. R. 2007. The etiology of steroid cataract. *J Ocul Pharmacol Ther,* 23**,** 403-20.

JAMES, E. R., ROBERTSON, L., EHLERT, E., FITZGERALD, P., DROIN, N. & GREEN, D. R. 2003. Presence of a transcriptionally active glucocorticoid receptor alpha in lens epithelial cells. *Invest Ophthalmol Vis Sci,* 44**,** 5269-76.

JAO, L. E., WENTE, S. R. & CHEN, W. 2013. Efficient multiplex biallelic zebrafish genome editing using a CRISPR nuclease system. *Proc Natl Acad Sci U S A,* 110**,** 13904-9.

JAYA, N., GARCIA, V. & VIERLING, E. 2009. Substrate binding site flexibility of the small heat shock protein molecular chaperones. *Proc Natl Acad Sci U S A,* 106**,** 15604-9.

JEHLE, S., RAJAGOPAL, P., BARDIAUX, B., MARKOVIC, S., KUHNE, R., STOUT, J. R., HIGMAN, V. A., KLEVIT, R. E., VAN ROSSUM, B. J. & OSCHKINAT, H. 2010. Solid-state NMR and SAXS studies provide a structural basis for the activation of alpha B-crystallin oligomers. *Nature Structural & Molecular Biology,* 17**,** 1037-U1.

JEHLE, S., VOLLMAR, B. S., BARDIAUX, B., DOVE, K. K., RAJAGOPAL, P., GONEN, T., OSCHKINAT, H. & KLEVIT, R. E. 2011. N-terminal domain of alphaB-crystallin provides a conformational switch for multimerization and structural heterogeneity. *Proc Natl Acad Sci U S A,* 108**,** 6409-14.

JINEK, M., CHYLINSKI, K., FONFARA, I., HAUER, M., DOUDNA, J. A. & CHARPENTIER, E. 2012. A programmable dual-RNA-guided DNA endonuclease in adaptive bacterial immunity. *Science,* 337**,** 816-21.

JOBLING, A. I. & AUGUSTEYN, R. C. 2001. Is there a glucocorticoid receptor in the bovine lens? *Exp Eye Res,* 72**,** 687-94.

JOBLING, A. I. & AUGUSTEYN, R. C. 2002. What causes steroid cataracts? A review of steroid-induced posterior subcapsular cataracts. *Clin Exp Optom,* 85**,** 61-75.

JOBLING, A. I., STEVENS, A. & AUGUSTEYN, R. C. 2001. Binding of dexamethasone by alpha-crystallin. *Invest Ophthalmol Vis Sci,* 42**,** 1829-32.

JONASOVA, K. & KOZMIK, Z. 2008. Eye evolution: lens and cornea as an upgrade of animal visual system. *Semin Cell Dev Biol,* 19**,** 71-81.

KADMIEL, M. & CIDLOWSKI, J. A. 2013. Glucocorticoid receptor signaling in health and disease. *Trends Pharmacol Sci,* 34**,** 518-30.

KAGANOVICH, D., KOPITO, R. & FRYDMAN, J. 2008. Misfolded proteins partition between two distinct quality control compartments. *Nature,* 454**,** 1088-95.

KAKKAR, V., MEISTER-BROEKEMA, M., MINOIA, M., CARRA, S. & KAMPINGA, H. H. 2014. Barcoding heat shock proteins to human diseases: looking beyond the heat shock response. *Dis Model Mech,* 7**,** 421-34.

KAPPE, G., BOELENS, W. C. & DE JONG, W. W. 2010. Why proteins without an alpha-crystallin domain should not be included in the human small heat shock protein family HSPB. *Cell Stress Chaperones,* 15**,** 457-61.

KAPPE, G., FRANCK, E., VERSCHUURE, P., BOELENS, W. C., LEUNISSEN, J. A. & DE JONG, W. W. 2003. The human genome encodes 10 alpha-crystallin-related small heat shock proteins: HspB1-10. *Cell Stress Chaperones,* 8**,** 53-61.

KAYES-WANDOVER, K. M. & WHITE, P. C. 2000. Steroidogenic enzyme gene expression in the human heart. *J Clin Endocrinol Metab,* 85**,** 2519-25.

KHAIRALLAH, M., KAHLOUN, R., BOURNE, R., LIMBURG, H., FLAXMAN, S. R., JONAS, J. B., KEEFFE, J., LEASHER, J., NAIDOO, K., PESUDOVS, K., PRICE, H., WHITE, R. A., WONG, T. Y., RESNIKOFF, S., TAYLOR, H. R. & VISION LOSS EXPERT GROUP OF THE GLOBAL BURDEN OF DISEASE, S. 2015. Number of People Blind or Visually Impaired by Cataract Worldwide and in World Regions, 1990 to 2010. *Invest Ophthalmol Vis Sci,* 56**,** 6762-9.

KIKIS, E. A., GIDALEVITZ, T. & MORIMOTO, R. I. 2010. Protein Homeostasis in Models of Aging and Age-Related Conformational Disease. *In:* TAVERNARAKIS, N. (ed.) *Protein Metabolism and Homeostasis in Aging.*

KIM, Y. E., HIPP, M. S., BRACHER, A., HAYER-HARTL, M. & HARTL, F. U. 2013. Molecular chaperone functions in protein folding and proteostasis. *Annu Rev Biochem,* 82**,** 323-55.

KINYAMU, H. K., COLLINS, J. B., GRISSOM, S. F., HEBBAR, P. B. & ARCHER, T. K. 2008. Genome wide transcriptional profiling in breast cancer cells reveals distinct changes in hormone receptor target genes and chromatin modifying enzymes after proteasome inhibition. *Mol Carcinog,* 47**,** 845-85.

KIRSCHKE, E., GOSWAMI, D., SOUTHWORTH, D., GRIFFIN, P. R. & AGARD, D. A. 2014. Glucocorticoid receptor function regulated by coordinated action of the Hsp90 and Hsp70 chaperone cycles. *Cell,* 157**,** 1685-97.

KLAIPS, C. L., JAYARAJ, G. G. & HARTL, F. U. 2018. Pathways of cellular proteostasis in aging and disease. *J Cell Biol,* 217**,** 51-63.

KLEMENZ, R., SCHEIER, B., MULLER, A., STEIGER, R. & AOYAMA, A. 1994. Alpha B crystallin expression in response to hormone, oncogenes and stress. *Verh Dtsch Ges Pathol,* 78**,** 34-5.

KNOLL, R., BUYANDELGER, B. & LAB, M. 2011. The sarcomeric Z-disc and Z-discopathies. *J Biomed Biotechnol,* 2011**,** 569628.

KOBERLEIN, J., BEIFUS, K., SCHAFFERT, C. & FINGER, R. P. 2013. The economic burden of visual impairment and blindness: a systematic review. *BMJ Open,* 3**,** e003471.

KOK, F. O., SHIN, M., NI, C. W., GUPTA, A., GROSSE, A. S., VAN IMPEL, A., KIRCHMAIER, B. C., PETERSON-MADURO, J., KOURKOULIS, G., MALE, I., DESANTIS, D. F., SHEPPARD-TINDELL, S., EBARASI, L., BETSHOLTZ, C., SCHULTE-MERKER, S., WOLFE, S. A. & LAWSON, N. D. 2015. Reverse genetic screening reveals poor correlation between morpholino-induced and mutant phenotypes in zebrafish. *Dev Cell,* 32**,** 97-108.

KOSANO, H. & NISHIGORI, H. 2002. Steroid-induced cataract: other than in the whole animal system, in the lens culture system, androgens, estrogens and progestins as well as glucocorticoids produce a loss of transparency of the lens. *Dev Ophthalmol,* 35**,** 161-8.

KOTEICHE, H. A., BERENGIAN, A. R. & MCHAOURAB, H. S. 1998. Identification of protein folding patterns using site-directed spin labeling. Structural

characterization of a beta-sheet and putative substrate binding regions in the conserved domain of alpha A-crystallin. *Biochemistry,* 37**,** 12681-8.
KOTEICHE, H. A., CHIU, S., MAJDOCH, R. L., STEWART, P. L. & MCHAOURAB, H. S. 2005. Atomic models by cryo-EM and site-directed spin labeling: application to the N-terminal region of Hsp16.5. *Structure,* 13**,** 1165-71.
KOTEICHE, H. A., CLAXTON, D. P., MISHRA, S., STEIN, R. A., MCDONALD, E. T. & MCHAOURAB, H. S. 2015. Species-Specific Structural and Functional Divergence of alpha-Crystallins: Zebrafish alphaBa- and Rodent alphaA(ins)-Crystallin Encode Activated Chaperones. *Biochemistry,* 54**,** 5949-58.
KOTEICHE, H. A., KUMAR, M. S. & MCHAOURAB, H. S. 2007. Analysis of betaB1-crystallin unfolding equilibrium by spin and fluorescence labeling: evidence of a dimeric intermediate. *FEBS Lett,* 581**,** 1933-8.
KOTEICHE, H. A. & MCHAOURAB, H. S. 1999. Folding pattern of the alpha-crystallin domain in alphaA-crystallin determined by site-directed spin labeling. *J Mol Biol,* 294**,** 561-77.
KOTEICHE, H. A. & MCHAOURAB, H. S. 2002. The determinants of the oligomeric structure in Hsp16.5 are encoded in the alpha-crystallin domain. *FEBS Lett,* 519**,** 16-22.
KOTEICHE, H. A. & MCHAOURAB, H. S. 2003. Mechanism of chaperone function in small heat-shock proteins. Phosphorylation-induced activation of two-mode binding in alphaB-crystallin. *J Biol Chem,* 278**,** 10361-7.
KOTEICHE, H. A. & MCHAOURAB, H. S. 2004. Site-directed spin labeling study of the structure of the multidrug transporter EmrE. *Protein Science,* 13**,** 180-180.
KOTEICHE, H. A. & MCHAOURAB, H. S. 2006. Mechanism of a hereditary cataract phenotype. Mutations in alphaA-crystallin activate substrate binding. *J Biol Chem,* 281**,** 14273-9.
KOTTER, S., UNGER, A., HAMDANI, N., LANG, P., VORGERD, M., NAGEL-STEGER, L. & LINKE, W. A. 2014. Human myocytes are protected from titin aggregation-induced stiffening by small heat shock proteins. *J Cell Biol,* 204**,** 187-202.
KRIEHUBER, T., RATTEI, T., WEINMAIER, T., BEPPERLING, A., HASLBECK, M. & BUCHNER, J. 2010. Independent evolution of the core domain and its flanking sequences in small heat shock proteins. *FASEB J,* 24**,** 3633-42.
KRISHNAMOORTHY, V., DONOFRIO, A. J. & MARTIN, J. L. 2013. O-GlcNAcylation of alphaB-crystallin regulates its stress-induced translocation and cytoprotection. *Mol Cell Biochem,* 379**,** 59-68.
KULTZ, D. 2003. Evolution of the cellular stress proteome: from monophyletic origin to ubiquitous function. *J Exp Biol,* 206**,** 3119-24.
KUMAR, L. V. S., RAMAKRISHNA, T. & RAO, C. M. 1999. Structural and Functional Consequences of the Mutation of a Conserved Arginine Residue in αA and αB Crystallins. *Journal of Biological Chemistry,* 274**,** 24137-24141.
KUMAR, M. S., KOTEICHE, H. A., CLAXTON, D. P. & MCHAOURAB, H. S. 2009. Disulfide cross-links in the interaction of a cataract-linked alphaA-crystallin mutant with betaB1-crystallin. *FEBS Lett,* 583**,** 175-9.

KWAN, K. M., FUJIMOTO, E., GRABHER, C., MANGUM, B. D., HARDY, M. E., CAMPBELL, D. S., PARANT, J. M., YOST, H. J., KANKI, J. P. & CHIEN, C. B. 2007. The Tol2kit: a multisite gateway-based construction kit for Tol2 transposon transgenesis constructs. *Dev Dyn,* 236**,** 3088-99.

KWONG, R. W., KUMAI, Y. & PERRY, S. F. 2013. Evidence for a role of tight junctions in regulating sodium permeability in zebrafish (Danio rerio) acclimated to ion-poor water. *J Comp Physiol B,* 183**,** 203-13.

LABBADIA, J. & MORIMOTO, R. I. 2015. The biology of proteostasis in aging and disease. *Annu Rev Biochem,* 84**,** 435-64.

LAGANOWSKY, A., BENESCH, J. L., LANDAU, M., DING, L., SAWAYA, M. R., CASCIO, D., HUANG, Q., ROBINSON, C. V., HORWITZ, J. & EISENBERG, D. 2010. Crystal structures of truncated alphaA and alphaB crystallins reveal structural mechanisms of polydispersity important for eye lens function. *Protein Sci,* 19**,** 1031-43.

LAMB, T. D., COLLIN, S. P. & PUGH, E. N., JR. 2007. Evolution of the vertebrate eye: opsins, photoreceptors, retina and eye cup. *Nat Rev Neurosci,* 8**,** 960-76.

LAND, M. F. 2005. The optical structures of animal eyes. *Curr Biol,* 15**,** R319-23.

LEBOWITZ, J., LEWIS, M. S. & SCHUCK, P. 2002. Modern analytical ultracentrifugation in protein science: a tutorial review. *Protein Sci,* 11**,** 2067-79.

LEE, G. J., ROSEMAN, A. M., SAIBIL, H. R. & VIERLING, E. 1997. A small heat shock protein stably binds heat-denatured model substrates and can maintain a substrate in a folding-competent state. *EMBO J,* 16**,** 659-71.

LEE, G. J. & VIERLING, E. 2000. A small heat shock protein cooperates with heat shock protein 70 systems to reactivate a heat-denatured protein. *Plant Physiol,* 122**,** 189-98.

LELJ-GAROLLA, B. & MAUK, A. G. 2012. Roles of the N- and C-terminal sequences in Hsp27 self-association and chaperone activity. *Protein Sci,* 21**,** 122-33.

LESKE, M. C., CHYLACK, L. T., JR., HE, Q., WU, S. Y., SCHOENFELD, E., FRIEND, J. & WOLFE, J. 1997. Incidence and progression of cortical and posterior subcapsular opacities: the Longitudinal Study of Cataract. The LSC Group. *Ophthalmology,* 104**,** 1987-93.

LEVINTHAL, C. 1968. Are There Pathways for Protein Folding. *Journal De Chimie Physique Et De Physico-Chimie Biologique,* 65**,** 44-+.

LEVINTHAL, C. How to Fold Graciously. Mössbaun Spectroscopy in Biological Systems Proceedings, 1969 Urbana, IL.

LEWINTER, M. M. & GRANZIER, H. L. 2014. Cardiac titin and heart disease. *J Cardiovasc Pharmacol,* 63**,** 207-12.

LI, Y., LUBCHENKO, V. & VEKILOV, P. G. 2011. The use of dynamic light scattering and brownian microscopy to characterize protein aggregation. *Rev Sci Instrum,* 82**,** 053106.

LINKE, W. A. & HAMDANI, N. 2014. Gigantic business: titin properties and function through thick and thin. *Circ Res,* 114**,** 1052-68.

LIU, S. & PIATIGORSKY, J. 2011. Regulation of mouse small heat shock protein alphab-crystallin gene by aryl hydrocarbon receptor. *PLoS One,* 6**,** e17904.

LOPEZ-OTIN, C., BLASCO, M. A., PARTRIDGE, L., SERRANO, M. & KROEMER, G. 2013. The hallmarks of aging. *Cell,* 153**,** 1194-217.
LOREDO, A., RODRIGUEZ, R. S. & MURILLO, L. 1972. Cataracts after short-term corticosteroid treatment. *N Engl J Med,* 286**,** 160.
LOWE, J., MCDERMOTT, H., PIKE, I., SPENDLOVE, I., LANDON, M. & MAYER, R. J. 1992. alpha B crystallin expression in non-lenticular tissues and selective presence in ubiquitinated inclusion bodies in human disease. *J Pathol,* 166**,** 61-8.
LU, N. Z. & CIDLOWSKI, J. A. 2004. The origin and functions of multiple human glucocorticoid receptor isoforms. *Ann N Y Acad Sci,* 1024**,** 102-23.
LU, N. Z. & CIDLOWSKI, J. A. 2006. Glucocorticoid receptor isoforms generate transcription specificity. *Trends Cell Biol,* 16**,** 301-7.
LYNNERUP, N., KJELDSEN, H., HEEGAARD, S., JACOBSEN, C. & HEINEMEIER, J. 2008. Radiocarbon dating of the human eye lens crystallines reveal proteins without carbon turnover throughout life. *PLoS One,* 3**,** e1529.
MA, Z., HANSON, S. R., LAMPI, K. J., DAVID, L. L., SMITH, D. L. & SMITH, J. B. 1998. Age-related changes in human lens crystallins identified by HPLC and mass spectrometry. *Exp Eye Res,* 67**,** 21-30.
MAAROUFI, H. & TANGUAY, R. M. 2013. Analysis and phylogeny of small heat shock proteins from marine viruses and their cyanobacteria host. *PLoS One,* 8**,** e81207.
MACARIO, A. J. & CONWAY DE MACARIO, E. 2007. Chaperonopathies and chaperonotherapy. *FEBS Lett,* 581**,** 3681-8.
MACARIO, A. J., GRIPPO, T. M. & CONWAY DE MACARIO, E. 2005. Genetic disorders involving molecular-chaperone genes: a perspective. *Genet Med,* 7**,** 3-12.
MACARIO, A. J. L., CONWAY DE MACARIO, E. & CAPPELLO, F. 2013. Chaperones: General Characteristics and Classifications. *The Chaperonopathies.* Dordrecht: Springer Netherlands.
MAINZ, A., PESCHEK, J., STAVROPOULOU, M., BACK, K. C., BARDIAUX, B., ASAMI, S., PRADE, E., PETERS, C., WEINKAUF, S., BUCHNER, J. & REIF, B. 2015. The chaperone alphaB-crystallin uses different interfaces to capture an amorphous and an amyloid client. *Nat Struct Mol Biol,* 22**,** 898-905.
MANDAL, N., HEEGAARD, S., PRAUSE, J. U., HONORE, B. & VORUM, H. 2009. Ocular proteomics with emphasis on two-dimensional gel electrophoresis and mass spectrometry. *Biol Proced Online,* 12**,** 56-88.
MAO, L. & SHELDEN, E. A. 2006. Developmentally regulated gene expression of the small heat shock protein Hsp27 in zebrafish embryos. *Gene Expr Patterns,* 6**,** 127-33.
MARQUARDT, D. W. 1963. An Algorithm for Least-Squares Estimation of Nonlinear Parameters. *Journal of the Society for Industrial and Applied Mathematics,* 11**,** 431-441.
MARSHMAN, E., BOOTH, C. & POTTEN, C. S. 2002. The intestinal epithelial stem cell. *Bioessays,* 24**,** 91-8.

MARVIN, M., O'ROURKE, D., KURIHARA, T., JULIANO, C. E., HARRISON, K. L. & HUTSON, L. D. 2008. Developmental expression patterns of the zebrafish small heat shock proteins. *Dev Dyn,* 237**,** 454-63.

MASTERS, P. M., BADA, J. L. & ZIGLER, J. S., JR. 1977. Aspartic acid racemisation in the human lens during ageing and in cataract formation. *Nature,* 268**,** 71-3.

MATTHEWS, L. C., BERRY, A. A., MORGAN, D. J., POOLMAN, T. M., BAUER, K., KRAMER, F., SPILLER, D. G., RICHARDSON, R. V., CHAPMAN, K. E., FARROW, S. N., NORMAN, M. R., WILLIAMSON, A. J., WHETTON, A. D., TAYLOR, S. S., TUCKERMANN, J. P., WHITE, M. R. & RAY, D. W. 2015. Glucocorticoid receptor regulates accurate chromosome segregation and is associated with malignancy. *Proc Natl Acad Sci U S A,* 112**,** 5479-84.

MATTOO, R. U. & GOLOUBINOFF, P. 2014. Molecular chaperones are nanomachines that catalytically unfold misfolded and alternatively folded proteins. *Cell Mol Life Sci,* 71**,** 3311-25.

MC, E. W. 1959. The yellow pigment of human lenses. *Am J Ophthalmol,* 47**,** 144-6.

MCCARTY, C. A., NANJAN, M. B. & TAYLOR, H. R. 2000. Attributable risk estimates for cataract to prioritize medical and public health action. *Invest Ophthalmol Vis Sci,* 41**,** 3720-5.

MCDONALD, E. T., BORTOLUS, M., KOTEICHE, H. A. & MCHAOURAB, H. S. 2012. Sequence, structure, and dynamic determinants of Hsp27 (HspB1) equilibrium dissociation are encoded by the N-terminal domain. *Biochemistry,* 51**,** 1257-68.

MCEWEN, B. S. 2007. Physiology and neurobiology of stress and adaptation: central role of the brain. *Physiol Rev,* 87**,** 873-904.

MCHAOURAB, H. S., BERENGIAN, A. R. & KOTEICHE, H. A. 1997. Site-directed spin-labeling study of the structure and subunit interactions along a conserved sequence in the alpha-crystallin domain of heat-shock protein 27. Evidence of a conserved subunit interface. *Biochemistry,* 36**,** 14627-34.

MCHAOURAB, H. S., DODSON, E. K. & KOTEICHE, H. A. 2002. Mechanism of chaperone function in small heat shock proteins. Two-mode binding of the excited states of T4 lysozyme mutants by alphaA-crystallin. *J Biol Chem,* 277**,** 40557-66.

MCHAOURAB, H. S., GODAR, J. A. & STEWART, P. L. 2009. Structure and mechanism of protein stability sensors: chaperone activity of small heat shock proteins. *Biochemistry,* 48**,** 3828-37.

MCHAOURAB, H. S., KOTEICHE, H. A., SHASHIDHARAMURTHY, R. & YANG, G. 2005. Mechanism of a protein sensor: The chaperone activity of a-crystallin. *Investigative Ophthalmology & Visual Science,* 46.

MCHAOURAB, H. S., KUMAR, M. S. & KOTEICHE, H. A. 2007. Specificity of alphaA-crystallin binding to destabilized mutants of betaB1-crystallin. *FEBS Lett,* 581**,** 1939-43.

MCHAOURAB, H. S., LIETZOW, M. A., HIDEG, K. & HUBBELL, W. L. 1996. Motion of spin-labeled side chains in T4 lysozyme. Correlation with protein structure and dynamics. *Biochemistry,* 35**,** 7692-704.

MCHAOURAB, H. S., LIN, Y. L. & SPILLER, B. W. 2012. Crystal structure of an activated variant of small heat shock protein Hsp16.5. *Biochemistry,* 51**,** 5105-12.

MCHAOURAB, H. S., MISHRA, S., KOTEICHE, H. A. & AMADI, S. H. 2008. Role of sequence bias in the topology of the multidrug transporter EmrE. *Biochemistry,* 47**,** 7980-2.

MCHAOURAB, H. S., MISHRA, S., KOTEICHE, H. A., SHI, J., WILLIAMS, D. & STEWART, P. L. 2011a. Role of the N-terminal Domain in Polydispersity and Substrate Binding by Small Heat Shock Proteins: Lessons from Hsp16.5. *ARVO Annual Meeting Abstract Search and Program Planner,* 2011**,** 1612-1612.

MCHAOURAB, H. S., STEED, P. R. & KAZMIER, K. 2011b. Toward the fourth dimension of membrane protein structure: insight into dynamics from spin-labeling EPR spectroscopy. *Structure,* 19**,** 1549-61.

MEDINA-MARTINEZ, O., SHAH, R. & JAMRICH, M. 2009. Pitx3 controls multiple aspects of lens development. *Dev Dyn,* 238**,** 2193-201.

MEEHAN, S., BERRY, Y., LUISI, B., DOBSON, C. M., CARVER, J. A. & MACPHEE, C. E. 2004. Amyloid fibril formation by lens crystallin proteins and its implications for cataract formation. *J Biol Chem,* 279**,** 3413-9.

MEEHAN, S., KNOWLES, T. P., BALDWIN, A. J., SMITH, J. F., SQUIRES, A. M., CLEMENTS, P., TREWEEK, T. M., ECROYD, H., TARTAGLIA, G. G., VENDRUSCOLO, M., MACPHEE, C. E., DOBSON, C. M. & CARVER, J. A. 2007. Characterisation of amyloid fibril formation by small heat-shock chaperone proteins human alphaA-, alphaB- and R120G alphaB-crystallins. *J Mol Biol,* 372**,** 470-84.

MELLERIO, J. 1987. Yellowing of the human lens: nuclear and cortical contributions. *Vision Res,* 27**,** 1581-7.

MERCK, K. B., DE HAARD-HOEKMAN, W. A., OUDE ESSINK, B. B., BLOEMENDAL, H. & DE JONG, W. W. 1992. Expression and aggregation of recombinant alpha A-crystallin and its two domains. *Biochim Biophys Acta,* 1130**,** 267-76.

MICHAEL, R. & BRON, A. J. 2011. The ageing lens and cataract: a model of normal and pathological ageing. *Philos Trans R Soc Lond B Biol Sci,* 366**,** 1278-92.

MICHAUD, S., MARIN, R. & TANGUAY, R. M. 1997. Regulation of heat shock gene induction and expression during Drosophila development. *Cell Mol Life Sci,* 53**,** 104-13.

MISHRA, S., CHANDLER, S. A., WILLIAMS, D., CLAXTON, D. P., KOTEICHE, H. A., STEWART, P. L., BENESCH, J. L. P. & MCHAOURAB, H. S. 2018. Engineering of a Polydisperse Small Heat-Shock Protein Reveals Conserved Motifs of Oligomer Plasticity. *bioRxiv*.

MISHRA, S., STEIN, R. A. & MCHAOURAB, H. S. 2012. Cataract-linked gammaD-crystallin mutants have weak affinity to lens chaperones alpha-crystallins. *FEBS Lett,* 586**,** 330-6.

MOBERG, C., BOURLEV, V., ILYASOVA, N. & OLOVSSON, M. 2015. Levels of oestrogen receptor, progesterone receptor and alphaB-crystallin in eutopic endometrium in relation to pregnancy in women with endometriosis. *Hum Fertil (Camb),* 18**,** 30-7.

MOFFAT, B. A., LANDMAN, K. A., TRUSCOTT, R. J., SWEENEY, M. H. & POPE, J. M. 1999. Age-related changes in the kinetics of water transport in normal human lenses. *Exp Eye Res,* 69**,** 663-9.

MOORMAN, A., WEBB, S., BROWN, N. A., LAMERS, W. & ANDERSON, R. H. 2003. Development of the heart: (1) formation of the cardiac chambers and arterial trunks. *Heart,* 89**,** 806-14.

MOREAU, K. L. & KING, J. A. 2012. Protein misfolding and aggregation in cataract disease and prospects for prevention. *Trends Mol Med,* 18**,** 273-82.

MORIMOTO, R. I. & CUERVO, A. M. 2009. Protein homeostasis and aging: taking care of proteins from the cradle to the grave. *J Gerontol A Biol Sci Med Sci,* 64**,** 167-70.

MORIMOTO, R. I. & CUERVO, A. M. 2014. Proteostasis and the aging proteome in health and disease. *J Gerontol A Biol Sci Med Sci,* 69 Suppl 1**,** S33-8.

MORROW, G., BATTISTINI, S., ZHANG, P. & TANGUAY, R. M. 2004. Decreased lifespan in the absence of expression of the mitochondrial small heat shock protein Hsp22 in Drosophila. *J Biol Chem,* 279**,** 43382-5.

MOU, H., SMITH, J. L., PENG, L., YIN, H., MOORE, J., ZHANG, X. O., SONG, C. Q., SHEEL, A., WU, Q., OZATA, D. M., LI, Y., ANDERSON, D. G., EMERSON, C. P., SONTHEIMER, E. J., MOORE, M. J., WENG, Z. & XUE, W. 2017. CRISPR/Cas9-mediated genome editing induces exon skipping by alternative splicing or exon deletion. *Genome Biol,* 18**,** 108.

MOUTAOUFIK, M. T., MORROW, G., FINET, S. & TANGUAY, R. M. 2017. Effect of N-terminal region of nuclear Drosophila melanogaster small heat shock protein DmHsp27 on function and quaternary structure. *PLoS One,* 12**,** e0177821.

MUCHOWSKI, P. J., BASSUK, J. A., LUBSEN, N. H. & CLARK, J. I. 1997. Human alphaB-crystallin. Small heat shock protein and molecular chaperone. *J Biol Chem,* 272**,** 2578-82.

MUCHOWSKI, P. J. & WACKER, J. L. 2005. Modulation of neurodegeneration by molecular chaperones. *Nat Rev Neurosci,* 6**,** 11-22.

MULDER, F. A., MITTERMAIER, A., HON, B., DAHLQUIST, F. W. & KAY, L. E. 2001. Studying excited states of proteins by NMR spectroscopy. *Nat Struct Biol,* 8**,** 932-5.

MUNOZ, V., CAMPOS, L. A. & SADQI, M. 2016. Limited cooperativity in protein folding. *Curr Opin Struct Biol,* 36**,** 58-66.

MURTHY, S. R., KOTEICHE, H. A., HASIGE, S. A. & MCHAOURAB, H. S. 2004. Mechanistic studies of small heat-shock proteins chaperone activity. *Protein Science,* 13**,** 111-112.

MYMRIKOV, E. V., DAAKE, M., RICHTER, B., HASLBECK, M. & BUCHNER, J. 2017. The Chaperone Activity and Substrate Spectrum of Human Small Heat Shock Proteins. *J Biol Chem,* 292**,** 672-684.

NAHOMI, R. B., HUANG, R., NANDI, S. K., WANG, B., PADMANABHA, S., SANTHOSHKUMAR, P., FILIPEK, S., BISWAS, A. & NAGARAJ, R. H. 2013. Acetylation of lysine 92 improves the chaperone and anti-apoptotic activities of human alphaB-crystallin. *Biochemistry,* 52**,** 8126-38.

NAKAMOTO, H. & VIGH, L. 2007. The small heat shock proteins and their clients. *Cell Mol Life Sci,* 64**,** 294-306.
NEMET, A. Y., VINKER, S., LEVARTOVSKY, S. & KAISERMAN, I. 2010. Is cataract associated with cardiovascular morbidity? *Eye (Lond),* 24**,** 1352-8.
NEPPL, R. L., KATAOKA, M. & WANG, D. Z. 2014. Crystallin-alphaB regulates skeletal muscle homeostasis via modulation of argonaute2 activity. *J Biol Chem,* 289**,** 17240-8.
NESAN, D. & VIJAYAN, M. M. 2012. Embryo exposure to elevated cortisol level leads to cardiac performance dysfunction in zebrafish. *Mol Cell Endocrinol,* 363**,** 85-91.
NEU-YILIK, G., AMTHOR, B., GEHRING, N. H., BAHRI, S., PAIDASSI, H., HENTZE, M. W. & KULOZIK, A. E. 2011. Mechanism of escape from nonsense-mediated mRNA decay of human beta-globin transcripts with nonsense mutations in the first exon. *RNA,* 17**,** 843-54.
NGUYEN, C. T., LU, Q., WANG, Y. & CHEN, J. N. 2008. Zebrafish as a model for cardiovascular development and disease. *Drug Discov Today Dis Models,* 5**,** 135-140.
NICHOLL, I. D. & QUINLAN, R. A. 1994. Chaperone activity of alpha-crystallins modulates intermediate filament assembly. *EMBO J,* 13**,** 945-53.
NIELSEN, J., HEDEHOLM, R. B., HEINEMEIER, J., BUSHNELL, P. G., CHRISTIANSEN, J. S., OLSEN, J., RAMSEY, C. B., BRILL, R. W., SIMON, M., STEFFENSEN, K. F. & STEFFENSEN, J. F. 2016. Eye lens radiocarbon reveals centuries of longevity in the Greenland shark (Somniosus microcephalus). *Science,* 353**,** 702-4.
NILSSON, D. E. 2009. The evolution of eyes and visually guided behaviour. *Philos Trans R Soc Lond B Biol Sci,* 364**,** 2833-47.
NINKOVIC, J., PINTO, L., PETRICCA, S., LEPIER, A., SUN, J., RIEGER, M. A., SCHROEDER, T., CVEKL, A., FAVOR, J. & GOTZ, M. 2010. The transcription factor Pax6 regulates survival of dopaminergic olfactory bulb neurons via crystallin alphaA. *Neuron,* 68**,** 682-94.
OAKLEY, R. H. & CIDLOWSKI, J. A. 2011. Cellular processing of the glucocorticoid receptor gene and protein: new mechanisms for generating tissue-specific actions of glucocorticoids. *J Biol Chem,* 286**,** 3177-84.
OAKLEY, R. H. & CIDLOWSKI, J. A. 2013. The biology of the glucocorticoid receptor: new signaling mechanisms in health and disease. *J Allergy Clin Immunol,* 132**,** 1033-44.
OAKLEY, R. H. & CIDLOWSKI, J. A. 2015. Glucocorticoid signaling in the heart: A cardiomyocyte perspective. *J Steroid Biochem Mol Biol,* 153**,** 27-34.
OAKLEY, R. H., REN, R., CRUZ-TOPETE, D., BIRD, G. S., MYERS, P. H., BOYLE, M. C., SCHNEIDER, M. D., WILLIS, M. S. & CIDLOWSKI, J. A. 2013. Essential role of stress hormone signaling in cardiomyocytes for the prevention of heart disease. *Proc Natl Acad Sci U S A,* 110**,** 17035-40.
OAKLEY, R. H., SAR, M. & CIDLOWSKI, J. A. 1996. The human glucocorticoid receptor beta isoform. Expression, biochemical properties, and putative function. *J Biol Chem,* 271**,** 9550-9.

OGURA, A., YOSHIDA, M. A., MORITAKI, T., OKUDA, Y., SESE, J., SHIMIZU, K. K., SOUSOUNIS, K. & TSONIS, P. A. 2013. Loss of the six3/6 controlling pathways might have resulted in pinhole-eye evolution in Nautilus. *Sci Rep,* 3**,** 1432.

OHTO-FUJITA, E., FUJITA, Y. & ATOMI, Y. 2007. Analysis of the alphaB-crystallin domain responsible for inhibiting tubulin aggregation. *Cell Stress Chaperones,* 12**,** 163-71.

ONUCHIC, J. N., LUTHEY-SCHULTEN, Z. & WOLYNES, P. G. 1997. Theory of protein folding: the energy landscape perspective. *Annu Rev Phys Chem,* 48**,** 545-600.

OWENS, D. A. 2000. A natural history of vision. *Journal of the History of the Behavioral Sciences,* 36**,** 50-52.

PACE, C. N., FISHER, L. M. & CUPO, J. F. 1981. Globular protein stability: aspects of interest in protein turnover. *Acta Biol Med Ger,* 40**,** 1385-92.

PAGE-MCCAW, P. S., CHUNG, S. C., MUTO, A., ROESER, T., STAUB, W., FINGER-BAIER, K. C., KORENBROT, J. I. & BAIER, H. 2004. Retinal network adaptation to bright light requires tyrosinase. *Nat Neurosci,* 7**,** 1329-36.

PAL, C., PAPP, B. & LERCHER, M. J. 2006. An integrated view of protein evolution. *Nat Rev Genet,* 7**,** 337-48.

PAPACONSTANTINOU, J. 1967. Molecular aspects of lens cell differentiation. *Science,* 156**,** 338-46.

PARKER, A. 2004. *In the blink of an eye : how vision sparked the big bang of evolution,* New York, Basic Books.

PASTA, S. Y., RAMAN, B., RAMAKRISHNA, T. & RAO CH, M. 2002. Role of the C-terminal extensions of alpha-crystallins. Swapping the C-terminal extension of alpha-crystallin to alphaB-crystallin results in enhanced chaperone activity. *J Biol Chem,* 277**,** 45821-8.

PASTA, S. Y., RAMAN, B., RAMAKRISHNA, T. & RAO CH, M. 2003. Role of the conserved SRLFDQFFG region of alpha-crystallin, a small heat shock protein. Effect on oligomeric size, subunit exchange, and chaperone-like activity. *J Biol Chem,* 278**,** 51159-66.

PASTA, S. Y., RAMAN, B., RAMAKRISHNA, T. & RAO CH, M. 2004. The IXI/V motif in the C-terminal extension of alpha-crystallins: alternative interactions and oligomeric assemblies. *Mol Vis,* 10**,** 655-62.

PAULIN, D. & LI, Z. 2004. Desmin: a major intermediate filament protein essential for the structural integrity and function of muscle. *Exp Cell Res,* 301**,** 1-7.

PESCHEK, J., BRAUN, N., FRANZMANN, T. M., GEORGALIS, Y., HASLBECK, M., WEINKAUF, S. & BUCHNER, J. 2009. The eye lens chaperone alpha-crystallin forms defined globular assemblies. *Proc Natl Acad Sci U S A,* 106**,** 13272-7.

PESCHEK, J., BRAUN, N., ROHRBERG, J., BACK, K. C., KRIEHUBER, T., KASTENMULLER, A., WEINKAUF, S. & BUCHNER, J. 2013. Regulated structural transitions unleash the chaperone activity of alphaB-crystallin. *Proc Natl Acad Sci U S A,* 110**,** E3780-9.

PESCOSOLIDO, N., BARBATO, A., GIANNOTTI, R., KOMAIHA, C. & LENARDUZZI, F. 2016. Age-related changes in the kinetics of human lenses: prevention of the cataract. *Int J Ophthalmol,* 9**,** 1506-1517.

PIATIGORSKY, J. 1993. Puzzle of crystallin diversity in eye lenses. *Dev Dyn,* 196**,** 267-72.

PIERSCIONEK, B. K. & REGINI, J. W. 2012. The gradient index lens of the eye: an opto-biological synchrony. *Prog Retin Eye Res,* 31**,** 332-49.

PINZ, I., ROBBINS, J., RAJASEKARAN, N. S., BENJAMIN, I. J. & INGWALL, J. S. 2008. Unmasking different mechanical and energetic roles for the small heat shock proteins CryAB and HSPB2 using genetically modified mouse hearts. *FASEB J,* 22**,** 84-92.

POSNER, M., KANTOROW, M. & HORWITZ, J. 1999. Cloning, sequencing and differential expression of alphaB-crystallin in the zebrafish, Danio rerio. *Biochim Biophys Acta,* 1447**,** 271-7.

POSNER, M., LOW, S., RUNKLE, S., HILL, J., KANTOROW, M. & HORWITZ, J. 2002. Sequencing, tissue specific expression and chaperone activity of zebrafish (Danio rerio) alpha crystallin. *Investigative Ophthalmology & Visual Science,* 43**,** U1317-U1317.

POSNER, M., SMITH, A., VIHTELIC, T. S. & WISTOW, G. J. 2005. A second alpha B crystallin from the zebrafish (Danio rerio). *Investigative Ophthalmology & Visual Science,* 46.

POSNER, M., WAGES, P. A., HORWITZ, J. & DING, L. 2011. Developmental Changes In Zebrafish (Danio rerio) Lens Crystallin Expression. *ARVO Annual Meeting Abstract Search and Program Planner,* 2011**,** 2773-2773.

POULAIN, P., GELLY, J. C. & FLATTERS, D. 2010. Detection and architecture of small heat shock protein monomers. *PLoS One,* 5**,** e9990.

POUNTNEY, D. L., TREWEEK, T. M., CHATAWAY, T., HUANG, Y., CHEGINI, F., BLUMBERGS, P. C., RAFTERY, M. J. & GAI, W. P. 2005. Alpha B-crystallin is a major component of glial cytoplasmic inclusions in multiple system atrophy. *Neurotox Res,* 7**,** 77-85.

POWERS, E. T. & BALCH, W. E. 2013. Diversity in the origins of proteostasis networks--a driver for protein function in evolution. *Nat Rev Mol Cell Biol,* 14**,** 237-48.

POWERS, E. T., MORIMOTO, R. I., DILLIN, A., KELLY, J. W. & BALCH, W. E. 2009. Biological and chemical approaches to diseases of proteostasis deficiency. *Annu Rev Biochem,* 78**,** 959-91.

PRATT, W. B., MORISHIMA, Y., MURPHY, M. & HARRELL, M. 2006. Chaperoning of glucocorticoid receptors. *Handb Exp Pharmacol***,** 111-38.

PRIVALOV, P. L. 1979. Stability of proteins: small globular proteins. *Adv Protein Chem,* 33**,** 167-241.

QUARLES, E. K., DAI, D. F., TOCCHI, A., BASISTY, N., GITARI, L. & RABINOVITCH, P. S. 2015. Quality control systems in cardiac aging. *Ageing Res Rev,* 23**,** 101-15.

RAJU, I., OONTHONPAN, L. & ABRAHAM, E. C. 2012. Mutations in human alphaA-crystallin/sHSP affect subunit exchange interaction with alphaB-crystallin. *PLoS One,* 7**,** e31421.

RAJU, T. N. 1999. The Nobel chronicles. 1950: Edward Calvin Kendall (1886-1972); Philip Showalter Hench (1896-1965); and Tadeus Reichstein (1897-1996). *Lancet,* 353**,** 1370.

RAMSAY, J. M., FEIST, G. W., VARGA, Z. M., WESTERFIELD, M., KENT, M. L. & SCHRECK, C. B. 2006. Whole-body cortisol is an indicator of crowding stress in adult zebrafish, Danio rerio. *Aquaculture,* 258**,** 565-574.

RAYNER, K., CHEN, Y. X., SIEBERT, T. & O'BRIEN, E. R. 2010. Heat shock protein 27: clue to understanding estrogen-mediated atheroprotection? *Trends Cardiovasc Med,* 20**,** 54-8.

REDDY, V. S. & REDDY, G. B. 2015. Emerging role for alphaB-crystallin as a therapeutic agent: pros and cons. *Curr Mol Med,* 15**,** 47-61.

RENFRO, L. & SNOW, J. S. 1992. Ocular effects of topical and systemic steroids. *Dermatol Clin,* 10**,** 505-12.

RENNELL, D., BOUVIER, S. E., HARDY, L. W. & POTEETE, A. R. 1991. Systematic mutation of bacteriophage T4 lysozyme. *J Mol Biol,* 222**,** 67-88.

REYNAUD, E. 2010. Protein Misfolding and Degenerative Diseases. *Nature Education,* 3**,** 28.

RHEN, T. & CIDLOWSKI, J. A. 2005. Antiinflammatory action of glucocorticoids--new mechanisms for old drugs. *N Engl J Med,* 353**,** 1711-23.

RICHARDSON, R., TRACEY-WHITE, D., WEBSTER, A. & MOOSAJEE, M. 2017. The zebrafish eye-a paradigm for investigating human ocular genetics. *Eye (Lond),* 31**,** 68-86.

RICHTER, K., HASLBECK, M. & BUCHNER, J. 2010. The heat shock response: life on the verge of death. *Mol Cell,* 40**,** 253-66.

RISLEY, S. D. 1915. Hereditary aniridia - An interesting family history. *Journal of the American Medical Association,* 64**,** 1310-1312.

ROBINSON, A. A., DUNN, M. J., MCCORMACK, A., DOS REMEDIOS, C. & ROSE, M. L. 2010. Protective effect of phosphorylated Hsp27 in coronary arteries through actin stabilization. *J Mol Cell Cardiol,* 49**,** 370-9.

ROBINSON, M. L. & OVERBEEK, P. A. 1996. Differential expression of alpha A- and alpha B-crystallin during murine ocular development. *Invest Ophthalmol Vis Sci,* 37**,** 2276-84.

ROG-ZIELINSKA, E. A., RICHARDSON, R. V., DENVIR, M. A. & CHAPMAN, K. E. 2014. Glucocorticoids and foetal heart maturation; implications for prematurity and foetal programming. *J Mol Endocrinol,* 52**,** R125-35.

ROSE, G. D., FLEMING, P. J., BANAVAR, J. R. & MARITAN, A. 2006. A backbone-based theory of protein folding. *Proc Natl Acad Sci U S A,* 103**,** 16623-33.

ROY, S. G., DE, P., MUKHERJEE, D., CHANDER, V., KONAR, A., BANDYOPADHYAY, D. & BANDYOPADHYAY, A. 2009. Excess of glucocorticoid induces cardiac dysfunction via activating angiotensin II pathway. *Cell Physiol Biochem,* 24**,** 1-10.

RUJANO, M. A., BOSVELD, F., SALOMONS, F. A., DIJK, F., VAN WAARDE, M. A., VAN DER WANT, J. J., DE VOS, R. A., BRUNT, E. R., SIBON, O. C. &

KAMPINGA, H. H. 2006. Polarised asymmetric inheritance of accumulated protein damage in higher eukaryotes. *PLoS Biol,* 4**,** e417.

RUNKLE, S., HILL, J., KANTOROW, M., HORWITZ, J. & POSNER, M. 2002. Sequence and spatial expression of zebrafish (Danio rerio) alpha A-crystallin. *Molecular Vision,* 8**,** 45-50.

RUNKLE, S. A., HILL, J. & POSNER, M. 2001. Differential expression of alpha crystallin in the zebrafish, Danio rerio. *Ohio Journal of Science,* 101**,** A.32-A.33.

SACCONI, S., FEASSON, L., ANTOINE, J. C., PECHEUX, C., BERNARD, R., COBO, A. M., CASARIN, A., SALVIATI, L., DESNUELLE, C. & URTIZBEREA, A. 2012. A novel CRYAB mutation resulting in multisystemic disease. *Neuromuscul Disord,* 22**,** 66-72.

SAINTE-MARIE, Y., NGUYEN DINH CAT, A., PERRIER, R., MANGIN, L., SOUKASEUM, C., PEUCHMAUR, M., TRONCHE, F., FARMAN, N., ESCOUBET, B., BENITAH, J. P. & JAISSER, F. 2007. Conditional glucocorticoid receptor expression in the heart induces atrio-ventricular block. *FASEB J,* 21**,** 3133-41.

SALLIN, P. & JAZWINSKA, A. 2016. Acute stress is detrimental to heart regeneration in zebrafish. *Open Biol,* 6.

SANBE, A., OSINSKA, H., VILLA, C., GULICK, J., KLEVITSKY, R., GLABE, C. G., KAYED, R. & ROBBINS, J. 2005. Reversal of amyloid-induced heart disease in desmin-related cardiomyopathy. *Proc Natl Acad Sci U S A,* 102**,** 13592-7.

SANBE, A., YAMAUCHI, J., MIYAMOTO, Y., FUJIWARA, Y., MURABE, M. & TANOUE, A. 2007. Interruption of CryAB-amyloid oligomer formation by HSP22. *J Biol Chem,* 282**,** 555-63.

SANTHOSHKUMAR, P., MURUGESAN, R. & SHARMA, K. K. 2009. Deletion of (54)FLRAPSWF(61) residues decreases the oligomeric size and enhances the chaperone function of alphaB-crystallin. *Biochemistry,* 48**,** 5066-73.

SANTHOSHKUMAR, P., XIE, L., RAJU, M., RENEKER, L. & SHARMA, K. K. 2014. Lens crystallin modifications and cataract in transgenic mice overexpressing acylpeptide hydrolase. *J Biol Chem,* 289**,** 9039-52.

SATHISH, H. A., KOTEICHE, H. A. & MCHAOURAB, H. S. 2004. Binding of destabilized betaB2-crystallin mutants to alpha-crystallin: the role of a folding intermediate. *J Biol Chem,* 279**,** 16425-32.

SATHISH, H. A., STEIN, R. A., YANG, G. & MCHAOURAB, H. S. 2003. Mechanism of chaperone function in small heat-shock proteins. Fluorescence studies of the conformations of T4 lysozyme bound to alphaB-crystallin. *J Biol Chem,* 278**,** 44214-21.

SAX, C. M., CVEKL, A. & PIATIGORSKY, J. 1997. Transcriptional regulation of the mouse alpha A-crystallin gene: binding of USF to the -7/+5 region. *Gene,* 185**,** 209-16.

SCHAAF, M. J., CHAMPAGNE, D., VAN LAANEN, I. H., VAN WIJK, D. C., MEIJER, A. H., MEIJER, O. C., SPAINK, H. P. & RICHARDSON, M. K. 2008. Discovery of a functional glucocorticoid receptor beta-isoform in zebrafish. *Endocrinology,* 149**,** 1591-9.

SCHAAF, M. J., CHATZOPOULOU, A. & SPAINK, H. P. 2009. The zebrafish as a model system for glucocorticoid receptor research. *Comp Biochem Physiol A Mol Integr Physiol,* 153**,** 75-82.
SCHEIER, B., FOLETTI, A., STARK, G., AOYAMA, A., DOBBELING, U., RUSCONI, S. & KLEMENZ, R. 1996. Glucocorticoids regulate the expression of the stressprotein alpha B-crystallin. *Mol Cell Endocrinol,* 123**,** 187-98.
SCHMITT, E. A. & DOWLING, J. E. 1994. Early eye morphogenesis in the zebrafish, Brachydanio rerio. *J Comp Neurol,* 344**,** 532-42.
SCHREIBER, G., BUCKLE, A. M. & FERSHT, A. R. 1994. Stability and function: two constraints in the evolution of barstar and other proteins. *Structure,* 2**,** 945-51.
SCHRODER, H., LANGER, T., HARTL, F. U. & BUKAU, B. 1993. DnaK, DnaJ and GrpE form a cellular chaperone machinery capable of repairing heat-induced protein damage. *EMBO J,* 12**,** 4137-44.
SCHUCK, P. 2000. Size-distribution analysis of macromolecules by sedimentation velocity ultracentrifugation and lamm equation modeling. *Biophys J,* 78**,** 1606-19.
SCHWAB, I. R., DUBIELZIG, R. R. & SCHOBERT, C. 2012. *Evolution's witness : how eyes evolved,* New York, Oxford University Press.
SEIM, I., MA, S. & GLADYSHEV, V. N. 2016. Gene expression signatures of human cell and tissue longevity. *NPJ Aging Mech Dis,* 2**,** 16014.
SELCEN, D. 2011. Myofibrillar myopathies. *Neuromuscul Disord,* 21**,** 161-71.
SELCEN, D. & ENGEL, A. G. 2003. Myofibrillar myopathy caused by novel dominant negative alpha B-crystallin mutations. *Ann Neurol,* 54**,** 804-10.
SENYO, S. E., STEINHAUSER, M. L., PIZZIMENTI, C. L., YANG, V. K., CAI, L., WANG, M., WU, T. D., GUERQUIN-KERN, J. L., LECHENE, C. P. & LEE, R. T. 2013. Mammalian heart renewal by pre-existing cardiomyocytes. *Nature,* 493**,** 433-6.
SERRANO, L., DAY, A. G. & FERSHT, A. R. 1993. Step-wise mutation of barnase to binase. A procedure for engineering increased stability of proteins and an experimental analysis of the evolution of protein stability. *J Mol Biol,* 233**,** 305-12.
SHARMA, K. K., KAUR, H. & KESTER, K. 1997. Functional elements in molecular chaperone alpha-crystallin: identification of binding sites in alpha B-crystallin. *Biochem Biophys Res Commun,* 239**,** 217-22.
SHASHIDHARAMURTHY, R., KOTEICHE, H. A., DONG, J. & MCHAOURAB, H. S. 2005. Mechanism of chaperone function in small heat shock proteins: dissociation of the HSP27 oligomer is required for recognition and binding of destabilized T4 lysozyme. *J Biol Chem,* 280**,** 5281-9.
SHEELADEVI, S., LAWRENSON, J. G., FIELDER, A. R. & SUTTLE, C. M. 2016. Global prevalence of childhood cataract: a systematic review. *Eye (Lond),* 30**,** 1160-9.
SHEN, Y., GU, J., HUANG, L. H., ZHENG, S. C., LIU, L., XU, W. H., FENG, Q. L. & KANG, L. 2011. Cloning and expression analysis of six small heat shock protein genes in the common cutworm, Spodoptera litura. *J Insect Physiol,* 57**,** 908-14.
SHI, J., KOTEICHE, H. A., MCDONALD, E. T., FOX, T. L., STEWART, P. L. & MCHAOURAB, H. S. 2013. Cryoelectron microscopy analysis of small heat

shock protein 16.5 (Hsp16.5) complexes with T4 lysozyme reveals the structural basis of multimode binding. *J Biol Chem,* 288**,** 4819-30.

SHI, J., KOTEICHE, H. A., MCHAOURAB, H. S. & STEWART, P. L. 2006a. Cryoelectron microscopy and EPR analysis of engineered symmetric and polydisperse Hsp16.5 assemblies reveals determinants of polydispersity and substrate binding. *J Biol Chem,* 281**,** 40420-8.

SHI, X., LUO, Y., HOWLEY, S., DZIALO, A., FOLEY, S., HYDE, D. R. & VIHTELIC, T. S. 2006b. Zebrafish foxe3: roles in ocular lens morphogenesis through interaction with pitx3. *Mech Dev,* 123**,** 761-82.

SHIH, Y. H., ZHANG, Y., DING, Y., ROSS, C. A., LI, H., OLSON, T. M. & XU, X. 2015. Cardiac transcriptome and dilated cardiomyopathy genes in zebrafish. *Circ Cardiovasc Genet,* 8**,** 261-9.

SHOICHET, B. K., BAASE, W. A., KUROKI, R. & MATTHEWS, B. W. 1995. A relationship between protein stability and protein function. *Proc Natl Acad Sci U S A,* 92**,** 452-6.

SHROFF, N. P., CHERIAN-SHAW, M., BERA, S. & ABRAHAM, E. C. 2000. Mutation of R116C Results in Highly Oligomerized αA-Crystallin with Modified Structure and Defective Chaperone-like Function. *Biochemistry,* 39**,** 1420-1426.

SIDDIQUE, M., GERNHARD, S., VON KOSKULL-DORING, P., VIERLING, E. & SCHARF, K. D. 2008. The plant sHSP superfamily: five new members in Arabidopsis thaliana with unexpected properties. *Cell Stress Chaperones,* 13**,** 183-97.

SIMON, S., FONTAINE, J. M., MARTIN, J. L., SUN, X., HOPPE, A. D., WELSH, M. J., BENNDORF, R. & VICART, P. 2007. Myopathy-associated alphaB-crystallin mutants: abnormal phosphorylation, intracellular location, and interactions with other small heat shock proteins. *J Biol Chem,* 282**,** 34276-87.

SKALKA, H. W. & PRCHAL, J. T. 1980. Effect of corticosteroids on cataract formation. *Arch Ophthalmol,* 98**,** 1773-7.

SLINGSBY, C., WISTOW, G. J. & CLARK, A. R. 2013. Evolution of crystallins for a role in the vertebrate eye lens. *Protein Sci,* 22**,** 367-80.

SMITH, A. A., WYATT, K., VACHA, J., VIHTELIC, T. S., ZIGLER, J. S., JR., WISTOW, G. J. & POSNER, M. 2006. Gene duplication and separation of functions in alphaB-crystallin from zebrafish (Danio rerio). *FEBS J,* 273**,** 481-90.

SORGER, P. K. 1991. Heat shock factor and the heat shock response. *Cell,* 65**,** 363-6.

SOTO, C. 2001. Protein misfolding and disease; protein refolding and therapy. *FEBS Lett,* 498**,** 204-7.

SOULES, K. A. & LINK, B. A. 2005. Morphogenesis of the anterior segment in the zebrafish eye. *BMC Dev Biol,* 5**,** 12.

SPALDING, K. L., ARNER, E., WESTERMARK, P. O., BERNARD, S., BUCHHOLZ, B. A., BERGMANN, O., BLOMQVIST, L., HOFFSTEDT, J., NASLUND, E., BRITTON, T., CONCHA, H., HASSAN, M., RYDEN, M., FRISEN, J. & ARNER, P. 2008. Dynamics of fat cell turnover in humans. *Nature,* 453**,** 783-7.

SPALDING, K. L., BHARDWAJ, R. D., BUCHHOLZ, B. A., DRUID, H. & FRISEN, J. 2005a. Retrospective birth dating of cells in humans. *Cell,* 122**,** 133-43.

SPALDING, K. L., BUCHHOLZ, B. A., BERGMAN, L. E., DRUID, H. & FRISEN, J. 2005b. Forensics: age written in teeth by nuclear tests. *Nature,* 437**,** 333-4.
SPECTOR, A. 1965. The Soluble Proteins of the Lens. *Invest Ophthalmol,* 4**,** 579-91.
SREELAKSHMI, Y., SANTHOSHKUMAR, P., BHATTACHARYYA, J. & SHARMA, K. K. 2004. AlphaA-crystallin interacting regions in the small heat shock protein, alphaB-crystallin. *Biochemistry,* 43**,** 15785-95.
SRINIVASAN, A. N., NAGINENI, C. N. & BHAT, S. P. 1992. alpha A-crystallin is expressed in non-ocular tissues. *J Biol Chem,* 267**,** 23337-41.
STEENBERGEN, P. J., RICHARDSON, M. K. & CHAMPAGNE, D. L. 2011. The use of the zebrafish model in stress research. *Prog Neuropsychopharmacol Biol Psychiatry,* 35**,** 1432-51.
STENGEL, F., BALDWIN, A. J., PAINTER, A. J., JAYA, N., BASHA, E., KAY, L. E., VIERLING, E., ROBINSON, C. V. & BENESCH, J. L. 2010. Quaternary dynamics and plasticity underlie small heat shock protein chaperone function. *Proc Natl Acad Sci U S A,* 107**,** 2007-12.
STEWART, E. J., MADDEN, R., PAUL, G. & TADDEI, F. 2005. Aging and death in an organism that reproduces by morphologically symmetric division. *PLoS Biol,* 3**,** e45.
STRAUCH, A. & HASLBECK, M. 2016. The function of small heat-shock proteins and their implication in proteostasis. *Essays Biochem,* 60**,** 163-172.
STROIKIN, Y., DALEN, H., BRUNK, U. T. & TERMAN, A. 2005. Testing the "garbage" accumulation theory of ageing: mitotic activity protects cells from death induced by inhibition of autophagy. *Biogerontology,* 6**,** 39-47.
STUDER, S., OBRIST, M., LENTZE, N. & NARBERHAUS, F. 2002. A critical motif for oligomerization and chaperone activity of bacterial alpha-heat shock proteins. *Eur J Biochem,* 269**,** 3578-86.
SULAIMAN, R. S., KADMIEL, M. & CIDLOWSKI, J. A. 2018. Glucocorticoid receptor signaling in the eye. *Steroids,* 133**,** 60-66.
SUN, S. T., TANAKA, T., NISHIO, I., PEETERMANS, J., MAIZEL, J. V., JR. & PIATIGORSKY, J. 1984. Direct observation of delta-crystallin accumulation by laser light-scattering spectroscopy in the chicken embryo lens. *Proc Natl Acad Sci U S A,* 81**,** 785-7.
SUN, Y. & MACRAE, T. H. 2005a. The small heat shock proteins and their role in human disease. *FEBS J,* 272**,** 2613-27.
SUN, Y. & MACRAE, T. H. 2005b. Small heat shock proteins: molecular structure and chaperone function. *Cell Mol Life Sci,* 62**,** 2460-76.
SUSS, O. & REICHMANN, D. 2015. Protein plasticity underlines activation and function of ATP-independent chaperones. *Front Mol Biosci,* 2**,** 43.
SUZUKI, A., SUGIYAMA, Y., HAYASHI, Y., NYU-I, N., YOSHIDA, M., NONAKA, I., ISHIURA, S., ARAHATA, K. & OHNO, S. 1998a. MKBP, a novel member of the small heat shock protein family, binds and activates the myotonic dystrophy protein kinase. *J Cell Biol,* 140**,** 1113-24.

SUZUKI, T. C., KRAWITZ, D. C. & VIERLING, E. 1998b. The chloroplast small heat-shock protein oligomer is not phosphorylated and does not dissociate during heat stress in vivo. *Plant Physiol,* 116**,** 1151-61.

SWAMYNATHAN, S. K. & PIATIGORSKY, J. 2007. Regulation of the mouse alphaB-crystallin and MKBP/HspB2 promoter activities by shared and gene specific intergenic elements: the importance of context dependency. *Int J Dev Biol,* 51**,** 689-700.

TABIBZADEH, S. & BROOME, J. 1999. Heat shock proteins in human endometrium throughout the menstrual cycle. *Infect Dis Obstet Gynecol,* 7**,** 5-9.

TAIPALE, M., JAROSZ, D. F. & LINDQUIST, S. 2010. HSP90 at the hub of protein homeostasis: emerging mechanistic insights. *Nat Rev Mol Cell Biol,* 11**,** 515-28.

TANGUAY, R. M. & HIGHTOWER, L. E. 2015. *The Big Book on Small Heat Shock Proteins*, Springer International Publishing.

TANNOUS, P., ROTHERMEL, B. A. & HILL, J. A. 2010. Protein Quality Control in Heart Disease: Small Heat Shock Proteins and Autophagy. *Small Stress Proteins and Human Diseases***,** 171-188.

TANNU, N. S. & HEMBY, S. E. 2006. Two-dimensional fluorescence difference gel electrophoresis for comparative proteomics profiling. *Nat Protoc,* 1**,** 1732-42.

TAYLOR, R. C. & DILLIN, A. 2011. Aging as an event of proteostasis collapse. *Cold Spring Harb Perspect Biol,* 3.

THAYER, N. H., LEVERICH, C. K., FITZGIBBON, M. P., NELSON, Z. W., HENDERSON, K. A., GAFKEN, P. R., HSU, J. J. & GOTTSCHLING, D. E. 2014. Identification of long-lived proteins retained in cells undergoing repeated asymmetric divisions. *Proc Natl Acad Sci U S A,* 111**,** 14019-26.

THISSE, B. & THISSE, C. 2014. In situ hybridization on whole-mount zebrafish embryos and young larvae. *Methods Mol Biol,* 1211**,** 53-67.

THOMSON, J. A. & AUGUSTEYN, R. C. 1985. Ontogeny of human lens crystallins. *Exp Eye Res,* 40**,** 393-410.

THOMSON, J. A. & AUGUSTEYN, R. C. 1989. On the structure of alpha-crystallin: construction of hybrid molecules and homopolymers. *Biochim Biophys Acta,* 994**,** 246-52.

THORNELL, E. & AQUILINA, A. 2015. Regulation of alphaA- and alphaB-crystallins via phosphorylation in cellular homeostasis. *Cell Mol Life Sci,* 72**,** 4127-37.

TOKURIKI, N., KINJO, M., NEGI, S., HOSHINO, M., GOTO, Y., URABE, I. & YOMO, T. 2004. Protein folding by the effects of macromolecular crowding. *Protein Sci,* 13**,** 125-33.

TOMOKANE, N., IWAKI, T., TATEISHI, J., IWAKI, A. & GOLDMAN, J. E. 1991. Rosenthal fibers share epitopes with alpha B-crystallin, glial fibrillary acidic protein, and ubiquitin, but not with vimentin. Immunoelectron microscopy with colloidal gold. *Am J Pathol,* 138**,** 875-85.

TOWER, J. 2011. Heat shock proteins and Drosophila aging. *Exp Gerontol,* 46**,** 355-62.

TREISMAN, J. E. 2004. How to make an eye. *Development,* 131**,** 3823-7.

TREWEEK, T. M., ECROYD, H., WILLIAMS, D. M., MEEHAN, S., CARVER, J. A. & WALKER, M. J. 2007. Site-directed mutations in the C-terminal extension of

human alphaB-crystallin affect chaperone function and block amyloid fibril formation. *PLoS One,* 2**,** e1046.
TREWEEK, T. M., MEEHAN, S., ECROYD, H. & CARVER, J. A. 2015. Small heat-shock proteins: important players in regulating cellular proteostasis. *Cell Mol Life Sci,* 72**,** 429-451.
TROKEL, S. 1962. The physical basis for transparency of the crystalline lens. *Invest Ophthalmol,* 1**,** 493-501.
TRUSCOTT, R. J. & FRIEDRICH, M. G. 2016. The etiology of human age-related cataract. Proteins don't last forever. *Biochim Biophys Acta,* 1860**,** 192-8.
TRUSCOTT, R. J. W., SCHEY, K. L. & FRIEDRICH, M. G. 2016. Old Proteins in Man: A Field in its Infancy. *Trends Biochem Sci,* 41**,** 654-664.
TSAI, A. M., UDOVIC, T. J. & NEUMANN, D. A. 2001. The inverse relationship between protein dynamics and thermal stability. *Biophys J,* 81**,** 2339-43.
TYEDMERS, J., MOGK, A. & BUKAU, B. 2010. Cellular strategies for controlling protein aggregation. *Nat Rev Mol Cell Biol,* 11**,** 777-88.
ULYANOVA, V., VERSHININA, V. & ILINSKAYA, O. 2011. Barnase and binase: twins with distinct fates. *FEBS J,* 278**,** 3633-43.
UNG, C. Y. & MOLTENO, A. C. 2004. An enigmatic eye: the histology of the tuatara pineal complex. *Clin Exp Ophthalmol,* 32**,** 614-8.
URBAN, R. C., JR. & COTLIER, E. 1986. Corticosteroid-induced cataracts. *Surv Ophthalmol,* 31**,** 102-10.
VALLEE-BELISLE, A. & MICHNICK, S. W. 2007. Multiple tryptophan probes reveal that ubiquitin folds via a late misfolded intermediate. *J Mol Biol,* 374**,** 791-805.
VALLEE-BELISLE, A. & MICHNICK, S. W. 2012. Visualizing transient protein-folding intermediates by tryptophan-scanning mutagenesis. *Nat Struct Mol Biol,* 19**,** 731-6.
VAN DEN BERG, B., ELLIS, R. J. & DOBSON, C. M. 1999. Effects of macromolecular crowding on protein folding and aggregation. *EMBO J,* 18**,** 6927-33.
VAN DEN OETELAAR, P. J., VAN SOMEREN, P. F., THOMSON, J. A., SIEZEN, R. J. & HOENDERS, H. J. 1990. A dynamic quaternary structure of bovine alpha-crystallin as indicated from intermolecular exchange of subunits. *Biochemistry,* 29**,** 3488-93.
VAN MONTFORT, R., SLINGSBY, C. & VIERLING, E. 2001a. Structure and function of the small heat shock protein/alpha-crystallin family of molecular chaperones. *Adv Protein Chem,* 59**,** 105-56.
VAN MONTFORT, R., SLINGSBY, C. & VIERLING, E. 2002. Structure and function of the small heat shock protein/alpha-crystallin family of molecular chaperones. *Protein Folding in the Cell,* 59**,** 105-156.
VAN MONTFORT, R. L., BASHA, E., FRIEDRICH, K. L., SLINGSBY, C. & VIERLING, E. 2001b. Crystal structure and assembly of a eukaryotic small heat shock protein. *Nat Struct Biol,* 8**,** 1025-30.
VANDER HEIDE, R. S. 2002. Increased expression of HSP27 protects canine myocytes from simulated ischemia-reperfusion injury. *Am J Physiol Heart Circ Physiol,* 282**,** H935-41.

VANDEWALLE, J., LUYPAERT, A., DE BOSSCHER, K. & LIBERT, C. 2018. Therapeutic Mechanisms of Glucocorticoids. *Trends Endocrinol Metab,* 29**,** 42-54.

VEENSTRA, D. L., BEST, J. H., HORNBERGER, J., SULLIVAN, S. D. & HRICIK, D. E. 1999. Incidence and long-term cost of steroid-related side effects after renal transplantation. *Am J Kidney Dis,* 33**,** 829-39.

VICART, P., CARON, A., GUICHENEY, P., LI, Z., PREVOST, M. C., FAURE, A., CHATEAU, D., CHAPON, F., TOME, F., DUPRET, J. M., PAULIN, D. & FARDEAU, M. 1998. A missense mutation in the alphaB-crystallin chaperone gene causes a desmin-related myopathy. *Nat Genet,* 20**,** 92-5.

VOISINE, C., PEDERSEN, J. S. & MORIMOTO, R. I. 2010. Chaperone networks: tipping the balance in protein folding diseases. *Neurobiol Dis,* 40**,** 12-20.

VOS, M. J., ZIJLSTRA, M. P., KANON, B., VAN WAARDE-VERHAGEN, M. A., BRUNT, E. R., OOSTERVELD-HUT, H. M., CARRA, S., SIBON, O. C. & KAMPINGA, H. H. 2010. HSPB7 is the most potent polyQ aggregation suppressor within the HSPB family of molecular chaperones. *Hum Mol Genet,* 19**,** 4677-93.

VRIES, H. D. 1958. Atomic Bomb Effect - Variation of Radiocarbon in Plants, Shells, and Snails in the Past 4 Years. *Science,* 128**,** 250-251.

VYAS, S., RODRIGUES, A. J., SILVA, J. M., TRONCHE, F., ALMEIDA, O. F., SOUSA, N. & SOTIROPOULOS, I. 2016. Chronic Stress and Glucocorticoids: From Neuronal Plasticity to Neurodegeneration. *Neural Plast,* 2016**,** 6391686.

WADE, N. J. 1998. *A natural history of vision,* Cambridge, Mass., MIT Press.

WAGES, P., HORWITZ, J., DING, L., CORBIN, R. W. & POSNER, M. 2013. Changes in zebrafish (Danio rerio) lens crystallin content during development. *Mol Vis,* 19**,** 408-17.

WANG, K., CHENG, C., LI, L., LIU, H., HUANG, Q., XIA, C. H., YAO, K., SUN, P., HORWITZ, J. & GONG, X. 2007. GammaD-crystallin associated protein aggregation and lens fiber cell denucleation. *Invest Ophthalmol Vis Sci,* 48**,** 3719-28.

WANG, M., HERRMANN, C. J., SIMONOVIC, M., SZKLARCZYK, D. & VON MERING, C. 2015. Version 4.0 of PaxDb: Protein abundance data, integrated across model organisms, tissues, and cell-lines. *Proteomics,* 15**,** 3163-8.

WANG, X., GARCIA, C. M., SHUI, Y. B. & BEEBE, D. C. 2004. Expression and regulation of alpha-, beta-, and gamma-crystallins in mammalian lens epithelial cells. *Invest Ophthalmol Vis Sci,* 45**,** 3608-19.

WANG, X., OSINSKA, H., KLEVITSKY, R., GERDES, A. M., NIEMAN, M., LORENZ, J., HEWETT, T. & ROBBINS, J. 2001. Expression of R120G-alphaB-crystallin causes aberrant desmin and alphaB-crystallin aggregation and cardiomyopathy in mice. *Circ Res,* 89**,** 84-91.

WANG, Z., HAN, J., DAVID, L. L. & SCHEY, K. L. 2013. Proteomics and phosphoproteomics analysis of human lens fiber cell membranes. *Invest Ophthalmol Vis Sci,* 54**,** 1135-43.

WASHINGTON, N. L., HAENDEL, M. A., MUNGALL, C. J., ASHBURNER, M., WESTERFIELD, M. & LEWIS, S. E. 2009. Linking human diseases to animal models using ontology-based phenotype annotation. *PLoS Biol,* 7**,** e1000247.

WAWROUSEK, E. F. & BRADY, J. P. 1997. Lens fiber cell inclusion bodies in alpha A-crystallin gene knockout mice are composed predominantly of alpha B-crystallin polypeptides. *Investigative Ophthalmology & Visual Science,* 38**,** 2733-2733.

WEEKS, S. D., BARANOVA, E. V., HEIRBAUT, M., BEELEN, S., SHKUMATOV, A. V., GUSEV, N. B. & STRELKOV, S. V. 2014. Molecular structure and dynamics of the dimeric human small heat shock protein HSPB6. *J Struct Biol,* 185**,** 342-54.

WELMAN, A., BARRACLOUGH, J. & DIVE, C. 2006. Generation of cells expressing improved doxycycline-regulated reverse transcriptional transactivator rtTA2S-M2. *Nat Protoc,* 1**,** 803-11.

WENDELAAR BONGA, S. E. 1997. The stress response in fish. *Physiol Rev,* 77**,** 591-625.

WHITE, H. E., ORLOVA, E. V., CHEN, S., WANG, L., IGNATIOU, A., GOWEN, B., STROMER, T., FRANZMANN, T. M., HASLBECK, M., BUCHNER, J. & SAIBIL, H. R. 2006. Multiple distinct assemblies reveal conformational flexibility in the small heat shock protein Hsp26. *Structure,* 14**,** 1197-204.

WIERSMA, M., HENNING, R. H. & BRUNDEL, B. J. 2016. Derailed Proteostasis as a Determinant of Cardiac Aging. *Can J Cardiol,* 32**,** 1166 e11-20.

WILKINSON, R. N., JOPLING, C. & VAN EEDEN, F. J. M. 2014. Chapter Four - Zebrafish as a Model of Cardiac Disease. *In:* CHICO, T. J. A. (ed.) *Progress in Molecular Biology and Translational Science.* Academic Press.

WILLIS, M. S. & PATTERSON, C. 2010. Hold me tight: Role of the heat shock protein family of chaperones in cardiac disease. *Circulation,* 122**,** 1740-51.

WINKLHOFER, K. F., TATZELT, J. & HAASS, C. 2008. The two faces of protein misfolding: gain- and loss-of-function in neurodegenerative diseases. *EMBO J,* 27**,** 336-49.

WISTOW, G. 1993. Lens crystallins: gene recruitment and evolutionary dynamism. *Trends Biochem Sci,* 18**,** 301-6.

WOODCOCK, E. A. & MATKOVICH, S. J. 2005. Cardiomyocytes structure, function and associated pathologies. *Int J Biochem Cell Biol,* 37**,** 1746-51.

WU, S. Y., ZOU, P., FULLER, A. W., MISHRA, S., WANG, Z., SCHEY, K. L. & MCHAOURAB, H. S. 2016. Expression of Cataract-linked gamma-Crystallin Variants in Zebrafish Reveals a Proteostasis Network That Senses Protein Stability. *J Biol Chem,* 291**,** 25387-25397.

WYATT, P. J. 2014. Measurement of special nanoparticle structures by light scattering. *Anal Chem,* 86**,** 7171-83.

XU, X., MEILER, S. E., ZHONG, T. P., MOHIDEEN, M., CROSSLEY, D. A., BURGGREN, W. W. & FISHMAN, M. C. 2002. Cardiomyopathy in zebrafish due to mutation in an alternatively spliced exon of titin. *Nat Genet,* 30**,** 205-9.

YANG, Y. & CVEKL, A. 2005. Tissue-specific regulation of the mouse alphaA-crystallin gene in lens via recruitment of Pax6 and c-Maf to its promoter. *J Mol Biol,* 351**,** 453-69.

YELON, D., HORNE, S. A. & STAINIER, D. Y. 1999. Restricted expression of cardiac myosin genes reveals regulated aspects of heart tube assembly in zebrafish. *Dev Biol,* 214**,** 23-37.

YOSHIDA, K., AKI, T., HARADA, K., SHAMA, K. M., KAMODA, Y., SUZUKI, A. & OHNO, S. 1999. Translocation of HSP27 and MKBP in ischemic heart. *Cell Struct Funct,* 24**,** 181-5.

YUDT, M. R., JEWELL, C. M., BIENSTOCK, R. J. & CIDLOWSKI, J. A. 2003. Molecular origins for the dominant negative function of human glucocorticoid receptor beta. *Mol Cell Biol,* 23**,** 4319-30.

ZHAO, H., BROWN, P. H. & SCHUCK, P. 2011a. On the distribution of protein refractive index increments. *Biophys J,* 100**,** 2309-17.

ZHAO, H., MAGONE, M. T. & SCHUCK, P. 2011b. The role of macromolecular crowding in the evolution of lens crystallins with high molecular refractive index. *Phys Biol,* 8**,** 046004.

ZHENG, J. 2010. FRET and Its Biological Application as a Molecular Ruler. *In:* JUE, T. (ed.) *Biomedical Applications of Biophysics.* Totowa, NJ: Humana Press.

ZOU, P., WU, S. Y., KOTEICHE, H. A., MISHRA, S., LEVIC, D. S., KNAPIK, E., CHEN, W. & MCHAOURAB, H. S. 2015. A conserved role of alphaA-crystallin in the development of the zebrafish embryonic lens. *Exp Eye Res,* 138**,** 104-13.

ZWANZIG, R. 1997. Two-state models of protein folding kinetics. *Proc Natl Acad Sci U S A,* 94**,** 148-50.